

**DETECTION, CLASSIFICATION AND MATCHING OF ALTERED  
FINGERPRINTS USING RIDGE AND MINUTIAE FEATURES**

Submitted to  
**COCHIN UNIVERSITY OF SCIENCE AND TECHNOLOGY**

for the award of the degree of

**Doctor of Philosophy**

by

**ANOOP T.R.**

Under the guidance of

**Dr. Mini M. G.**

RESEARCH GUIDE  
DEPARTMENT OF ELECTRONICS ENGINEERING  
MODEL ENGINEERING COLLEGE  
COCHIN - 682 021, INDIA

**MAY 2016**

**DETECTION, CLASSIFICATION AND MATCHING OF ALTERED FINGERPRINTS  
USING RIDGE AND MINUTIAE FEATURES**

**Ph.D. Thesis in the field of Biometrics Image Processing**

**Author**

Anoop T.R.  
Research Scholar  
Department of Electronics  
Model Engineering College  
Cochin-682 021, India  
e-mail: anooptr234@gmail.com

**Research Advisor**

Dr. M. G. Mini  
Research Guide  
Department of Electronics  
Model Engineering College  
Cochin-682 021, India  
e-mail: mininair@mec.ac.in

May, 2016

Dedicated to.....

*My Parents, Wife & Son*



## ***CERTIFICATE***

This is to certify that this thesis entitled ***Detection, Classification and Matching of Altered Fingerprints using Ridge and Minutiae Features*** is a bonafide record of the research work carried out by Sri. Anoop T. R. under my supervision in the Department of Electronics Engineering, Model Engineering College, Kochi.. The results presented in this thesis or part of it have not been presented for the award of any other degree(s).

I further certify that the corrections and modifications suggested by the audience during pre-synopsis seminar recommended by the Doctoral committee of Mr. Anoop T. R. are incorporated in this thesis.

*Cochin-682 021*  
18-5-2016

Dr. Mini M. G.  
(Supervising Guide)



## **DECLARATION**

I hereby declare that the work presented in the thesis entitled “*Detection, Classification and Matching of Altered Fingerprints Using Ridge and Minutiae Features*” is a bonafide record of the research work done by me under supervision of Dr. Mini.M.G, Associate Professor, in the Department of Electronics Engineering, College of Engineering, Cherthala and Research Guide, Model engineering College, Thrikkakara, Kochi. The result presented in this thesis or parts of it have not been presented for other degree(s).

Cochin -21  
19<sup>th</sup> May 2016

Anoop T.R





# Acknowledgement

I would like to express my heartfelt gratitude to my research guide **Dr. Mini M. G.**, Associate Professor and Principal, College of Engineering, Cherthala, for her excellent guidance and support. With her constant enquiries, help and suggestions, she has been a great source of inspiration for me.

I sincerely thank **Prof. (Dr.) V. P. Devassia**, Principal, Model Engineering College, Thrikkakara, for extending the facilities in the college for the research work and for his valuable suggestions and encouraging words throughout the research.

I sincerely thank **Prof. (Dr.) N. Unnikrishnan**, Former Vice Chancellor of Cochin University of Science and Technology, for his valuable suggestions and encouraging words.

Let me express my sincere gratitude to **Dr. Jayasree V.K.**, Former Head, Department of Electronics, Model Engineering College, for her valuable suggestions and comments.

I sincerely thank **Dr. Vinu Thomas**, Associate Professor, Department of Electronics, Model Engineering College, for his valuable suggestions.

My sincere thank to Assistant Prof. **Jagadesh Kumar P**, for providing the lab facilities and his encouraging words throughout the research.

I thank all the research scholars of the department, especially Mrs. Simi Zerin Sleeba, Mrs. Neethu M. Sasi, Mrs. Rekha Lakshmanan and Mrs. Arya Devi P.S. for their friendly and supportive attitude.

My sincere thanks to all the faculty members, particularly, Dr. Laila D., Ms. Jiby John, Ms. Shiji T. P., Ms. Vineetha George, Associate Professors, Model Engineering College, for their support.

I also thank Ms. Aparna Devi P.S, Mr. Joseph George K.N, Mr. Bineesh T. and Mr. Rashid, Assistant Professors Model Engineering College, for their support and help.

I thank the non-teaching, library and administrative staff of the Model Engineering College for their cooperation and support.

I also take this opportunity to thank Mr. Jeevan K.M. and Mr. Deepak P., Department of Electronics, S.N.G.C.E. who have collaborated with me.

It is beyond words to express my gratitude to my wife Asha R.S., Sachu, my parents and brother Dr. Binu for their sacrifice and help. Without their cooperation, I am sure I could not have accomplished this task. I also thank my in-laws for their support and understanding.

Anoop T.R.

# Abstract

**Key Words:** Alteration, Detection, Classification, Hough Transform, Ridge endings, Orientation, Reconstruction, Wavelet transform, Matching, Region of Interest, Ridge frequency, Ridge texture.

This thesis presents a solution to prevent the attack of altered fingerprint on Automatic Fingerprint Identification systems (AFIS). Alteration also called obfuscation is the process of making the regular ridge structure irregular to mask the identity from a watch list of FP so that the criminals can easily enter into the restricted area. Different mechanical and chemical process used in alteration creates various patterns on the ridge structure. Subjective analysis of the ridge patterns and process leads to the classification of altered FP into three groups. They are obliteration, distortion and imitation. Obliteration of the FP is obtained by process like cutting and abrasion with blades or knives, burning and poring strong chemicals. Obliteration is again divided into scar and mutilation. Distortion type of altered FP is obtained by surgical ways. The interchanging of one portion of the fingertip with other portion of the same fingertip or with the palm or leg print leads to distortion type of altered FP. There is a special type of distortion known as 'Z' cut. The path of the surgical cut forms the alphabet Z. Imitation type of alteration is created by the replacement of large area of fingertip with other fingertip, palm print or leg print by plastic surgery.

The thesis covers detection, classification, reconstruction and matching of altered fingerprint. The first step to defeat altered fingerprint is alteration detection. A method is proposed for altered FP detection using three features viz. Minutiae Density, Ridge Discontinuity and Scars.

If the detected fingerprint is obliteration type, it needs to be matched with unaltered mates in the database. The matching of distortion and imitation type is impossible since the reconstruction of transplanted region is not possible. It also reduces the matching rate while increases the false match rate. This necessitates the classification of altered fingerprint. A Hough transform based method for classification of a given FP into normal FP and different types of altered fingerprint have been developed. This method uses variation of ridge ending density possessed by normal and different types of altered FP.

Wavelet transform approximation based method is proposed for the reconstruction of ridge orientation of altered fingerprints. An orthogonal wavelet is used to decompose the complex ridge orientation to a desired level. After decomposition, the orientation is reconstructed using the approximation coefficients.

After classifying the given fingerprint into obliteration, successful matching is essential since it helps to find the criminals and prevents the breaking of fingerprint based security system. Proposed method of matching uses the reconstructed ridge orientation and features in the unaltered region. Matching method is implemented in two stages. First stage utilizes the approximated ridge orientation. Second stages uses Ridge Texture and Ridge Frequency in the unaltered region of altered fingerprints. A matching is declared as successful, if genuine match occurs in both the stage.

# Contents

	<b>Page No.</b>
<i>Acknowledgements</i>	<i>ix</i>
<i>Abstract</i>	<i>xi</i>
<i>Contents</i>	<i>xiii</i>
<i>List of Figures</i>	<i>xix</i>
<i>List of Tables</i>	<i>xxv</i>
<i>Abbreviations</i>	<i>xxvii</i>
<b>CHAPTER 1</b>	
<b>INTRODUCTION</b>	<b>1</b>
1.1. History of Biometrics	4
1.2. General Biometrics Recognition System	5
1.3. Fingerprint Based Biometrics System	7
1.3.1. Fingerprint Scanning	8
1.3.2. Features of Fingerprint	9
1.4. Specifications of Fingerprint Images	12
1.5. Quality Assessment of Fingerprint Images	13
1.6. Objectives of Research	13
1.7. Motivation of the Research	14
1.7.1. Fingerprint Alteration Detection	14
1.7.2. Fingerprint Alteration Classification	15
1.7.3. Altered Fingerprint Matching	16
1.8. Database	16

	<b>Page No.</b>
1.9. Organization of the Thesis	17
<b>CHAPTER 2</b>	
<b>LITERATURE REVIEW</b>	<b>19</b>
2.1. Threats on Fingerprint based Biometrics System	21
2.2. History of Altered Fingerprints	24
2.3. Altered Fingerprint Detection	26
2.4. Orientation Field Estimation	28
2.5. Hough Transform	32
2.6. Fingerprint Matching	33
2.7. Fingerprint Image Enhancement	40
<b>CHAPTER 3</b>	
<b>THEORY OF FINGERPRINT IMAGE PROCESSING</b>	<b>43</b>
3.1. Fingerprint Image Preprocessing	45
3.1.1. Fingerprint Image Segmentation	45
3.1.2. Fingerprint Image Enhancement	46
3.2. Fingerprint Matching	47
3.3. Receiver Operating Characteristics Curve	49
3.4. Support Vector Machine	50
3.5. Hough Transforms	53
3.6. Introduction to Wavelet Transform	54
3.6.1. Multi Resolution Approximation	56
3.6.2. Continuous Wavelet Transform	59
3.6.3. Discrete Wavelet Transform	59

	<b>Page No.</b>
3.6.4. Discrete Wavelet Transform Computation	60
3.6.5. Two Dimensional Discrete Wavelet Transform (2D-DWT)	61
<b>CHAPTER 4</b>	
<b>ALTERED FINGERPRINT DETECTION</b>	<b>65</b>
4.1. Fingerprint Enhancement	67
4.2. Minutiae Density Extraction	68
4.2.1. Binarization	69
4.2.2. Thinning	69
4.3. Ridge Discontinuity Analysis	71
4.4. Analysis of Scar	73
4.4.1. Adaptive Average Filtering	73
4.4.2. Thresholding	74
4.5. Feature Extraction and Classification	75
4.6. Experiments and Results	76
4.7. Conclusion	79
<b>CHAPTER 5</b>	
<b>ALTERED FINGERPRINT CLASSIFICATION</b>	<b>81</b>
5.1. Introduction	83
5.1.1. Obliteration	83
5.1.2. Distortion	83
5.1.3. Imitation	84

	<b>Page No.</b>
5.2. Detection and Classification of Fingerprint Alteration	
by Hough Accumulator	86
5.2.1. Hough Accumulator Enhancement	89
5.3. Separation of Natural Scar from Altered Scar	94
5.4. Database	97
5.5. Results	98
5.5.1. Classification Based on Normal Hough	
Accumulator	98
5.5.2. Classification Based on Enhanced Hough	
Accumulator	100
5.5.3. Two Stage Classification	101
5.5.4. Classification of Scar	102
5.5.5. Comparison with state of the Art Algorithm	103
5.6. Conclusion	103

## **CHAPTER 6**

### **ORIENTATION FIELD RECONSTRUCTION 105**

6.1. Transformation of Orientation into Continuous	
Complex Function	107
6.2. Selection of Level of Decomposition	110
6.3. Comparison of Orthogonal Wavelets	113
6.4. Results	115
6.4.1. Reconstructed Orientation of Altered Fingerprints	115



	<b>Page No.</b>
6.4.2. Reconstructed Orientation of Synthetically Altered Fingerprints	116
6.4.3. Reconstructed Orientation of Low Quality Fingerprints	117
6.5. Conclusion	118
<b>CHAPTER 7</b>	
<b>ALTERED FINGERPRINT MATCHING</b>	<b>119</b>
7.1. Verification of Altered Fingerprint Detection	121
7.2. Proposed Method	122
7.3. Ridge orientation Based Matching	124
7.3.1. Orientation Based Matching Score	125
7.4. Selection of Region of Interest	126
7.5. Ridge Frequency Extraction	127
7.6. Matching Score Computation from ridge Frequency	129
7.7. Matching score Computation from Ridge Texture	130
7.8. Matching score Fusion	130
7.9. Results and Discussion	131
7.10. Conclusion	133
<b>CHAPTER 8</b>	
<b>CONCLUSION AND FUTURE SCOPE</b>	<b>135</b>
8.1. Conclusion	135
8.2. Future Scope	136

<i>References</i>	137
<i>Publications</i>	155
<i>Resume</i>	157
<i>Subject Index</i>	159

# List of Figures

	<b>Page No.</b>
Fig. 1.1 Enrollment process	5
Fig. 1.2 Verification system	6
Fig. 1.3 Identification system	6
Fig. 1.4 Block diagram of fingerprint scanner	8
Fig. 1.5 Different classes of fingerprint with core and delta marked	10
Fig. 1.6 Local ridge details	11
Fig. 2.1 Attacks at different levels of biometric recognition system	21
Fig. 2.2 Breaking of border control security system	24
Fig. 3.1 Fingerprint image with foreground and background regions marked	45
Fig. 3.2 Example of genuine and imposter distribution	48
Fig. 3.3 Basic ROC curve showing five discrete classifiers	50
Fig. 3.4 Linear two class problem	51
Fig. 3.5 Example of non linear classification	52
Fig 3.6(a) XY plane	53
Fig. 3.6(b) Parameter space	53
Fig. 3.6(c) Accumulator cell	53
Fig. 3.7 Illustration of Hough transform of normal representation of line	54
Fig. 3.8 (a) Time frequency representation of FT	55
Fig. 3.8 (b) Time frequency representation of STFT	55

	<b>Page No.</b>
Fig. 3.8 (c) Time frequency representation of WT	55
Fig. 3.9 Schematic of MRA decomposition	58
Fig. 4.1(a) Ridge ending	70
Fig. 4.1(b) Bifurcation	70
Fig. 4.2 (a) 3X3 window for ridge ending	70
Fig. 4.2 (b) 3X3 window for bifurcation	70
Fig. 4.3 (a) MD map of altered FP	71
Fig. 4.3 (b) MD map of normal FP	71
Fig. 4.4 (a) RD map of Obliteration	72
Fig. 4.4 (b) RD map of distortion	72
Fig. 4.4 (c) RD map of imitation	72
Fig. 4.4 (d) RD map of normal FP	72
Fig. 4.5(a) Dry FP	74
Fig. 4.5(b) Wet FP	74
Fig. 4.5(c) Normal FP	74
Fig. 4.6 Scar detected from obliteration type of altered FP	74
Fig. 4.7(a) Scar detected from distortion type of altered FP	75
Fig. 4.7(b) Scar detected from imitation type of altered FP	75
Fig. 4.8 ROC curve for altered FP detection	78
Fig. 5.1 (a) Mutilation	84
Fig. 5.1(b) Scar	84
Fig. 5.1(c) Z type distortion	84
Fig. 5.1(d) Imitation	84
Fig. 5.2(a) Variation of ridge ending density in normal FP	85

	<b>Page No.</b>
Fig. 5.2(b) Variation of ridge ending density in imitation	85
Fig. 5.2(c) Variation of ridge ending density in distortion	85
Fig. 5.2(d) Variation of ridge ending density in obliteration	85
Fig. 5.3(a) Collinear ridge end points detected by Hough transform in normal FP	87
Fig. 5.3(b) Collinear ridge end points detected by Hough transform in altered FP	87
Fig. 5.4(a) Variation of $H_{th1}$	89
Fig. 5.4(b) Variation of $H_{th2}$	89
Fig. 5.5 Mesh plot of Hough accumulator	90
Fig. 5.6(a) Mesh plot of Hough accumulator of normal FP before enhancement	92
Fig. 5.6(b) Mesh plot of Hough accumulator of normal FP after enhancement	92
Fig. 5.7(a) Mesh plot of Hough accumulator of altered FP before enhancement	92
Fig. 5.7(b) Mesh plot of Hough accumulator of altered FP after enhancement	92
Fig. 5.8 Variation of $R_{min}$ and $R_{max}$ of enhanced accumulator	93
Fig. 5.9 Classification algorithm	94
Fig. 5.10(a) Scar in normal fingerprint	95
Fig. 5.10(b) & (c) scar in altered fingerprints	95
Fig. 5.11(a) Normal FP with scar	95
Fig. 5.11(b) Altered FP with scar	95
Fig. 5.11(c) Line detected from ridge ending images of normal FP	95

	<b>Page No.</b>
Fig. 5.11(d) Line detected from ridge ending images of altered FP	95
Fig. 5.12 Classification of scar	96
Fig. 5.13(a) Obliteration type of synthetically altered FP	97
Fig. 5.13(b) Distortion type of synthetically altered FP	97
Fig. 5.14 Imitation type of synthetically altered FP	98
Fig. 6.1 Block diagram of proposed method	109
Fig. 6.2(a) Normal FP	110
Fig. 6.2(b) Altered FP	110
Fig. 6.3(a) $\sin^2(x,y)$ and $\cos^2(x,y)$ of normal FP	111
Fig. 6.3(b) $\sin^2(x,y)$ and $\cos^2(x,y)$ of altered FP	111
Fig. 6.4(a) R.O.D. map for decomposition level of 3	112
Fig. 6.4(b) R.O.D. map for decomposition level of 4	112
Fig. 6.4(c) R.O.D. map for decomposition level of 5	112
Fig. 6.4(d) R.O.D. map for decomposition level of 6	112
Fig. 6.4(e) R.O.D. map for decomposition level of 7	112
Fig. 6.4(f) R.O.D map for decomposition level of 8	112
Fig. 6.5(a) Orientation of unaltered mate $u_n(x,y)$	112
Fig. 6.5(b) Reconstructed orientation of altered mate at level 4	112
Fig. 6.5(c) Reconstructed orientation of altered mate at level 5	112
Fig. 6.5(d) Reconstructed orientation of altered mate at level 6	112
Fig. 6.5(e) Reconstructed orientation of altered mate at level 7	112
Fig. 6.5(f) Reconstructed orientation of altered mate at level 8	112
Fig. 6.6 (a) Altered FP	113
Fig. 6.6 (b) Orientation of altered FP	113
Fig. 6.6 (c) Orientation of unaltered mate	113

	<b>Page No.</b>
Fig. 6.7 ROD map of altered FP given in Fig. 6.6 (a) for db 5	114
Fig. 6.7 ROD map of altered FP given in Fig. 6.6 (a) for Sym 5	114
Fig. 6.7 ROD map of altered FP given in Fig. 6.6 (a) for Coif 5	114
Fig. 6.8(a) Reconstructed orientation of mutilation type of altered FP	115
Fig. 6.8(b) Reconstructed orientation of scar type of altered FP	115
Fig. 6.9 (a), (b) & (c) Synthetically altered FPs	116
Fig. 6.10 (a) ROF of altered FP in 6.9(a)	116
Fig. 6.10 (b) ROF of unaltered mate	116
Fig. 6.10 (c) Reconstructed ROF	116
Fig. 6.11 (a) ROF of altered FP in 6.9(b)	117
Fig. 6.11 (b) ROF of unaltered mate	117
Fig. 6.11 (c) Reconstructed ROF	117
Fig. 6.12 (a) ROF of altered FP in 6.9(c)	117
Fig. 6.12 (b) ROF of unaltered mate	117
Fig. 6.12 (c) Reconstructed ROF	117
Fig. 6.13 Reconstructed orientation of low quality FPs	118
Fig. 7.1 RD obtained by wavelet based approximation	121
Fig. 7.2 Block diagram of the proposed method	123
Fig. 7.3(a) Altered and its unaltered mate before alignment	124
Fig. 7.3(b) Altered and its unaltered mate after alignment	124
Fig. 7.4(a) Altered FP	126
Fig. 7.4(b) Segmented FP	126
Fig. 7.5(a) ROI marked as rectangle in synthetically altered FP	126

	<b>Page No.</b>
Fig. 7.5(b) ROI marked as rectangle in unaltered mate	126
Fig. 7.5(c)&(d) ROI marked as rectangle in unaltered FP in the database	126
Fig. 7.6 ROI selected from altered FPs	127
Fig. 7.7(a) 32X32 window is marked with rectangle	128
Fig. 7.7(b) 32X32 window with center $(x_i, y_j)$	128
Fig. 7.7(c) Rotated window with ridges points in the vertical direction	128
Fig. 7.8 x-signature	128
Fig. 7.9 (a) Fingerprint	129
Fig. 7.9 (b) Ridge frequency image	129
Fig. 7.10 ROC curve for the matching scores in first stage	131
Fig. 7.11 ROC curve for matching scores in second stage	132



# List of Tables

	<b>Page No.</b>
1.1. Comparison of general biometric traits	7
4.1. Detection of distortion type of alteration	76
4.2. Detection of imitation type of alteration	76
4.3. Detection of obliteration type of alteration	76
4.4. Result of detection in terms of TPR and FPR	77
4.5. Alteration detection by different combination of features	77
4.6. TPR and FPR for combination of features	78
4.7. Comparison of proposed method with existing method	78
5.1. Classification results on altered and normal FP using $H_{th1}$	99
5.2. Classification results using $H_{th1}$ in terms TPR and FPR	99
5.3. Classification results using $H_{th2}$	99
5.4. Classification result using $H_{th2}$ in terms TPR and FPR	100
5.5. Classification results on altered and normal FP using $R_{min}$	100
5.6. Classification results using $R_{min}$ in terms TPR and FPR	101
5.7. Altered FP Detection by $H_{th2}$	101
5.8. Classification results using $R_{min}$ in second stage	102
5.9. Classification results in second stage in terms of TPR and FPR	102
5.10. Classification results on altered and normal FP scar	103
5.11. Comparison results on altered detection	103
7.1. GAR and FAR for the thresholds 0.2213 and 0.0520	133
7.2. GAR and FAR for synthetically altered FP created from casia	133



# Abbreviations

2D-DWT	-	2 Dimensional Discrete Cosine Transform
A/D	-	Analog to Digital Converter
AFIS	-	Automatic Fingerprint Identification Systems
CCD	-	Charged Coupled Device
CDT	-	Constrained Delaunay Triangulation
CMOS	-	Complementary Metal Oxide Semiconductor
CWT	-	Continuous Wavelet Transform
db5	-	Daubichies 5
DCT	-	Discrete Cosine Transform
Dpi	-	Pixels Per Inch
DTMRA	-	Discrete Time Multi Resolution Analysis
DWT	-	Discrete Wavelet Transform
ECG	-	Electrocardiogram
EFS	-	Euclidian Distance Final Score
ERF	-	Euclidian distance for ridge frequency
ERM	-	Empirical Risk Minimization
ERT	-	Euclidian distance for ridge texture
FBI	-	Federal Burro of Investigation
FP	-	Fingerprint
FFT	-	Fast Fourier Transform
FAR	-	False Acceptance Rate
FMR	-	False Match Rate

FNR	-	False Negative Rate
FNMR		False Non-Match Rate
FPR	-	False Positive Rate
FRR	-	False Rejection Rate
FT	-	Fourier Transform
FVC	-	Fingerprint Verification Competition
GAR	-	Genuine Acceptance Rate
GHT	-	General Hough Transform
HT	-	Hough Transform
HtHT	-	Heteroscedastic Hough Transform
ID	-	Identity
IFFT	-	Inverse Fast Fourier Transform
LED	-	Light Emitting Diode
MD	-	Minutiae Density
MRA	-	Multi Resolution Analysis or Approximation
NIST	-	National Institute of Standards and Technology
NFIQ	-	NIST Fingerprint Image Quality
NFSM	-	Novel Fuzzy Similarity Measure
NN	-	Neural Networks
PCNN	-	Pulse Coupled Neural Network
PHT	-	Probabilistic Hough Transform
RD	-	Ridge Discontinuity
RF	-	Ridge Frequency
RHT	-	Randomized Hough Transform

RP	-	Reference Point
ROC	-	Receiver Operating Characteristic Curve
ROF	-	Ridge Orientation Field
ROD	-	Ridge Orientation Difference
RT	-	Ridge Texture
S	-	Scar
SIFT	-	Scale Invariant Feature Transform
SNR	-	Signal to Noise Ratio
SRM	-	Structural Risk Minimization
STFT	-	Short-Time Fourier Transform
SVM	-	Support Vector Machine
TNR	-	True Negative Rate
TPR	-	True Positive Rate
WT	-	Wavelet Transform
WSQ	-	Wavelet Scalar Quantization
sym5	-	Symlet 5









# Chapter 1

## Introduction

---

### **Abstract**

This chapter briefs about the general fingerprint based biometric systems including history of biometrics. A section is set aside for deliberations about different features of fingerprint including ridge and minutiae features. Chapter ends up with objectives, motivation, description about the database used and organization of the thesis.



Biometric recognition or biometrics is defined as the application of anatomical or behavioral identifiers or traits that are highly unique in nature for personal identification [1]. Examples for biometric traits are fingerprint (FP), iris, ear, face, facial thermo gram, hand thermo gram, hand vein, hand geometry, face, retina, signature and voice. The word biometrics is derived from Greek words bios (life) and metron (measurement). Biometric identifiers are measurements from living human body. Any biometric trait can be used for personal identification as long as it satisfies the following requirements [1]:

- Universality: Each person should have the particular biometric.
- Distinctiveness: The biometrics of any two persons should be sufficiently different.
- Permanence: Biometric should be invariant over a period of time.
- Collectability: Biometrics can be measured quantitatively.
- Performance: This includes speed, recognition accuracy, resource requirements and robustness to environmental and operational factors.
- Acceptability: Whether the user is willing to accept the trait in their daily life.
- Circumvention: Ease with which traits can be circumvented by fraudulent methods.

Main advantages of biometrics that makes it suitable for personal identification systems are

- It cannot be lost or forgotten
- Difficult to imitate,
- Unchanged with time
- Increased user convenience.

These advantages made the biometric systems to get increased attention compared to conventional security systems (examples; password, token, pin number) during recent decades. Biometric recognition systems have applications in border crossing,

national ID cards, e-passports, computer network logon, mobile phones, web access and smart cards.

## **1.1. History of Biometrics**

First systematic capture of hand geometry for identification purpose is recorded in 1858. Sir William Herschel, Civil Service of India, recorded a handprint on the back of a contract for each worker to distinguish employees. Use of biometrics for personal identification has come into existence in 1879 when Alphonse Bertillon, a French criminologist, introduced body measurements for the identification of criminals [2]. Bertillon's system of body measurements, consisting of skull diameter, arm and foot length was used in the United States of America to identify prisoners until the 1920s.

William Herschel was the first FP expert to point out that the ridge patterns in the fingertips of an individual remains unchanged from birth till death and Henry Faulds was the first person to identify FPs at the crime scenes to identify the criminal [3].

In 1892, Francis Galton identified that finger pattern is unique for each human being [4]. The characteristics of the FP used to identify the person are known as Galton details which are also referred to as minutiae features. Ophthalmologist Frank Burch first proposed the concept of using iris pattern for identification in 1936 [5].

Biometric systems were started to automated in 1960s with the developments in digital signal processing techniques. Voice and FP based personal recognition systems were automated in 1960s. Development of hand geometry systems took place in 1970s, retinal, signature and face verification systems came in 1980s and iris recognition systems were developed in 1990s [6].

## 1.2. General Biometric Recognition System

A biometric system is essentially a pattern recognition system that operates by acquiring biometric data from an individual, extracting a feature set from the acquired data, and comparing this feature set against the template set in the database [7]. A generic biometric system basically consists of four modules [8]. They are

- (a) Scanner module: Acquires biometric data of an individual.
- (b) Feature extraction module: Process the acquired data to extract a feature set to represent biometric trait.
- (c) Matching module: The extracted feature set is compared against the templates residing in the database through the generation of matching scores.
- (d) Decision making module: Matching scores are used to either validate the user's claimed identity or determine his/her identity.

Depending on the application context, a biometric system may operate either in verification mode or identification mode [7]. Enrollment is a process of making a database of template and is common to both verification and identification system. This is shown in Fig. 1.1. An enrollment system consists of scanner to capture the FP image, a quality checker and a feature extractor. This process is usually carried under the supervision of a trained person with an aim to maintain the quality of the FP image used for making the template.

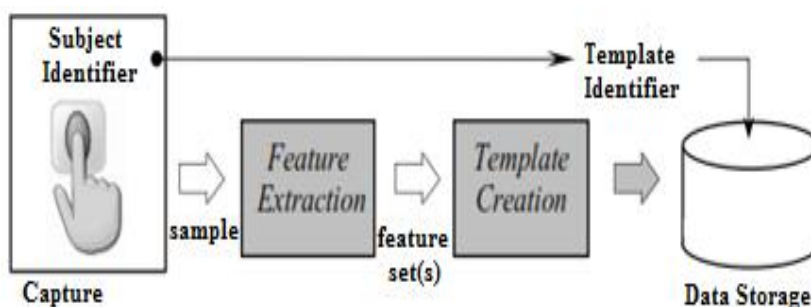


Fig. 1.1 Enrollment process

A verification system authenticates a person's identity by comparing captured biometric trait with his/her previously captured (enrolled) biometric reference template pre-stored in the system. An individual who wants to be recognized claims an identity; usually personal identification number, a user name or smartcard. Then it performs one to one comparison to either reject or accept the submitted claim of identity. Fig. 1.2 shows the block diagram of a verification system.

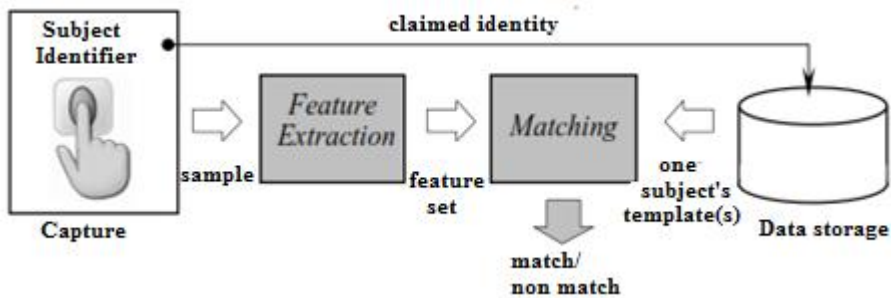


Fig. 1.2 Verification System

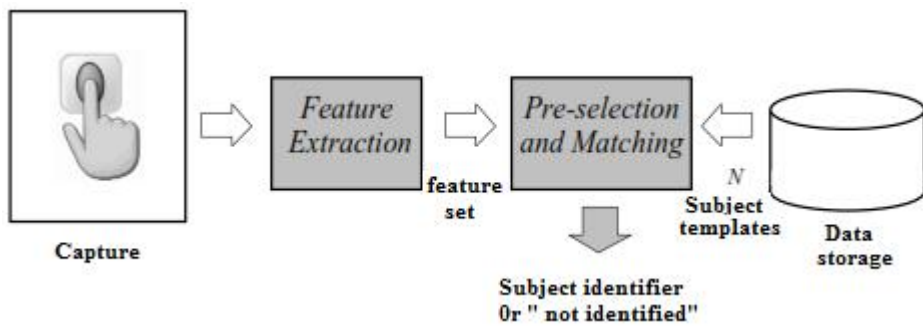


Fig. 1.3 Identification System

An identification system recognizes an individual by searching the entire enrollment template database for a match without claims for identity. It conducts one-to-many comparisons to establish if the individual is present in the database and if so, returns the identifier of the enrollment reference that matched. Fig. 1.3 shows the block diagram of an identification system. Depending upon area of application,

a biometric system can operate either as an online system or as an off line system. An online system requires quick response and is fully automatic. Offline system does not require quick response and is semi automatic. No single trait is expected to effectively meet the requirements of all the applications. The selection of biometric trait for a particular application depends upon the characteristics of the application and the properties of the trait [1].

### 1.3. FP Based Biometric Systems

A comparison of widely used biometric identifiers is given in Table 1.1. Entries in the table as given in second edition of Hand book of FP recognition [1]. The letters H, M and L denotes High, Medium and Low respectively. Table shows that FPs have very good balance between properties as compared to other biometrics.

Table 1.1 Comparison of general biometric traits

Biometric identifier	Universality	Distinctivene	Permanence	Collectability	Performance	Acceptability	Circumventi
Face	H	L	M	H	L	H	H
FP	M	H	H	M	H	M	M
Hand Geometry	M	M	M	H	M	M	M
Hand/Finger vein	M	M	M	M	M	M	L
Iris	H	H	H	M	H	L	L
Signature	L	L	L	H	L	H	H
Voice	M	L	L	M	L	H	H

All humans have FP that are distinctive from others. Their details are permanent, even if they temporarily change slightly due to cuts and bruises on the skin. FP

recognition has become one of the most matured biometric as far as technologies are concerned. It has wide use in forensic sciences to identify the criminals. Forensic experts use the latent FP obtained from the crime scenes and makes the match with a watch list of FP. FP scanners are small in size and can get with affordable prices. These reasons make FP one of the most widely used biometric traits in the world.

### 1.3.1. FP Scanning

FP scanning plays a very important role in FP recognition since the success of matching depends upon the quality of the image captured by the sensor. A basic block diagram of a FP scanner is shown in Fig. 1.4. It consists of a sensor that reads the ridge pattern on the finger surface, A/D (Analog to Digital) converter to convert the analog reading to the digital form, and interface module for communicating (sending images, receiving commands, etc.) with external devices such as personal computers [1].

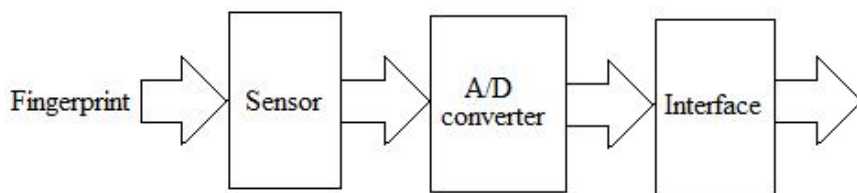


Fig. 1.4 Block diagram of a FP scanner

FP scanning is of 2 types, off-line acquisition and online acquisition [1]. In the former case, the finger is first smeared with a black ink and pressed or rolled on a paper card. Then this paper card is scanned by using a general purpose scanner to obtain the digital image. This technology was used by law enforcement agencies and has rare use today. In latter, the digital images are obtained by pressing the finger against the flat surface of an electronic FP sensor or FP reader. Nowadays,



most of the Automatic FP Identification Systems (AFIS) uses online acquisition technology also known as live scanning. This technology does not require ink to scan the FP. There are three families of electronic FP sensors based on different sensing technology [1]. They are

- **Solid state or silicon sensors:** These consist of an array of pixels, each pixel being a sensor itself. Users place the finger on the surface of the silicon, and four techniques are typically used to convert the ridge/valley information into an electrical signal: capacitive, thermal, electric field and piezoelectric.
- **Optical sensors:** The finger touches a glass prism and the prism is illuminated with diffused light. The light is reflected at the valleys and absorbed at the ridges. The reflected light is focused onto a CCD or CMOS sensor. Optical FP sensors provide good image quality and large sensing area but they cannot be miniaturized because as the distance between the prism and the image sensor is reduced, more optical distortion is introduced in the acquired image.
- **Ultrasound:** Acoustic signals are sent, capturing the echo signals that are reflected at the FP surface. Acoustic signals are able to cross dirt and oil that may be present in the finger, thus giving good quality images. On the other hand, ultrasound scanners are large and expensive, and take some seconds to acquire an image.

### **1.3.2. Features of FP**

The overall area of FP image captured by scanner contains foreground and background region. Foreground region is a pattern of ridges and furrows or valleys and possess the important features needed for matching. The background area has to be segmented off from the image and does not contain any information. The

features possessed by FP image are categorized into three levels [1]; level 1, level 2 and level 3 features.

Level 1 Features also known as global ridge pattern shows macro details of ridge flow. These features are a pattern of alternating convex skin called ridges and concave skin called valleys with spiral curve like line shape. There are two types of ridge flows: the pseudo-parallel ridge flows and high-curvature ridge flows located around the singular point [1]. This representation relies on the ridge structure, global landmarks and ridge pattern characteristics. The commonly used global or level 1 FP features are:

- Singular points: There are two types of singular points known as core and delta. A core is the uppermost point of the innermost curving ridge [1]. Delta is the junction point where three ridge flows meet. Both core and delta are shown in Fig. 1.5. They are usually used for FP registration and FP classification. According to the ridge flow around singular points and number of singular points, FP is classified into 6 classes. They are Right loop(R), Left loop(L), Whorl(W), Arch(A) and Tented Arch(T).(see Fig. 1.5)

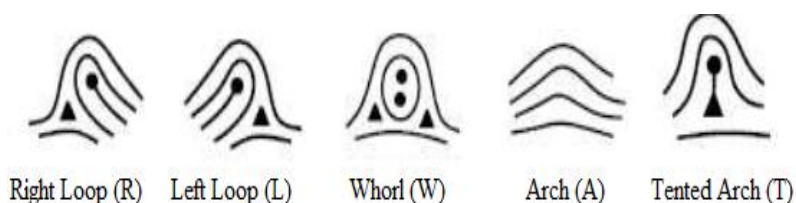


Fig. 1.5 Different classes of FP with core and delta marked.

- Ridge orientation Field: It gives the local direction of ridge-valley flow. It is widely used for classification, image enhancement, matching, minutiae feature verification and filtering [1].
- Ridge Frequency: The local ridge frequency (or density)  $f_{xy}$  at point  $[x, y]$  is the number of ridges per unit length along a hypothetical segment centered

at  $[x, y]$  and orthogonal to the local ridge orientation [1]. A frequency image  $\mathbf{F}$  can be defined if the frequency is estimated at discrete positions and arranged into a matrix.

Level 2 or local ridge details are the discontinuities of local ridge structure also known as minutiae. Most widely used minutiae features for matching are ridge ending and ridge bifurcation. The main reason that minutiae features are preferred is because they are relatively stable and robust to contrast, image resolutions, and global distortion when compared to other representations. They are also used for FP synthesis and reconstruction [10], [11]. There are 150 types of minutiae classified based on their configuration [9]. Some of the minutiae details are shown in 1.6. Extraction of ridge ending and bifurcation from low quality FP image is a difficult task since dryness and wetness causes spurious minutiae.

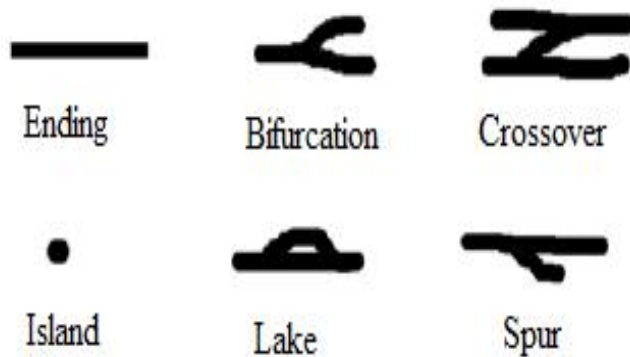


Fig. 1.6 Local ridge details

Level 3 features or inter-ridge details occur at very fine level. These consist of width, shape, curvature, edge contours of ridges, dots and incipient ridges. Other fine level detail is sweat pores and its position and shapes are highly distinctive. Extraction of sweat pores is possible only at high resolution (above 1000 dpi).

## 1.4. Specifications of FP Images

FP consists of pattern of ridges and valleys. The FP scanner converts this pattern into digital representation known as FP image. The quality of the FP image is affected by different parameters. These parameters are known as the specifications of the FP image as listed below; [1].

- **Resolution:** It denotes the number of dots or pixels per inch (dpi).
- **Area:** It represents the size of the rectangular area captured by FP scanner. For multi-finger scanners the area is usually as large as 2x3 square inches to allow four fingers to be placed simultaneously. In case of single-finger scanners, an area greater than or equal to 1x1 square inches permits a full plain FP impression to be acquired.
- **Number of Pixels:** This is obtained by multiplying the area of the image with resolution.
- **Geometric Accuracy:** It depends upon the geometric distortion produced by acquisition device.
- **Gray level quantization and gray range:** The gray-level quantization is defined as the maximum number of gray-levels in the output image and is related to the number of bits used to encode the intensity value of each pixel. The gray-range is the actual number of gray-levels used in an image disregarding the maximum given by the gray-level quantization.
- **Gray level uniformity and input/output linearity:** The gray level uniformity is defined as the gray-level homogeneity measured in the image obtained by scanning a uniform dark (or light) gray patch; the Input/Output linearity quantifies the deviation of the gray levels from a linear mapping when the input pattern is transformed into an output image.
- **Spatial frequency response:** denotes the ability of an acquisition device to transfer the details of the original pattern to the output image for different frequencies.

- **Signal-to-noise ratio (SNR):** the signal to noise ratio quantifies the magnitude of the noise with respect to the magnitude of the signal. The signal magnitude is related to the gray-range in the output image while the noise can be defined as the standard deviation of the gray-levels in uniform gray patches.

## **1.5. Quality Assessment of FP Images**

Successful matching of every FP based recognition system depends upon the quality of the FP image since the feature extraction stage fails in the low quality images. In general, FP quality can be estimated at a global level (i.e., a single quality value is derived for the whole image) or at a local level (i.e., a distinct value is estimated for each block/pixel of the image). Quality assessment of FP images are important in order to

- Reject very low-quality samples during enrollment or/and to select the best sample(s).
- Isolate unrecoverable regions where FP enhancement is counterproductive as it leads to the detection of several spurious features.
- Adapt the matching strategy to the quality of FPs.
- Assign weights to features (at matching stage) according to the quality.

FP alteration degrades the quality of the FP image and thus the alteration detection is a part of quality assessment.

## **1.6. Objectives of Research**

The countermeasures to defeat altered FP threats are detection, classification and matching. Detection is first step needed against the altered FP threats. Once the

altered FP is detected, it has to be matched with unaltered mates available in the database to find criminals who have altered the FP. In order to match the altered FP successfully, classification of altered FP has to be performed. This is due to the fact that altered FP consists of transplanted region and this increase the rate of false matching.

## **1.7. Motivation of Research**

FP is one of the most successful and matured biometric trait for the personal identification all over the world. Due to this, threats to AFIS are also increasing. FP alteration is one among them especially in border control security systems [12],[13]. The increased use of AFIS in immigration control and forensic application motivated the illegal immigrants and criminals to alter the FP for masking their identity. A number of websites are available in the internet that discusses the different ways of alteration of the FP. Cases related to altered FP is also reported all over the world. The above facts motivated to find a solution to defeat this problem.

The development of the methods or algorithms for alteration detection, classification and matching is also motivated by different reasons explained in following subsections.

### **1.7.1. FP Alteration Detection**

The quality assessment software is not able to detect the altered FP, if the quality of the FP is good. It is reported in [12] and [13] that the NFIQ quality assessment software developed by National Institute of Standards and Technology (NIST) has been able to detect only 20% altered FPs.

Alteration is the process of making the regular ridge structure irregular in order to mask the identity from a watch list of FP so that the criminals can easily enter into the restricted area. The breaking of the security system can be prevented by employing a detection method along with AFIS.

Surgical cuts along the boundary of the altered region lead to scar and give important information about the alteration. This research aimed to include this surgical scar present in the altered region to improve the detection rate of existing alteration detection methods.

### **1.7.2. FP Alteration Classification**

Researchers have subjectively classified the altered FPs into three. They are obliteration, distortion, and imitation [12],[13].

Classification of alteration is important in the sense that it provides strong evidence against the criminals. For example, distortion and imitation type of alteration are produced by surgical means and once classified the given FP into distortion or imitation type, more evidence against the criminals can be obtained through identifying the doctor who had done the surgery [14].

Another advantage of alteration classification is that it can give important clue about whether the given FP is possible to reconstruct or not. Obliteration type of altered FP can be reconstructed, if the altered area is small. Distortion and imitation type of altered FP seems not possible to reconstruct since the surgery causes transplantation of ridge structure. The reconstruction of Z cut type of distortion may be possible. The manual classification of imitated and distorted FPs is sometimes very difficult even for an expert since the transplanted region resembles the normal FPs.

Automatic altered FP classification also helps the altered FP matching. Matching of distortion type of altered FP except 'z' type and imitation type are not possible since the altered region consists of transplanted ridge structure. Automatic classification can help to prevent the imitation and distortion type of FP from going into the matching stage and can reduce the false matching rate caused by transplanted region.

### **1.7.3. Altered FP Matching**

Successful matching of altered FP is essential since it helps the authority for the identification of the criminals or to get the information about the criminals. Matching of imitation type altered FP is not possible since reconstruction of altered region is not possible. Separation of unaltered region from the altered region is also difficult. Matching of Z-type distortion is possible because altered region can be reconstructed. Matching of obliteration is possible if the whole region of the FP is not altered.

## **1.8. Database**

Database used for this thesis work consists of 70 real altered FPs which consist of all types of alterations obtained from NIST SD14. Synthetically altered FP of 240 images with 80 each of obliteration, distortion and imitation is also used. Normal FP obtained from FVC 2000, 2002, 2004 and CASIA is used for the creation of synthetically altered FP and also for the conduct of the experiments.

Altered FP is synthetically created as follows. Obliteration type of altered FP is generated by making scratches and scars in the FPs. Synthetic distortion is made by transplantation of one region of the normal FP with other region of the same FP.



Scar is also created through the boundary of the transplanted region. Special type of distortion known as ‘Z’ cut is formed by selecting a square section, cutting it into two triangles, stretching it and joining back to the FP. After performing these steps, scars are created through the joints of the altered region. Imitation type is made by transplanting large area of the FP with other FPs.

## **1.9. Organization of Thesis**

Chapter 2 gives the literature review on different cases related to altered FP. Literature review on altered FP detection, ridge orientation estimation and matching of FP is also given in this chapter.

Chapter 3 discusses the theory of FP image processing, Receiver Operating Characteristics (ROC) curve, theory of Support vector Machines, Hough transform and wavelet transform.

Chapter 4 discusses the altered FP detection using three features namely ridge discontinuity, minutiae density and scar. Comparison of the proposed method with the state of the art method is also given.

Chapter 5 deals with Hough transform based FP alteration detection and classification. This method uses ridge ending density variation present in different types of altered FP.

Chapter 6 explains a method proposed for ridge orientation reconstruction of altered FP. This method uses orthogonal wavelets as a basis function for the reconstruction of orientation. Comparison of this method with polynomial based method is also given.

Chapter 7 gives a two stage method for altered FP matching. First stage is based on reconstructed ridge orientation and if the matching is successful, the FP goes to the second stage. Second stage uses ridge frequency and ridge texture in the unaltered region of the altered FP.

Chapter 8 gives conclusion and future works.

# Chapter 2

## Literature Review

---

### **Abstract**

This chapter starts with the discussion of different threats faced by the FP based biometric system. It discusses the fake and altered FP threats occurred at the sensor level and the cases related to altered FPs threats reported in press. Literature review on altered FP detection methods and ridge orientation estimation methods are also given. Chapter ends with the literature review on different methods developed for FP matching and FP image enhancement.



## 2.1. Threats on FP Biometric Systems

The researchers have pointed out different vulnerabilities or threats faced by FP based biometric systems. They also suggested different remedies to reduce these threats to a great extent. Ratha et.al identified eight attacks faced by the generic biometric systems with respect to different vulnerable points in the systems [15]. They are occurring at sensor, matcher, feature extraction module, database, in between these modules and at final decision level. These attacks are shown in Fig. 2.1. Attacks at sensor level include forcibly compelling a registered user to verify/identify, presenting a registered deceased person or dismembered body part, using a genetic clone, and introduction of fake biometric samples or spoofing [16]. Spoof is defined as any counterfeit biometric that is not obtained from live person.

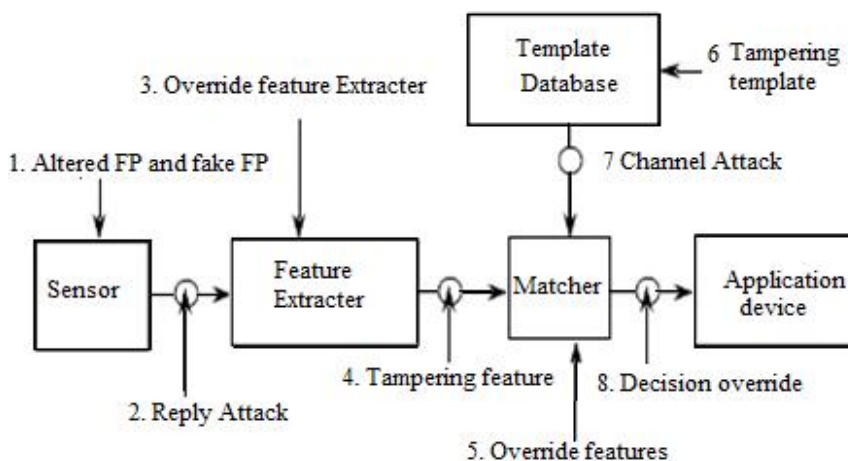


Fig. 2.1 Attacks at different levels of Biometric recognition system

Most of the methods used for fake FP detection are based on the design of hardware to measure overt characteristics of live fingers which are not present in the fake FPs [17-21].

Osten et. al. have used a combination of pulse oximetry, electrocardiography (ECG), and a temperature sensor to measure liveliness [17]. A CCD camera is used for the FP identification/verification, and the skin temperature, pulse and oxygen saturation of hemoglobin in the arterial blood, are used for a liveness measurement.

Two Light Emitting Diodes (LEDs) and a photo-detector are used to determine whether blood is flowing through the finger in [18]. This liveness detection method basically implements pulse oximetry, but only uses the pulse rate information.

A FP sensor that reduces the spoofing is given in [19]. This FP sensor includes an array of impedance sensing elements for generating signals related to an object positioned adjacent thereto. It also includes spoof reducing circuit for determining whether or not the impedance of the object positioned adjacent the array of impedance sensing elements corresponds to a live finger. A spoofing indicated may be used to block further processing.

A hardware based solution that uses temperature of the finger, electrical conductivity of the skin and pulse oximetry is proposed in [20].

Baldisserra.et.al have developed a method for fake FP detection based on the acquisition of the odor by means of an electronic nose, and differentiating the human skin from other material [21]. Even though this method is able to detect artificial reproductions, creation of a single model of human skin for each user is necessary.

Some of the techniques used the fusion of biometric traits to avoid the spoofing of identification systems [22-25]. Biometric fusion is the concept of using features from more than one biometric trait for personal identification. Biometric fusion involving FPs can be performed in one of the following manners

1. Multiple traits: FPs can be combined with some other trait such as iris or face.
2. Multiple fingers of the same person: FPs from two or more fingers of a person may be combined.
3. Multiple samples of the same finger acquired using different sensors: information obtained from different sensing technologies for the same finger is combined.
4. Multiple samples of the same finger: multiple impressions of the same finger are combined.
5. Multiple representations and matching algorithms: this involves combining different approaches to feature extraction and/or matching of FPs.

The disadvantages of fusion is that it is expensive and less user convenient since it needs more sensors which in turn cause the user to present their traits on more than one sensor. It is also difficult to select the features needed to combine together for fusion scheme.

Heeseung Choi .et. al used multiple static features including power spectrum, histogram, directional contrast, ridge thickness, and ridge signal to detect fake FPs [26].

Altered FP falls under the broader category of attack known as obfuscation [12]. Any deliberate attempt by an attacker to change his biometric characteristic in order to avoid detection by a biometric system is called obfuscation. The similarity between spoofing and obfuscation is that both occur at the sensor or user interface level. The difference is that spoofing is for positive recognition and obfuscation is for negative recognition (hiding the identity).

## 2.2. History of Altered FPs

FP alteration has been used by illegal immigrants to break the border control security system. Fig. 2.2 shows the breaking of the border control security system by using the altered FP. The border control security has a watch list of criminals. When the automatic Personal Identification System makes a matching of the altered FP of the illegal immigrants with their unaltered mates in the watch list, the result is non match. Thus the illegal immigrant is permitted to cross the border and enter into the country. Different criminal cases related to altered fingerprints are reported in press.

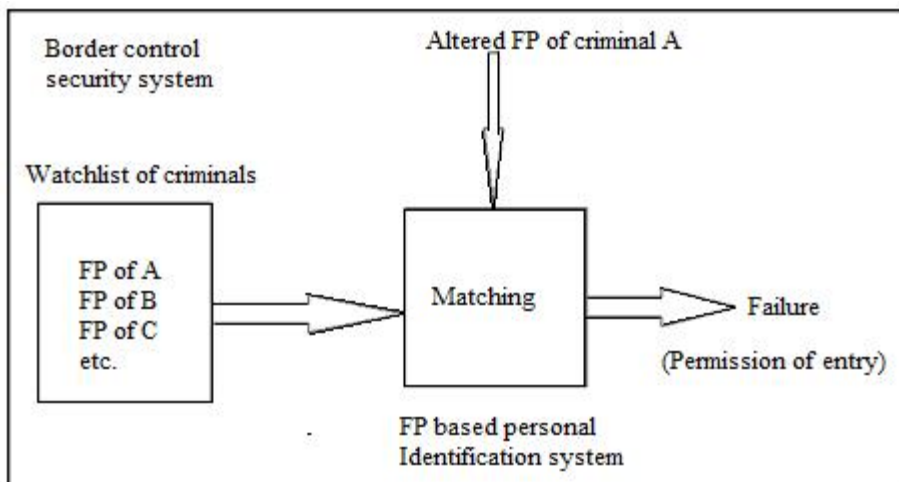


Fig. 2.2 Breaking of Border control Security System

The first case of altered FP has been reported way back in 1933[27]. John Dillinger, a notorious criminal in American history, altered his face by plastic surgery with the help of a doctor. Dillinger underwent several bouts of plastic surgery and he only managed to slightly alter his face. After this, one doctor suggested him to alter the FP as a way to escape being detected. By comparing the FP recorded before and after Dillinger's death, investigation agency found that all



the fingertips were altered. He altered the central portion of the ridge pattern by applying acid to fingertips. Even after this alteration the investigation agency successfully identified him after his death in 1934 by using the details in the undamaged portions of the fingertips.

Gus Winkler [27], another criminal, got the idea of FP alteration from an accidental damage occurred to his finger. Later he altered four fingers on the left hand excluding the thumb, by the combination of slashing and deep abrasion. His left middle finger is found to be converted from whorl class to loop class.

Jack Clutas altered index and ring finger of the right hand to evade identification [27]. After realizing the uselessness of first attempt, he made deep damage to fingertip with an aim of successful masking of his identity.

Dr. Howard L. Updegraff, had extensive experience in the area of FP alterations and he reported that the only way to permanently obliterate a FP is to graft skin from another part of the body over them [28]. In 1941, Robert Phillips attempted to alter the finger by grafting the skin from his chest to the fingertip [28].

Donald Roquierre altered the fingerprints by making circles in the middle of each finger, turned the circles upside down and replaced them on different fingers [29]

Jose Izequierdo altered the finger by exchanging two portion of the fingertip. After the alteration, the portions seems to be like 'z' shape. The officials reconstructed the fingertip manually for the identification purpose and they have taken 170 hours for manual and computer search to identify the person [30].

In 2007 a Mexican doctor was charged in Pennsylvania with surgically removing drug traffickers FP, substituting skin from the soles of their feet [14].

A Dominican doctor Jose Elias Zaiter-Pou had been jailed for a year and a day for plotting to surgically alter FPs of illegal immigrants [14].

In 2009, Lin Rong, a Chinese women illegally entered into Japan by having plastic surgery to alter her FPs [31]. She swapped the FPs from her right and left hands to evade the border control security systems. She removed the skin patches from the thumb and index fingers and re-grafted on to the fingers of the opposite hand.

Mateo Cruz-Cruz, a 25 year old man from Mexico got arrested by Border Patrol agents in Douglas, Arizona for allegedly jumping the fence from Mexico [32]. After his arrest, it is found that his fingers were blackened and burned. Many Other cases of evading border control security systems are reported in [33], [34].

### **2.3. Altered FP Detection**

Even though the cases regarding the altered FP are reported early in 1933, the researchers have started to focus this area only from 2009 onwards. Hence the work related to altered FP detection is limited in number.

Jianjiang Feng, Anil K. Jain and Arun Ross developed a method for FP alteration detection based on orientation field [12]. They considered distorted type of altered FP for this study. Orientation field of a FP can be decomposed into two components namely singular orientation field and continuous orientation field. Orientation field around the singular point or singular orientation in normal FP is discontinuous since it posses more curved nature as compared to that of other regions. Continuous orientation field of altered FP is not continuous and that of normal FP is continuous. They have used the discontinuity in the continuous orientation filed to detect the altered FP. High level features are extracted from the continuous orientation filed and feature vectors are created. These feature vectors are fed into the Support Vector Machine (SVM) for classifying the given FP into

normal or altered. They have simulated synthetically altered FPs from the normal FPs obtained from NIST SD14 database. This method is tested on this database and detected 92% of altered FP with a false positive rate of 7%.

Soweon Yoon, Jianjiang Feng and Anil K. Jain have developed another method for FP alteration detection based on orientation field discontinuity and minutiae density map [13]. Orientation field discontinuity is found by comparing the least square polynomial approximated ridge orientation of altered FP with its original orientation. Minutiae density map is obtained by Parzen window method with uniform kernel function. Feature vector are formed from the orientation field discontinuity and minutiae density map. These feature vectors are fused together and fed to SVM for classification. This algorithm achieves a True Positive Rate (TPR) of 70.2% with a False Positive Rate (FPR) of 2.1% while NFIQ achieves a FPR of 31.6%.

A method proposed by Adina.et.al based on Scale Invariant Feature Transform (SIFT) key points are given in [35] and these key points in a FP is represented by an orientation and magnitude. After finding an initial estimate of SIFT key points, they are refined to get a reduced set of key points. The normal FP consists of low density of SIFT key points located only at singular points and altered FP consists of large density of key points located at altered region. This feature is utilized for detection of altered FP.

Adina.et.al proposed another method based on orientation field reliability map [36], which has peaks at singular point locations. Alteration detection is based on the fact that altered FP s have many peaks as singular points with lower amplitude while normal FP has few peaks as singular points with higher amplitudes.

John H Ellingsgaard proposed a method based on singular point density and minutiae orientation analysis to detect altered FP [37]. Singular point density

analysis is based on local entropy and uncertainty of orientations around scarred and mutilated areas and uses common techniques to extract core features of a fingerprint.

## **2.4. Orientation Field Estimation**

Ridge orientation field is an important feature of FP that distinguishes it from other biometric traits. It is considered to be one of the important intermediate step in most of the FP image processing like enhancement, classification and matching [38-46]. Other main use of ridge orientation field is in the area of FP synthesis and reconstruction [47], [48], [49]. In case of altered FP, reconstructed orientation can be used for matching and reconstruction of altered region. It can also be used to extract ridge discontinuity which in turn can be used to detect altered FP.

Determination of Ridge orientation field is classified into two categories, local estimation and global modeling. In the former, the orientation is obtained for each pixel of the image and in the latter, the orientation for whole image is obtained by mathematical modeling. Most widely used local estimation is the gradient-based method. In this, the gradient at each pixel of the image, both in x and y direction, is found. Then the orientation is the direction perpendicular to the gradient. Local estimation fails in poor quality and noisy regions of the FP image.

Jain et al. performed the approximation of the ridge orientation of altered FP to find orientation field discontinuity for the detection of altered FP [13]. They decomposed the sine and cosine of doubled orientation using 6<sup>th</sup> degree two variable polynomial and reconstructed by least square approximation.

Sherlock and Monro developed an orientation model named zero-pole model by considering image plane as a complex plane with the core point as zero and delta

point as pole[50]. To find out orientation at a point, this method needs the distance with respect to singular points and the number of singular points.

Soweon Yoon and Anil K. Jain have developed another method for ridge orientation modeling of altered F in terms of ordinary differential equations which does not require any prior information such as singular points of a fingerprint [51]. They considered the doubled orientation as a vector field since it can be represented using ordinary differential equation. They first converted rational polynomial model proposed by Sherlock in [50] into an ordinary differential equation. Then constrains on the number of singular points are applied to estimate the model parameters. Finally difference between the approximated ridge orientation and original orientation is used to differentiate normal FP images from non-FP images and altered FPs.

Vizcaya and Gerhardt improved the zero pole model using a piecewise linear approximation model around singular points [52]. First, the neighborhood of each singular point is uniformly divided into eight regions and the influence of the singular point is assumed to change linearly in each region. An optimization implemented by gradient-descend is then carried on to get piecewise linear function.

A combinational model for orientation field estimation is presented in [53]. This consists of polynomial model for global orientation and point charge model to correct the orientation near singular region. Since orientation of FP is quite smooth and continuous except at singular points, they applied a polynomial model to approximate the global orientation field. At each singular point, a point-charge model similar with zero-pole model is used to describe the local region. Then, these two models are combined smoothly together through a weight function.

An orientation model for the entire FP orientation using high order phase portrait is developed in [54]. A low-order phase portrait near each of the singular

point is added as constraint to the high-order phase portrait to provide accurate orientation modeling for the entire FP image. The main advantage of the proposed approach is that the nonlinear model itself is able to model all type of FP orientations completely.

S.Ram used Legendre polynomial as a basis function for ridge orientation modeling and showed that singular points can be modeled by zero-poles of Legendre polynomial [55]. A two stage optimization procedure is used to find out the model parameters. This method requires 56 coefficients to represent the orientation field.

Wang presented an orientation estimation method using trigonometric polynomials that does not require any prior knowledge of singular points [56]. Phase doubled vector field of the ridge orientation is decomposed using trigonometric Fourier series. After the parameter optimization process, the coefficients of the trigonometric terms are found by Least Square method. These coefficients are used to model the ridge orientation field.

Huckemann et al. used a quadratic differential model that assumes actual location and type of the singular points of a FP [57].

In [58], Dass developed a Bayesian framework using the Markov random field model. This model needs the updating of ridge properties to find the orientation field around all over the FP and around the singular points. This model is class dependent.

Principal component analysis is used to estimate the ridge orientation field in [59]. A low pass filtering is applied to reduce the noise in the image but this cause the loss of information around singular points since frequency near these point is high.

Ridge orientation estimation using adaptive Gaussian filter is proposed in [60]. It computes orientation at two scales and the results are combined to estimate the orientation. Small scale defined by  $s = 5$  is used around the singular region and large scale  $s$  defined by  $s = 20$  is used around the scratches. This method gives better results compared to method based on principle component analysis.

An improved version of gradient based method known as enhanced gradient method is proposed by Wang in [61]. In this method, the image is divided into different blocks with each block consisting of  $8 \times 8$  pixels, and  $3 \times 3$  cells of such blocks are taken. The orientation of the centre block is obtained by averaging the orientations of the neighborhood blocks. This method also fails in high noisy regions.

The method proposed in [62] uses a neural network to select the correct orientation out of a number of orientation from a region of the FP. This neural network is trained in such a way that it responds to correct orientation with large value and to false orientation with low value.

A Constrained Delaunay Triangulation (CDT) based orientation field interpolation method is proposed in [63]. In this method, the orientation coherence is used to segment an image into foreground and background, valid regions and invalid regions, and the contours of the invalid regions are used to construct the CDT that is used to interpolate the orientations of the invalid regions. This method does not need pre-defined neighborhood and iteration.

Luping Ji and Zhang Yi proposed a method for estimating four-direction orientation field [64]. It consists of four steps: (i) preprocessing fingerprint image, (ii) determining the primary ridge of fingerprint block using neuron pulses of pulse coupled neural network (PCNN), (iii) estimating block direction by projective

distance variance of such a ridge, instead of a full block and (iv) correcting the estimated orientation field.

## **2.5. Hough Transform**

Hough transform was initially used for the detection of lines from the digital images. Later on this transform is generalized to detect other shapes such as circles, ellipse etc. Hough transform fails to correctly detect the lines from low quality or noisy image since Hough accumulator consists of a number of peaks and finding the exact peak is difficult. This section gives the peak isolation or Hough Accumulator enhancement using different strategies. Probabilistic Hough Transform (PHT) proposed by Kiryati et al is based on voting scheme in which only a subset of points 'm' out of 'M' edge points are used so that the complexity is reduced [65]. Smaller value of m can increase the speed of the algorithm but the accuracy gets reduced.

PHT depends upon the poll size and most of algorithm has fixed poll size and termination of the voting is not adaptive. Shaked et al. made the termination of the voting adaptive to increase the accuracy of the PHT [66].

Normal HT have some shortcomings such as computational cost, low detection accuracy, vulnerability to noise and possibility of missing objects. Randomized Hough Transform (RHT) aims to resolve these issues with random sampling in place of pixel scanning, converging mapping in place of diverging mapping and dynamic storage in place of accumulation storage.[67], [68].

The method given in [69] proposed HT based line recognition method, that utilizes both the HT parameter space and the image space. This method is able to detect the thickness of the line. This method uses an image-based gradient prediction to accelerate the accumulation, introduces a boundary recorder to eliminate redundant analyses in the line verification, and develops an image-based



line verification algorithm to detect line thickness and reduce false detections as well. It also avoids overlapping of lines by using pixel removal.

A HT is given in [70] which is able to solve the line fitting problem with the variables consisting of heteroscedastic errors with correlated noise. Thus this method is known as Heteroscedastic Hough Transform (HtHT).

Progressive probabilistic Hough transform given in [71] reduces the computation time by utilizing the difference in the fraction of votes needed to detect lines with different numbers of supporting points which exhibit the complexity of data.

A statistical based peak localization method is proposed in [72]. This method considered the butterfly structure of the Hough accumulator and computed the statistical standard variances and statistical means and used as parameters of fitting and interpolation processes. The peak localization method proposed in [73] focuses on reducing localization error.

## **2.6. FP Matching**

Fingerprint recognition or matching is defined as the comparison of two given fingerprints which gives either a degree of similarity (a score between 0 and 1) or a binary decision (mated or non-mated). Fingerprint recognition is basically divided into three types [1]; correlation based, minutiae based and texture features based techniques.

- Correlation based techniques: In this technique, two FP images are superimposed and the correlation between corresponding pixels is computed for different alignments [74-78].

- Minutiae Based methods: Ridge endings and bifurcation known as minutiae features is unique for each FP. Minutiae-based matching consists of finding the alignment between the template and the input minutiae feature sets that result in the maximum number of minutiae pairings [79-93]. Two important step in minutiae based FP recognition is minutiae extraction and matching. Minutiae points in the template is represented as  $m = \{x, y, \theta\}$ , where  $x$  and  $y$  gives the position of the minutiae and  $\theta$  gives direction of minutiae. A minutiae point in the captured image is also represented in the same way as in case of template. Matching is considered as a successful one, if the difference in position and directions of minutiae points are less than a threshold.
- Non minutiae based technique: These methods are developed since the minutiae based techniques are affected by the quality of the FP. Non-minutiae based techniques perform better than minutiae based methods when the area of the captured image is small. In non minutiae based matching, features of the ridge pattern like local orientation, frequency, ridge shape, texture information and number, type and position of singularities are used [94-96].

The richer gray-scale information of the fingerprints has been used for matching in [74]. This correlation-based FP verification system first selects appropriate templates in the primary FP, uses template matching to locate them in the secondary print, and compares the template positions of both FP. They have claimed that this method perform well in low quality images wherein minutiae feature extraction fails.

Vijaya Kumar et. al made an assessment about the performance of correlation filter techniques in FP verification[75]. They investigated the advanced correlation filters, such as synthetic discriminant function filters for face, fingerprint, and iris biometric verification.

Nandakumar and A.K.Jain proposed a minutiae matching algorithm that uses spatial correlation of regions around the minutiae to ascertain the quality of each minutia match[76]. They claimed that spatial correlation provides an accurate measure of the similarity between minutia regions. In this method, the quality of all the minutiae matches is accumulated to arrive at the final matching score between the template and query FP impressions.

A matching method based on cyclic structure of the FP image is proposed in [77]. The correlation value between a template and a sensed image, is obtained based on differential matching rate that utilizes the cyclic structure observed in the local area of a FP pattern, calculated by the maximum matching rate minus the minimum matching rate detected near the point where the matching rate is maximum.

In [78], a reference point (RP) on the fingerprint is found and alignment is performed based on this RP. Then the cross correlation factors between the gray scale intensities in region around the RP between the template and FP image is found. The mean of these cross correlation factors is used to perform the matching. If this mean is greater than a threshold, the matching is declared as successful otherwise unsuccessful.

In 1996, Ratha et al introduced HT in fingerprint matching by deriving an algorithm from the General Hough Transform (GHT) and applied it in minutiae-based fingerprint matching to determine transformation between two sets of minutiae points [79].

Later on some improvements on GHT for minutiae matching is proposed. Germain et al developed a method which is also derived from the GHT and improved it by first determining corresponding triangles that are formed using three minutiae points [80]. Another improved version of GHT was presented by Chang et

al which tried to reduce the accumulator array size by representing the alignment parameters by only the scale and rotation angle [81]. Pan-Gil et al [82], Pan-Moon et al [83] and Lomte and Nikam [84] presented improvement on Ratha et al's approach. The improvement is made by reducing the required memory usage for accumulator array so that it can take less computing resources such as memory space in smart cards. This was done by implementing the alignment more accurately, and performed more computations from a coarse-grain to fine grain resolution on the accumulator array.

Chouta et al introduced an improvement on GHT by reducing the error of transformation and deformation caused by the amount of pressure applied during the finger scanning process [85]. The error is reduced by including translation and rotation tolerances to overcome transformation and distortion errors. This method does not include the checking of direction difference for each possible pair of minutiae.

Chen et al [11] proposed a novel hierarchical minutiae matching algorithm for fingerprint identification systems. Alignment of the FP images is performed by the application of Hough Transform by estimating the alignment parameters. With this algorithm, the alignment process is decomposed to H steps, and each step uses  $n/H$  minutiae of the input FP to perform the alignment with the template FP in the database, where n is the total number of minutiae in the input FP [86].

A method based on Hough Transform approach is proposed to improve the SIFT method used in minutiae matching [87]. Low computational resource consumption such as memory usage is the main objective of this method. In this method, alignment is performed using Hough Transform for all closest pairs calculated by Euclidean Distance. The voting is performed on 2-dimensional and 1-dimensional accumulator arrays for translation and rotation values, respectively. The results revealed that time for searching peaks from a 3-dimensional accumulator array is decreased, and the memory requirement can also be decreased.

A new parameter known as Reliability of the minutiae which represents the quality of the minutiae is used for matching in [88]. This method used the relational information along with attribute information for the description of the FP for the enhancement of matching efficiency.

A FP minutiae matching algorithm is proposed in [89], which is claimed to be appropriate for the real time FP recognition system.

A matching method uses minutiae such as ridge endings and ridge bifurcation, which is more robust to nonlinear deformation, is proposed in [90].

A method that uses localized secondary features derived from relative minutiae information is introduced in [91] to perform the matching of partial print. A flow network-based matching technique is developed to obtain one-to-one correspondence of secondary features. A two-hidden-layer fully connected neural network is trained to generate the final similarity score.

Minutiae matching algorithm that uses minutiae-centered circular regions to increase the speed of matching and the robustness to non-linear distortion is presented in [92]. Region based matching is performed to find out the matched minutiae.

Distortion increases false minutiae, and hence makes it very difficult to find a perfect match. Algorithm proposed in [93] divides FP images into two concentric circular regions, inner and outer, based on the degree of distortion. The algorithm assigns weight-ages for a minutiae-pair match based on the region in which the pair exists.

Jain et.al divided the FP into different sectors and Gabor filters applied to each sectors to extract feature vectors [94]. These feature vectors are known as finger code and matching is performed based on the Euclidean distance between these

vectors. Finger code, is the collection of all the features (for every sector) in each filtered image. These features capture both the global pattern of ridges and valleys and the local characteristics.

Zin Mar Win and Myint Sein have used the Gabor filters for texture feature extraction and are combined with orientation features for matching [95].

Jayant et.al used the variance feature of ridge orientation for matching [96]. They made the matching rotation invariant by performing the alignment of the test and trainee FP image based on ridge orientation field.

In [97], Fuzzy theory is used for matching. This method starts with alignment of the FP with its template and a first stage of matching using local topological structure is performed. Finally a Novel Fuzzy Similarity Measure (NFSM) is computed for second stage of matching. This method is more robust against the non linear distortions in the FP image.

Wenzhen Zhou et al. proposed a method for FP matching based on global orientation field and local features [98]. Initially the preprocessing and alignment is performed to compensate the noises and rotation of the FP. The local features are those which are associated with the minutiae points in the FP. A combined similarity score is developed from global orientation field and local features of the minutiae points

Soweon Yoon and Anil K. Jain have performed the matching of 'Z' cut type of distortion by the restoration of minutiae distribution in the altered region [99]. Initially the given FP is classified in to altered or not altered. If it is an altered one, next step is to check whether it is z type or not. If it is Z type altered FP, restoration of the distorted region is carried out. The main aim of restoration of the distorted region is to relocate the minutiae points at the correct position by doing the reverse of the process used for making the Z cut.

Conventional minutiae based methods considered the minutiae point set including its position and orientation for matching. The accuracy of these methods gets reduced when the quality of FP image reduces. The other disadvantage is that these methods cannot provide enough distinguishing abilities for large-scale FP identification tasks. In order to compensate this, some of the researchers have developed the matching method which utilizes the non minutiae features along with minutiae features.

Method proposed in [100] is based on the fact that each minutiae detail is associated with its ridge orientation field. Thus the use of orientation field along with each minutiae point helps to develop a similarity function between minutiae and is used to identify corresponding features and evaluate the resemblance between two FP impressions.

The orientation is reconstructed from the minutiae points and used this orientation along with minutiae to improve the matching accuracy [101]. Initially a sparse area from the template is selected and orientation is interpolated from the minutiae points from this area. After the interpolation, the orientation field is obtained by modeling. This reconstructed orientation is used along with the minutiae points in the matching stage.

Matching algorithm proposed in [102] is based on the creation of feature vector for each FP minutia based on the global orientation field. These feature vectors allow the integration of orientation field information with the minutia details of FPs. The new feature vectors are rotation and translation invariant and capture more global information on FP ridges and furrows pattern. These features are used to identify corresponding minutiae between two FP impressions by computing the Euclidean distance between vectors.

## 2.7. FP Image Enhancement

FP image enhancement is one of the important preprocessing step before the feature extraction. Yang et al. [103] argue that the FP ridge and valley pattern does not always resemble a pure sinusoidal pattern, mainly because of the different values of ridge and valley width in some regions. Therefore they propose Gabor like filters whose positive and negative peaks can have different periods and contextually adjust the two periods based on the local ridge width and local valley width, respectively.

Zhu et al. implemented Gabor-based contextual filtering with squared mask [104].

Gabor filter have a shortcoming that the maximum bandwidth is limited. In order to overcome this limitation, Log-Gabor filter is used in [105]. The computational complexity in Gabor filter based methods can be reduced by using separable Gabor filters [106] or masks with sparse coefficients [107].

An overlapping block wise contextual filtering based on Short-Time Fourier transform (STFT) is proposed in [108].

Jirachaweng and Areekul implemented the block-wise contextual information computation and filtering in the Discrete Cosine Transform (DCT) domain instead of in the Fourier domain [109].

Multi resolution based FP image enhancement methods are proposed in literature. Enhancement method based on Gabor and Wavelet transform is proposed in [110-1122]. The image is first decomposed using wavelet transform. The Gabor filter is applied to decomposed images and is reconstructed back to obtain the enhanced image.



A FP image enhancement method using Contourlet Transform is proposed in [113]. The image is decomposed into low frequency and high frequency part using contourlet transform. The maximum modulus detection is applied to high frequency image and low frequency is used to compensate the high frequency part.

Enhancement method proposed in [114] consists of a smoothing operation which is adaptive based on the local ridge structure and it depends upon second moment descriptors. Normalized derivatives are used for the automatic scale selection of the smoothing operation.

Cheng and Tian proposed a method [115] which is based on dyadic space scale and the decomposition depth is determined according to the average ridge width in the image; the noise reduction relies on smoothing the differential images between successive scales (i.e., the details that are lost passing from one scale to the successive one).

Fronthaler et al. [116],[117] use a Laplacian like image-scale pyramid to decompose the original FP into three smaller images corresponding to different frequency bands. Each image is then processed through contextual filtering.



# Chapter 3

## Theory of Fingerprint Image Processing

---

### **Abstract**

Initial sections of this chapter describe FP-preprocessing methods including segmentation and enhancement. It also deals with FP matching and different parameters related to it. Receiver Operating Characteristics Curve, which can be used for assessing the performance of classification and matching systems, basic theory of Support Vector Machine classifier including the difference between linear and non-linear classifier, the Hough transform and wavelet transform, are also discussed.



### **3.1. FP Image Preprocessing**

FP preprocessing stages includes segmentation and enhancement. Segmentation is used to select the FP region which consists of necessary information. The enhancement is needed to increase the overall quality of the Fingerprint. The quality of the FP image is important since the success of matching methods depends upon the quality.

#### **3.1.1. FP Image Segmentation**

FP segmentation is an important step in automatic FP identification system. The image captured by a sensor involves foreground area that originated from the contact of the fingertip with the sensor and background area or noisy area which is the borders of the FP image. The task of the FP segmentation algorithm is to decide which part of the image belongs to the foreground and which part to the background [1]. Accurate segmentation is especially important for the reliable extraction of features like minutiae and singular points. Fig. 3.1 shows a FP with foreground and background marked. Region inside the boundary marked is foreground and region outside is background.



Fig. 3.1 Fingerprint image with foreground and background regions marked.

Different segmentation methods were developed based on local histogram of ridge orientation [118], [119], variance of gray levels in orthogonal direction to the ridge orientation [120], gradient response [121], Gabor filter response [122] and classifiers[123], [124].

### **3.1.2. FP Image Enhancement**

The success of an AFIS depends mainly on the quality of the FP since feature extraction fails in low quality images. The quality of the FP image captured by the scanner is affected by number of factors. They are physiological conditions of the friction ridge skin of fingers, performance of the capture devices, acquisition environment (external light, temperature and humidity weather conditions), user/device interaction, cleanliness of device surface, acquisition pressure and contact area of the finger with scanner. Depending upon the above factors, a FP image may contain good, medium and low quality regions. Common types of degradation associated with a FP image are [1]

- The ridges are not continuous.
- Parallel ridges are not well separated.
- Cuts, creases and bruises on the FP.

FP area resulting from segmentation can be divided into well defined region, recoverable region and unrecoverable region. The goal of an enhancement algorithm is to improve the quality of the recoverable region and mark the unrecoverable region too noisy for further processing. The FP image enhancement methods are broadly classified into pixel-wise enhancement, contextual filtering and multi-resolution enhancement [1]. Among these most widely used method is contextual filtering.

In pixel-wise enhancement, the new value of each pixel depends only on its previous value and some global parameters. These methods do not provide the needed results in the enhancement and are used as initial preprocessing methods.

Pixel-wise enhancement methods are developed based on contrast stretching, histogram manipulation and normalization [125], [126] and Wiener filtering [127].

The design of set of filters is the initial step in contextual filtering. A filter is selected for each region of the FP image depending upon the local context of the region. The local context is defined by ridge orientation and ridge frequency. Contextual filtering is performed based on bank of Gabor filters [128], [129]. The methods proposed by Erol et al. [128] and Wu et al. [130] relate the filter bandwidth to the local orientation coherence. Contextual filtering method proposed in frequency domain uses Fourier transform to convert the FP image from time domain to frequency domain [50]. The FFT (Fast Fourier Transform)  $F$  of each image  $I$  is computed. Each filter  $P$  is point-by-point multiplied by  $F$ , thus obtaining  $n$  filtered image transforms  $PF_i$ . Inverse FFT (IFFT) is computed for each  $PF_i$  to get the enhanced image in spatial domain.

Multi resolution analysis is used to remove the noise from the FP image [1]. As the name suggests, the FP image is decomposed in to different frequency bands and at higher levels (low and intermediate frequency bands) the rough ridge-valley flow is cleaned and gaps are closed, whereas at the lower levels (higher frequencies) the finer details are preserved. The enhanced image bands are then recombined to obtain the final image.

### **3.2.FP Matching**

FP recognition or matching is a process of comparison of two fingerprints and gives either a similarity score or a binary decision like mated or non-mated [1]. As stated in section 1.1.2, FP based biometric system can work either in verification mode or identification mode. A FP matcher take two fingerprints say ‘I’ and ‘T’ and produce a similarity measurement  $S(I, T)$ , which is normalized in the interval  $[0,1]$ . If  $S(I,T)$  is close to 1, the matcher has greater confidence that both FP come from the same

fingertip. The identity of a queried fingerprint is either a genuine type or an imposter type; hence, there are two statistical distributions of similarity scores, which are called genuine distribution and imposter distribution[1]. Fig. 3.2 gives an example of genuine distribution and imposter distribution. Each type of input identity has one of the two possible results, “match” or “non-match”, from a fingerprint matcher. Consequently, there are four possible scenarios:

1. A genuine individual is accepted (Genuine acceptance).
2. A genuine individual is rejected (False non match or False rejection).
3. An imposter individual is accepted (False acceptance or False match).
4. An imposter individual is rejected (Genuine rejection).

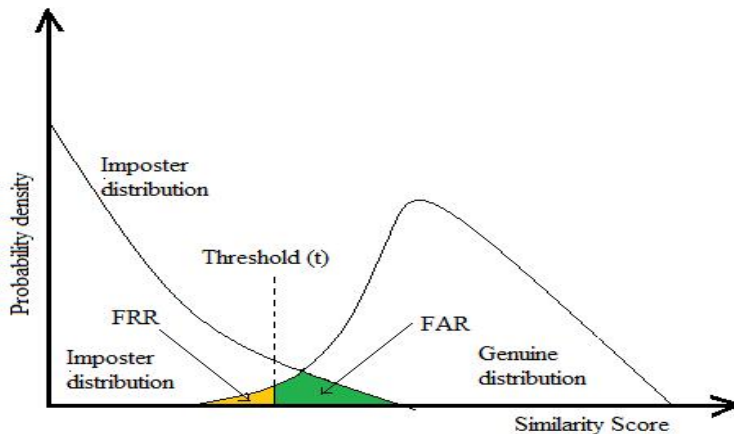


Fig. 3. 2 Example of genuine and imposter distribution.

Due to low quality of the fingerprint image, a genuine individual sometimes recognized as imposter. This situation is known as “false reject” and the corresponding error rate is called False Rejection Rate (FRR). The situation where the imposter individual is mistakenly recognized as genuine is known as “false accept” and the corresponding error rate is called False Acceptance Rate (FAR). FRR and FAR is also known as False Non Match Rate (FNMR) and False Match Rate (FMR) respectively. Complete separation of genuine distribution and imposter distribution is not possible with the selected threshold. This is shown in Fig. 3.2.



FAR and FRR are the function of threshold  $t$  and can be computed as follows

$$FAR = \int_0^t p_i(x) dx \quad (3.1)$$

$$FRR = \int_t^\infty p_g(x) dx \quad (3.2)$$

where  $p_i(x)$  and  $p_g(x)$  are the imposter and genuine distributions respectively. The Genuine Acceptance Rate (GAR) and False Acceptance Rate (FAR) are used] to analyze the performance of FP recognition systems.

### 3.3. Receiver Operating Characteristics (ROC) Curve

ROC curve is a graphical method used to measure the performance of the classification or personal recognition system. ROC graphs have been used in signal detection theory [132],[133], analyzing the behavior of diagnostic systems [134] medical diagnostic testing and compare and evaluate algorithms in machine learning [135],[136]. Performance of the classification systems can be assessed by plotting the ROC curve. Given a classifier and an instance, there are four possible outcomes [137].

1. Positive classified as positive class (True Positive Rate TPR).
2. Negative class classified as positive class (False Positive Rate FPR).
3. Negative class classified as negative class (True Negative Rate TNR)
4. Positive class classified as negative class (False Negative Rate FNR).

The TPR and FPR are calculated as

$$TPR = \frac{\text{Positives correctly classified}}{\text{total positives}} \quad (3.3)$$

$$FPR = \frac{\text{negatives incorrectly classified}}{\text{total negatives}} \quad (3.4)$$

Then ROC curve can be plotted between TPR and FPR (1-TPR) or between TNR and FNR(1-TNR) for varies thresholds. It is also used to analysis the performance

of the personal identification system. A discrete classifier is one that outputs only a class label. Each discrete classifier produces an FPR TPR pair, which corresponds to a single point in ROC space.

The classifiers in Fig. 3.3 are all discrete classifiers [137]. The lower left point (0, 0) is not having any positive classification; such a classifier commits no false positive errors but also gains no true positives. The opposite strategy, of unconditionally issuing positive classifications, is represented by the upper right point (1, 1). Performance of D is better since the point (0, 1) represents perfect classification.

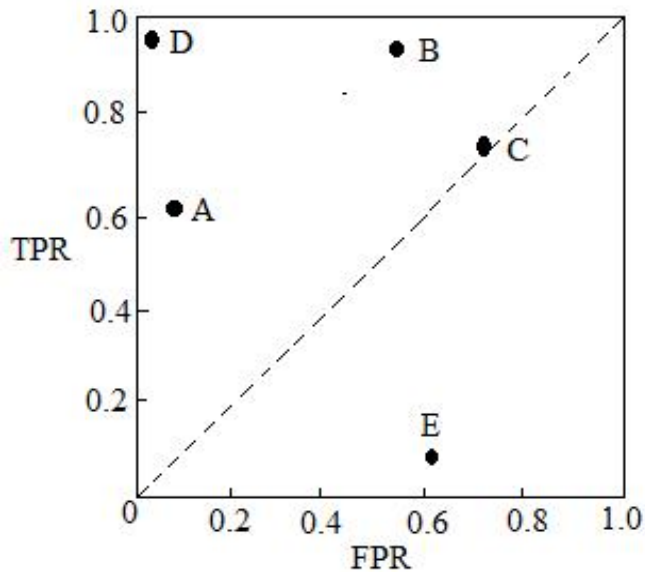


Fig. 3.3 Basic ROC curve showing five discrete classifiers.

### 3.4. Support Vector Machines (SVM)

Support Vector machines are first developed by Vapnik in 1992 and later on it have been widely used for linear or nonlinear classification and regression analysis. Theory of SVM is given in [138], [139], [140] and [141]. SVMs are basically based

on supervised learning models in which it classifies a set of data into two classes based on training data set. The formulation of SVM uses Structural Risk Minimization (SRM) principle whereas Neural Networks (NNs) are based on traditional Empirical Risk Minimization (ERM). SVMs evolved from the sound theory to implementation and experiments while NNs are evolved from applications and experiments to theory [138]. SVM performs the classification task by constructing hyperplanes in multidimensional space that separates the cases of different class labels. The data for two class learning problem consists of objects labeled with one of the two labels corresponding to the two classes; +1 for positive class and -1 for negative classes [139]. Thus the boundary that separates two classes is a line in two dimensions, a plane in three dimensions and more generally a hyperplane in higher dimensions.

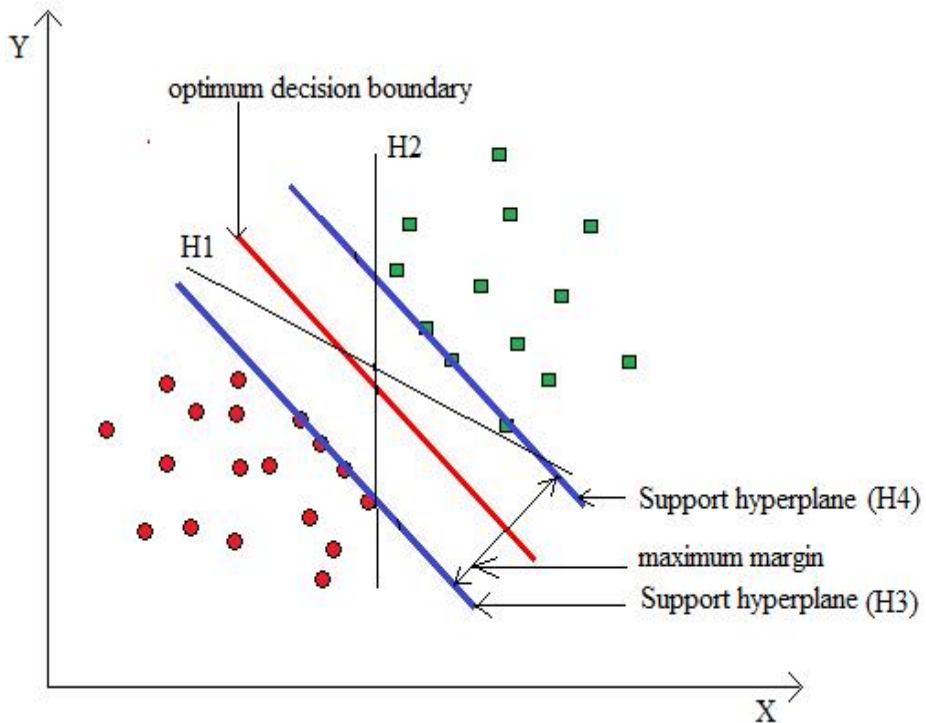


Fig. 3.4 Linear two class problem

The Fig. 3.4 illustrates the situation of a linear two class problem. The red and green dots are training samples belongs to negative and positive class respectively. The hyperplanes that are parallel to optimum decision boundary are called support hyperplanes. They are so called because the data vectors they contain support the plane. The data vectors on the support hyperplanes are known as support vectors. There are different hyperplanes that classifies the given data vector into two classes. They are H1, H2, H3 and H4. Selection of H1 and H2 as optimum solution increases the chance of false classification of testing data. Hyperplane H3 increases the chance of classifying red dots in the testing set as green while H4 increases the chance classifying green as red dots. Thus the problem of finding the optimum solution boundary is stated as “maximize the margin, subject to the constraints that all training cases fall on either side of the support hyper-planes. SVM finds the optimum solution by maximizing the margin between the support hyperplanes as shown in Fig.. This is done by finding a hyperplane parallel to and equidistant from support hyperplanes. This situation leads to the concept of non linear SVM. The original objects mapped or rearranged, using a set of mathematical functions, known as kernels. The process of rearranging the objects is known as mapping or transformation. Fig. 3.5 shows an example of non linear classifier. This training set in Fig. 3.5(a) is not possible to classify using a straight line. Thus it is transformed into feature space using kernels so that the training set can be linearly classified as shown in Fig. 3.5(b).

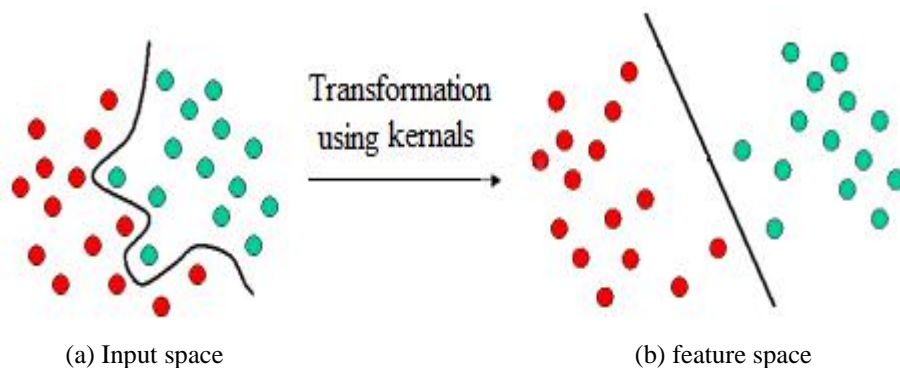


Fig. 3.5 Example of non linear classification

### 3.5. Hough Transform

Hough Transform is a technique invented by Paul Hough in 1962 to extract edge features from an image. Hough transform is mapping function which converts point in the image space into curve or line in Hough space [142]. Consider a point  $(x_1, y_1)$  and general equation of straight line in slope intercept form,  $y_1 = ax_1 + b$ . Hough transform maps the point in  $xy$  plane into a line in  $ab$  plane (also called parameter space). A second point  $(x_2, y_2)$  also has a line in parameter space associated with it, and this line intersects the line associated with  $(x_1, y_1)$  at  $(a^t, b^t)$  where  $a^t$  is the slope and  $b^t$  is intercept of the line containing both  $(x_1, y_1)$  and  $(x_2, y_2)$ . This is illustrated in Fig. 3.6. The parameter space is divided into so called accumulator cells and the expected range of slope and intercepts are  $(a_{max}, a_{min})$  and  $(b_{max}, b_{min})$  respectively. If there are  $Q$  points in  $xy$  plane lying on a line, then the corresponding accumulator cell have a value of  $Q$ . Cells with maximum values correspond to a line in the image. These cells are separated from other cell by setting a threshold to detect lines from the image.

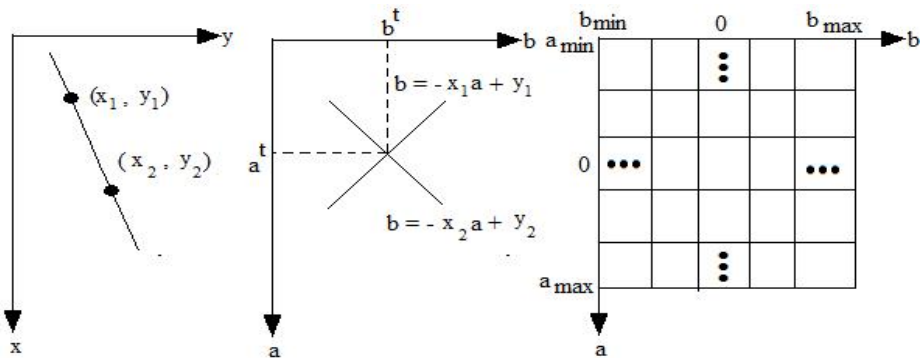


Fig. 3.6 (a)  $xy$  plane (b) Parameter space (c) Accumulator cell

A problem of using the equation  $y = ax + b$  to represent a line is that the slope approaches infinity as the line approaches vertical [142].

The above problem is solved by normal representation of line and the equation is

$$x \cdot \cos \theta + y \cdot \sin \theta = \rho \tag{3.5}$$

Fig. 3.7 gives the graphical representation of equation (3.5) and accumulator cell. Corresponds to every point lying on the line the parameter space consists of sinusoidal curves.  $Q$  collinear points lying on a line  $x \cdot \cos \theta + y \cdot \sin \theta = \rho$  yield  $Q$  sinusoidal curve that intersect at  $(\theta, \rho)$  in the parameter space. The range of angle  $\theta$  is  $+90$  to  $-90$  degree with respect to  $x$  axis. Hough transform is generalized to detect different shapes other than lines [143]. Hough transform is used for fingerprint recognition [79-86], [144] and crease detection of FP [145].

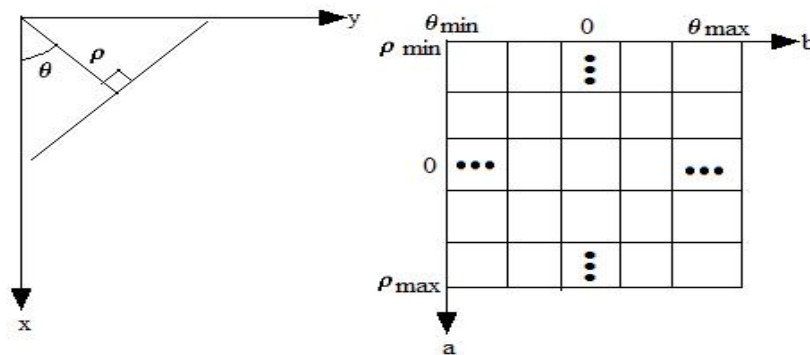


Fig. 3.7 Illustration of Hough transform of normal representation of line

### 3.6. Introduction of Wavelet Transform

In the first part of the 19th century, Joseph Fourier, a French mathematician and physicist, showed that any periodic function can be decomposed into series of sine and cosine functions or complex exponential. This expansion is known as Fourier series. After a century later generalization to the non-periodic signals has come to existence and is known as Fourier Transform (FT). Projecting the signal on complex exponentials leads to good frequency analysis, but no time localization. The poor time localizations or loss of time information while transforming into frequency domain is the main disadvantage of Fourier transform, making it not suitable for all kind of applications. In order to discount this disadvantage, Gabor in 1946

introduced Short Time Fourier Transform (STFT) [146]. In STFT the signal is first multiplied by a window of short time duration and then the Fourier transform of the obtained signal is computed. Even though STFT overcomes the limitation of Fourier transform, it has a fixed resolution in time and frequency since the length of the window is constant throughout the whole process.

In order to overcome the limitations of the Fourier Transform (poor time localization) and Short-Time Fourier Transform (fixed time and frequency localization), Grossman and Morlet introduced the Continuous Wavelet Transform in 1984. Unlike FT and STFT, wavelet transform provides a provision for analyzing the signal with short time interval for high frequency portion and long time interval for low frequency portion. This type of analysis is suitable for signals that have both low-frequency components with long time duration and high-frequency components with short time duration. Fig. 3.8 gives a comparative visualization of FT, STFT and Wavelet Transform (WT).

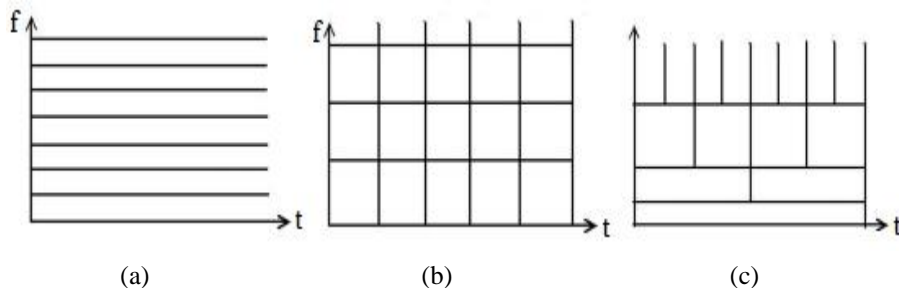


Fig. 3.8 Time frequency representation of (a) FT, (b)STFT, (c) WT

The term ‘wavelet’ refers to an oscillatory vanishing wave with limited duration of time that can be used to extract information from many kinds of data, including audio signals and images. There are various kinds of wavelets like compactly supported wavelets, symmetric and asymmetric wavelets, orthogonal and biorthogonal wavelets and smooth wavelets.

### 3.6.1. Multi Resolution Approximation

Mallat and Meyer in 1986 developed wavelet based Multi Resolution Analysis or Approximation (MRA) to analyze the functions at different resolution. MRA is performed by expressing a function with a shifted and scaled version of wavelet known as Mother Wavelet. MRA of a function adds more and more projections into detail spaces spanned by shifted and scaled versions of wavelet.

A function  $f(t)$  can be expressed as linear combination of real valued expansion function and if this expansion is unique, then the expansion function is known basis function. To find the MRA of a function  $x(t)$ , consider finite energy function  $x(t) \in L^2(\mathbb{R})$ , called scaling function, that generates a nested sequence  $\{A_j\}$ , namely

$$\{0\} \leftarrow K \subset A_{-1} \subset A_0 \subset A_1 \subset K \rightarrow L^2$$

and satisfies a dilation equation  $\phi(t) = \sum_k g_0(k)\phi(at - k)$  for some  $a > 0$  and coefficients  $\{g_0(k) \in \mathbb{R}\}$ . The space  $A_0$  is generated by  $\{\phi(-k): k \in \mathbb{Z}\}$  and in general  $A_s$  by  $\{\phi_k: k, s \in \mathbb{Z}\}$ . Consequently we have the following results.

$$X(t) \in A_s \quad x(2t) \in A_{s+1} \tag{3.6}$$

$$X(t) \in A_s \quad x(t + 2^{-s}) \in A_s \tag{3.7}$$

These dilation equations are unique to MRA.

For each  $s$ , since  $A_s$  is a proper subspace of  $A_{s+1}$  there is some space left in  $A_{s+1}$  called  $W_s$  which when combined with  $A_s$ , gives  $A_{s+1}$ .

This space  $\{W_s\}$  is called the wavelet sub-space and is complementary to  $A_s$ , in  $A_{s+1}$

This means that

$$A_s \perp W_s = \{0\}, \quad s \in \mathbb{Z} \tag{3.8}$$



Subspace  $\{W_s\}$  are generated by  $\psi(t) \in L^2(\mathbb{R})$ , called the wavelet, in the same way as  $A_s$  is generated by  $\phi(t)$ . i.e. for any  $x_s(t) \in A_s$ ,

$$x_s(t) = \sum_k a_{k,s} \phi(2^s t - k), \quad (3.9)$$

and any function  $y_s(t) \in W_s$  can be written as

$$y_s(t) = \sum_k w_{k,s} \psi(2^s t - k), \quad (3.10)$$

for same coefficients  $a_{k,s}, w_{k,s} \in \mathbb{R}$ .

Since we have

$$\begin{aligned} A_{s+1} &= W_s \oplus A_s \\ &= W_s \oplus W_{s-1} \oplus A_{s-1} \\ &= W_s \oplus W_{s-1} \oplus W_{s-2} \oplus \dots \oplus K \end{aligned} \quad (3.11)$$

We have

$$A_s = \bigoplus_{l=1}^{s-1} W_l \quad (3.12)$$

Here  $\{A_s\}$  are nested while  $\{W_s\}$  are mutually orthogonal. Thus we have

$$\begin{aligned} A_l \perp A_m &= \{0\}, & m > l \\ W_l \perp W_m &= \{0\}, & l = m \end{aligned} \quad (3.13)$$

In the case of an orthogonal decomposition, in addition to the wavelet space  $W$ , being complementary as, they are mutually orthogonal also, such that  $W_s \perp A_s, A_l \perp W_m = \{0\}, \quad l \neq m$

The hierarchical nature of  $A_s$ , and  $W_s$ , can be shown by the schematic representation in Fig. 3.9.

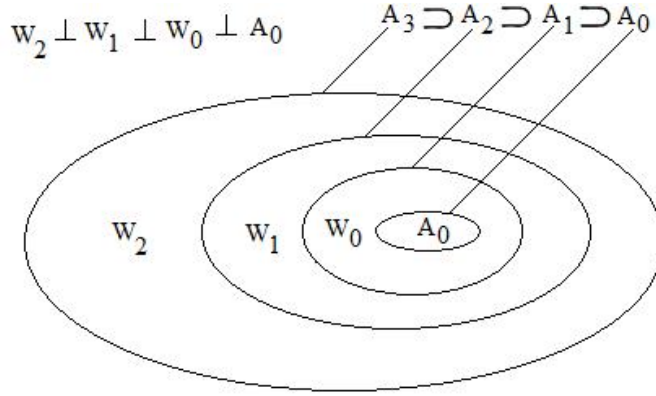


Fig. 3.9. Schematic of MRA decomposition

In order to analyze the discrete time signal with finite energy, Discrete Time Multi Resolution Analysis (DTMRA) has been developed [147-150].

Assume that basis are known, then approximation of a discrete time signal  $f(n)$  of finite energy in  $l^2(\mathbb{Z})$  is given by

$$f(n) = \frac{1}{\sqrt{M}} \sum_k W_\phi[j_0, k] \phi_{j_0, k}[n] + \frac{1}{\sqrt{M}} \sum_{j_0}^{\infty} \sum_k W_\psi[j, k] \psi_{j, k}[n] \quad (3.14)$$

Since the sets  $\{\phi_{j_0, k}[n]\}_{k \in \mathbb{Z}}$  and  $\{\psi_{j, k}[n]\}_{(j, k) \in \mathbb{Z}^2, j \geq j_0}$  are orthogonal to each other, the Wavelet coefficients are found by taking the inner products. Thus we have

$$W_\phi[j_0, k] = \frac{1}{\sqrt{M}} \sum_n f[n] \phi_{j_0, k}[n] \quad (3.15)$$

$$W_\psi[j, k] = \frac{1}{\sqrt{M}} \sum_n f(n) \psi_{j, k}[n] \quad (3.16)$$

### **3.6.2. Continuous Wavelet Transform (CWT)**

Continuous wavelet transform of signal is obtained by decomposing it with translated and dilated version of mother wavelet . The translated and dilated version of mother wavelet is

$$\psi_{\tau,s}(t) = \frac{1}{\sqrt{|s|}} \psi\left(\frac{t-\tau}{s}\right), \quad s \neq 0, \quad (3.17)$$

where 's' is a scaling or dilation factor that controls the width of the wavelet and is a translation parameter controlling the location of the wavelet. Scaling a wavelet means stretching it (if  $|s| > 1$ ) or compressing it (if  $|s| < 1$ ), while translating it means shifting its position in time. The CWT of a signal  $x(t)$  is obtained as follows.

$$W_{x;\psi(\tau,s)} = \int_{-\infty}^{+\infty} x(t) \frac{1}{\sqrt{|s|}} \psi^*\left(\frac{t-\tau}{s}\right) dt \quad (3.18)$$

where  $*$  is the complex conjugate of . The position of wavelet in time domain is given by , while its position in frequency domain is given by s. This transformation in theory is infinitely redundant, but it can be useful in recognizing certain characteristics of a signal.

### **3.6.3. Discrete Wavelet Transform (DWT)**

Discretization of scale and translation variables was introduced due to the redundancy of the CWT and is known as Discrete Wavelet Transform (DWT). The discretization is done by sampling the CWT on a 2-Dimensional (2-D) dyadic grid and yields countable set of coefficients in the transform domain. The grid is indexed by two integers; the first integer j, corresponds to discrete scale steps while the second integer n, corresponds to discrete translation steps. Then dilation and

translation parameters are changed in such a way that  $s = s_0^j$  and translation  $t = n_0 s_0^j$  where  $s_0$  and  $n_0$  are the discrete scale and translation steps respectively.

Then equation (1.6) becomes

$$\psi_{\tau,s}(t) = \frac{1}{\sqrt{|s_0^j|}} \psi\left(\frac{t - n\tau_0 s_0^j}{s_0^j}\right), \quad s \neq 0, \quad (3.19)$$

DWT is still the transform of a continuous time signal, with discretization performed in the  $s$  and  $t$  variables only. Hence it is analogous to the Fourier series, and also referred to as a continuous time wavelet series [151], [152].

### 3.6.4. Discrete Wavelet Transform (DWT) Computation

The equations that describes the wavelet decomposition of a signal  $f(t)$  is identical to the equations that defines perfect reconstruction in an orthogonal filter bank. The equations for perfect reconstruction in an orthogonal filter bank are given below.

$$\sum_n h_0(n)h_0(n - 2k) = \delta(k) \quad (3.20)$$

$$\sum_n h_1(n)h_1(n - 2k) = \delta(k) \quad (3.21)$$

$$\sum_n h_1(n)h_0(n - 2k) = 0 \quad (3.22)$$

The equations describes wavelet decomposition are as follows

The dilation equation and orthonormality of the functions  $\{ \psi(t-2k); k \in \mathbb{Z} \}$ :

$$\sum_k c(k)c(k - 2m) = \delta(m) \quad (3.23)$$

The wavelet equation and the orthogonality of the spaces  $V_0$  and  $W_0$  :

$$\sum_k c(k)d(k - 2m) = 0 \quad (3.24)$$

The decomposition relation and orthonormality of the functions  $\{ \phi(t-2k): k \in \mathbb{Z} \}$  :

$$\sum_k d(k)d(k-2m) = \delta(m) \quad (3.25)$$

Comparison of the filter bank and wavelet equation given above reveals the similarity in the double shift orthogonality and thus the coefficients  $c(n)$  and  $d(n)$  in a multi resolution analysis are also the filter coefficients in an orthogonal filter bank. This similarity allows the development of filter bank for the computation of DWT.

### 3.6.5. Two Dimensional Discrete Wavelet Transform (2-D DWT)

Wavelet transform uses a family of wavelet functions and its associated scaling functions to decompose the image into different sub bands [152], [153],[154]. The decomposition process is recursively applied to the sub bands to generate next level. For any scaling function and its corresponding wavelet function, we can construct three different 2-D wavelets and one 2-D approximation function using the tensor product approach. Thus 2D wavelet transform consists of one two dimensional scaling function  $\phi(x, y)$  and three two-dimensional wavelet functions,  $H(x,y)$ ,  $V(x,y)$  and  $D(x,y)$ . All these terms are products of a one dimensional scaling function and corresponding wavelet function as in equations below.

$$\phi(x, y) = \phi(x) \cdot \phi(y) \quad (3.26)$$

$$H(x, y) = \phi(x) \cdot \psi(y) \quad (3.27)$$

$$V(x, y) = \psi(x) \cdot \phi(y) \quad (3.28)$$

$$D(x, y) = \psi(x) \cdot \psi(y) \quad (3.29)$$

The scaling function  $\phi(x, y)$  gives the approximation coefficients corresponding to low frequency components. The terms  $H(x,y)$ ,  $V(x,y)$  and  $D(x,y)$  measures the variation of intensity along horizontal, vertical and diagonal directions respectively of the image.

The basis function for 2D wavelet transform is defined as

$$\phi_{j,m,n}(x, y) = 2^{j/2} \phi(2^j x - m, 2^j y - n), \quad (3.30)$$

$$\psi_{j,m,n}^i(x, y) = 2^{j/2} \psi^i(2^j x - m, 2^j y - n); i = \{H, V, D\}, \quad (3.31)$$

where index  $i$  defines the direction of wavelet function. Wavelet analysis of a function  $f(x, y)$  of size  $MN$  is obtained by following equations.

$$w_\phi(j_0, m, n) = \frac{1}{MN} \sum_{x=0}^{M-1} \sum_{y=0}^{N-1} f(x, y) \cdot \phi_{j_0, m, n}(x, y) \quad (3.32)$$

$$w_\psi^i(j, m, n) = \frac{1}{MN} \sum_{x=0}^{M-1} \sum_{y=0}^{N-1} f(x, y) \cdot \psi_{j, m, n}^i(x, y) \quad (3.33)$$

where  $i=\{H,V,D\}$ ,  $j_0$  is an arbitrary starting scale,  $w_\phi(j_0, m, n)$  define the approximation coefficients and  $w_\psi^i(j, m, n)$  defines the detailed coefficients in horizontal, vertical and diagonal directions. The function  $f(x, y)$  is reconstructed by inverse wavelet transform according to the equation given in (3.14).

$$\begin{aligned} f(x, y) = & \frac{1}{MN} \sum_n \sum_n w_\phi(j_0, m, n) \phi_{j_0, m, n}(x, y) \\ & + \frac{1}{MN} \sum_{i=H,V,D} \sum_{j=j_0}^{\infty} \sum_m \sum_n w_\psi^i(j, m, n) \psi_{j, m, n}^i(x, y) \end{aligned} \quad (3.34)$$

Wavelet transform finds numerous applications in signal and image analysis since it has the capability to analyze the local information in time-frequency plane. Main application of wavelet transform in image processing includes compression, de-noising, edge detection and enhancement. Excellent energy compaction property of the wavelet transform makes it suitable for use in image compression. The

extraction of high frequency components by multi resolution analysis leads to the edge detection from the images.

The use of wavelet transform in FP image processing is as follows. Because of the need of large amount of storage space for the FP, the Federal Bureau of Investigation (FBI) developed a new compression standard for 500 dpi images with small acceptable loss called Wavelet Scalar Quantization (WSQ) based on wavelet transform[1], [155].

Wavelet transform based FP recognition is given in [156-159]. Wavelet transform has also been used for FP based age estimation [160], [161] and gender classification [162].





# Chapter 4

## Altered Fingerprint Detection

---

### **Abstract**

The first step to defeat altered FP is alteration detection. This chapter proposes a method for altered FP detection using three features viz. Minutiae Density (MD), Ridge Discontinuity (RD), and Scars (S). The ridge flow in normal FP is continuous while that of altered FP is discontinuous in the altered region. The processes like burning, cutting and abrasion with blades, poring strong chemicals and surgery can cause broken ridges which in turn produce discontinuous ridges and high density of minutiae features as compared to normal FP. Apart from RD and MD, this method uses another feature known as Scar; the absence of ridges and valleys. Scar is present in the altered region as well as along surgical cuts.



Most of the AFIS existing today is based on minutiae features. Here the main aim of criminals is to change these features so as to evade the AFIS and all the FP image analysis methods. In fact altered FPs can be detected by finding the changes in the minutiae features of the FPs.

Alteration produces discontinuous ridges and these can be extracted changes occurred in these features by finding the discontinuity in the Ridge orientation field (ROF). It is a level 1 feature that is occurred at global level and minutiae points are level 2 features that occurred at local level. Finding ROF is an intermediate level for all FP image analysis. ROF is also used as feature for FP matching. Altered region consists of high density of minutiae points since the alteration process creates huge amount of broken ridges. Minutiae density is also an important feature for alteration detection. These two features have been used by the researchers to detect the altered FPs [12] [13]. The proposed work uses scar along with MD and RD which improved the alteration detection rate.

Scar is usually known as secondary feature of the FP. The different process used for alteration may wipe out the ridges and valleys and causes the introduction of scar in the altered region. The proposed method starts with FP image enhancement using Fourier Transform.

## **4.1. FP Enhancement**

The performance of the minutiae extraction algorithm relies heavily on quality of the FP images. Noises and dryness on the unaltered FP image causes broken ridges which in turn may increase minutiae density and be wrongly detected as altered FP images. The purpose of enhancement is to aid the extraction of the ridge endings produced by alteration and remove spurious ridge endings produced by dryness and noises in the image. Enhancing the FP by Fourier Transform techniques [51], [126]

gives directional smoothing to the ridges and fills the broken ridges produced by dryness in the FP while retains ridge endings produced by alteration process.

FP image is initially divided into 32X32 processing blocks. Then Fast Fourier Transform is performed on each block so that each block is converted into frequency domain. Fast Fourier Transform (FFT) is performed according to the equation.

$$F(u,v) = \sum_{x=0}^{M-1} \sum_{y=0}^{N-1} f(x,y) \times \exp \left\{ -j2\pi \times \left( \frac{ux}{M} + \frac{vy}{N} \right) \right\} \quad (4.1)$$

For  $u = 0, 1, 2, \dots, 31$  and  $v = 0, 1, 2, \dots, 31$ .

In order to enhance a specific block by its dominant frequencies, the FFT of the block is multiplied by its magnitude  $K$  times. The value of  $K$  is selected as 0.3 by iteration. The enhanced block is obtained by

$$g(x,y) = \text{IFFT} \left\{ F(u,v) \times |F(u,v)|^K \right\} \quad (4.2)$$

where  $F^{-1}(u, v)$  is obtained by

$$f(x,y) = \frac{1}{MN} \sum_{u=0}^{M-1} \sum_{v=0}^{N-1} F(u,v) \times \exp \left\{ j2\pi \times \left( \frac{ux}{M} + \frac{vy}{N} \right) \right\} \quad (4.3)$$

for  $x = 0, 1, 2, \dots, 31$  and  $y = 0, 1, 2, \dots, 31$ . Higher values of  $K$  improve the appearance of the ridges by filling up small holes in ridges, but very high values can result in false joining of ridges. Thus a termination might become a bifurcation.

## 4.2. Minutiae Density Extraction

The first step in minutiae density feature extraction is the detection of minutiae points known as ridge ending and bifurcation. There are two methods used for

finding the ridge ending and bifurcation from the FP image. One is based on gray scale image and other is based on binarized image [1]. The second method is used in this work. The different steps applied for finding minutiae points are explained below.

#### **4.2.1. Binarization**

Image binarization is a process which transforms the 8 bit gray scale image to a '1'-bit image with '0' value for ridges and '1' value for furrows. It is used for the extraction of ridge and valleys and to suppress all other gray scale values. After the operation, ridges in the fingerprint are highlighted with black color while furrows are white.

#### **4.2.2. Thinning**

Thinning is done to make the ridges one pixel wide so that the ridge endings are easily found by scanning with a 3x3 window. It is a morphological operation that successively erodes away the foreground pixels until they are one pixel wide. The application of a thinning algorithm to a fingerprint image preserves the connectivity of the ridge structures while forming a skeletonized version of the binary image which is then used in the subsequent extraction of ridge ending.

Minutiae consist of two features; namely ridge endings and bifurcations as shown in Fig. 4.1 (a) and (b) respectively. Fig. 4.2 (a) and (b) shows 3X3 window for scanning the thinned image to find ridge ending and bifurcation respectively. In this method, if the central pixel is zero and has exactly 3 zero-valued neighbors, then the central pixel is considered as a ridge branch or bifurcation. If it has only one zero-valued neighbor, then the central pixel is a ridge branch or bifurcation.

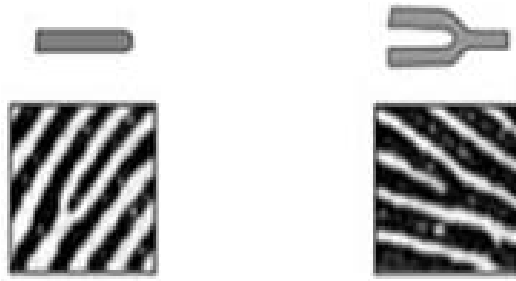


Fig. 4.1 (a) Ridge ending (b) Bifurcation

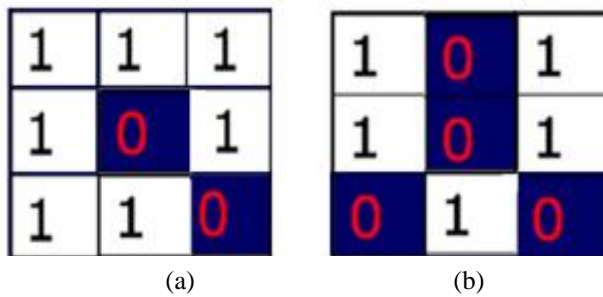


Fig. 4.2 3X3 window for (a) Ridge ending, (b) Bifurcation

After the extraction of minutiae features as described above, MD map is plotted for different types of altered fingerprints using Parzen window method with uniform kernel function [13], as explained below.

Let  $S_m$  is a set of minutiae of the fingerprint such as  $S_m = \{x|x = (x,y) \text{ is the position of the minutiae}\}$ . Then minutiae density map is constructed as follows.

ridge ending density map  $M_d(x,y)$  is obtained by

$$M_d(x,y) = \sum_{x_0 \in S_m} K_r(x - x_0) \tag{4.4}$$

where  $K_r(x-x_0)$  is a uniform kernel function centered at  $(x-x_0)$  with radius  $r$ ,  $M_d(x,y)$  is smoothed by a Gaussian filter of size  $30 \times 30$  pixels with standard deviation of 10 pixels so that  $M_d(x,y)$  is transformed to lie in the interval  $[0,1]$ .

Fig. 4.3 shows the minutiae density map obtained for normal and altered fingerprints. It clearly indicate that minutiae density is high in altered FP as compared to normal fp.

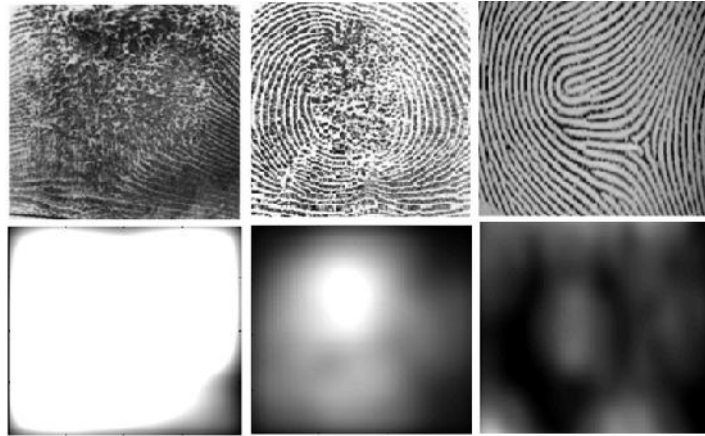


Fig. 4.3 MD map of (a) altered FP                      (b) normal FP

### 4.3. Ridge Discontinuity Analysis

Ridge Orientation of altered FP is determined using gradient based method [1] described as follows. Denote the gradient of an image at a point  $(x, y)$  as  $[G_x(x,y), G_y(x,y)]$ , then  $G_x$  and  $G_y$  gives the variation of intensity in  $x$  and  $y$  directions respectively. The principal axis of variation of gradients in  $x$  direction, diagonal directions and  $y$  direction is obtained as

$$\begin{aligned} G_{xx} &= G_x * G_x \\ G_{xy} &= G_x * G_y \\ G_{yy} &= G_y * G_y \end{aligned} \tag{4.5}$$

$$\text{Then } \sin 2\theta = G_{xy} / [(G_{xy})^2 + (G_{xx} - G_{yy})^2] \quad \text{and} \tag{4.6}$$

$$\cos 2\theta = (G_{xx} - G_{yy}) / [(G_{xy})^2 + (G_{xx} - G_{yy})^2] \tag{4.7}$$

where  $\theta(x, y)$  is the orientation field at point  $(x,y)$ .

Orientation  $\theta_{org}(x, y)$  is obtained as

$$\theta_{org}(x, y) = \pi/2 + \text{atan2}(\sin 2\theta, \cos 2\theta) / 2 \quad (4.8)$$

where  $\theta_{org}(x, y)$  denotes the orientation of altered FP before enhancement. After finding the orientation  $\theta_{org}$ , the altered FP is enhanced by FFT as explained in section 4.1.

The orientation field of enhanced FP is again found by gradient based method and is denoted as  $\theta_{en}$ . Enhancement gives more smoothing to the altered region while normal region is smoothed by lesser amounts. Thus, the ridge discontinuity map is obtained by comparing the ridge orientation field before and after the FFT enhancement as given in equation (4.9) below.

$$RD = \min(|\theta_{org}(i, j) - \theta_{en}(i, j)|, \pi - (|\theta_{org}(i, j) - \theta_{en}(i, j)|)) / (\pi/2) \quad (4.9)$$

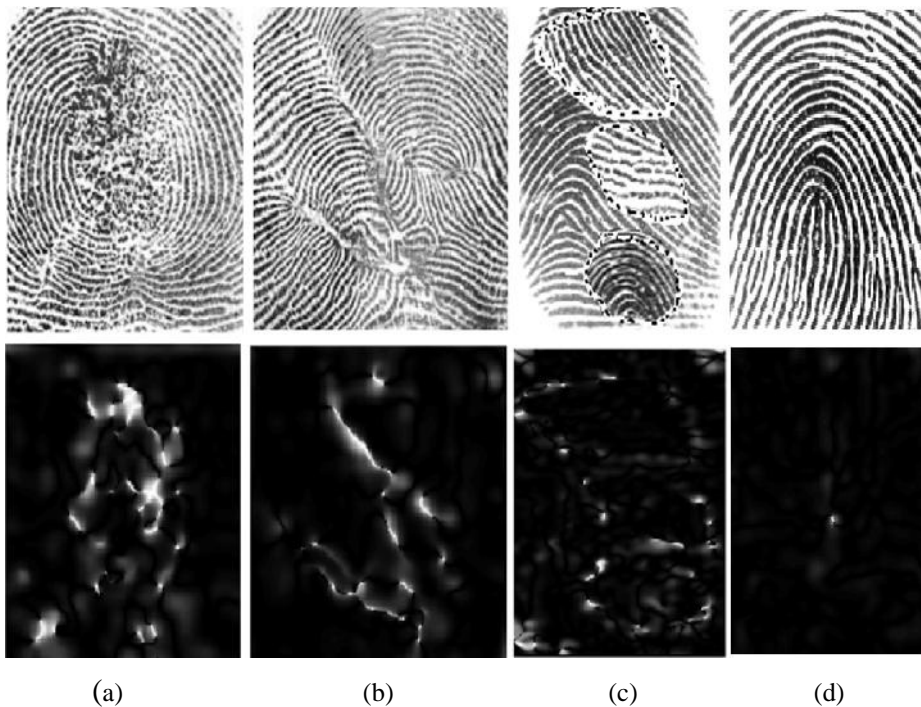


Fig. 4.4 RD map of (a) Obliteration, (b) Distortion (c) Imitation and (d) normal FP



## **4.4. Analysis of Scar**

Pontus Hymer developed two methods for the detection of scar present in the normal FP [163]. First method is based on average filtering and thresholding. The average filter is used to remove the high frequency components from the FP. Once these are removed, thresholding is applied to detect the scar. Second method is based on Gabor filtering. David Vernon used Hough transform for the detection of scar [145]. He considered the co linearity of ridge endings present at the boundary of the scar for the detection. In the proposed work, average filtering is made adaptive by changing the window size of the filter with respect to dryness present in the image.

### **4.4.1. Adaptive Average Filtering**

The quality of FP changes with the dryness of the fingers being scanned. Dry, wet and normal (good quality) FPs are shown in Fig. 4.5. The lack of moisture in the finger is the cause of dry FP. This leads to broken ridges and valleys in the fingerprint image. Excess of moisture in the fingertip causes the wet images. The ridges and valleys in the wet images are not well separated. The averaging filter preserves the sharp edges in the image. The image is convolved with average filter in the spatial domain to accentuate the present scars. The dryness on the fingerprint affects the preservation of scars in the fingerprint. This difficulty is solved by changing the window size by setting a threshold for mean of pixel intensity of the image. The mean varies for dry, wet and good quality images. Pixel intensity mean for dry FP varies between 190 to 250 while for wet images, it lies in between 30 and 120. For good quality normal fingerprint images, the pixel intensity lies between 120 and 190. Thus the filter is adapted to the dryness of the fingerprint. The mean and standard deviation varies for wet, dry and normal fingerprint images. Window size is selected as  $3 \times 3$ ,  $5 \times 5$  and  $7 \times 7$  for wet, normal and dry FPs respectively.



Fig. 4.5 (a) Dry FP

(b) Wet FP

(c) Normal FP

#### 4.4.2. Thresholding

Thresholding is used for segmenting the scars from the filtered FP image. Fig. 4.6 shows the segmented scars from the obliteration type altered fingerprint images. Both mutilation and scar type is shown in the Fig.

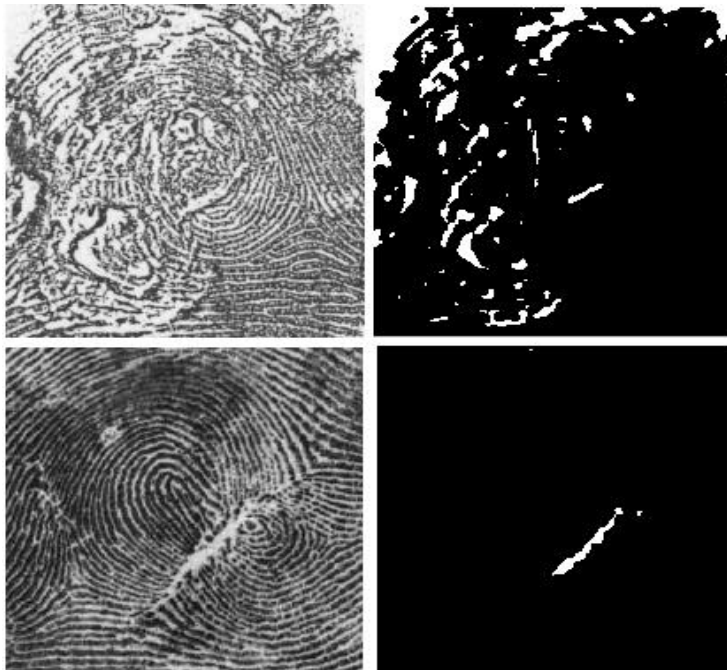
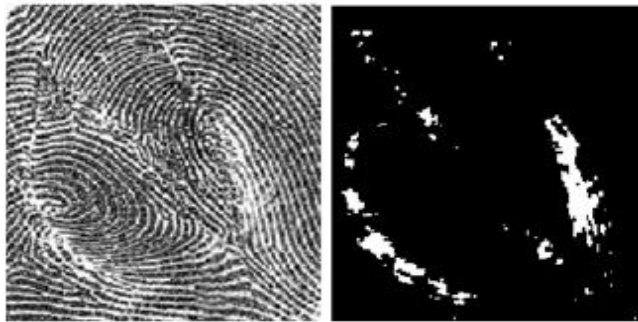


Fig. 4.6 Scar detected from obliteration type of altered FP



(a) Scar detected from distortion type of altered FP

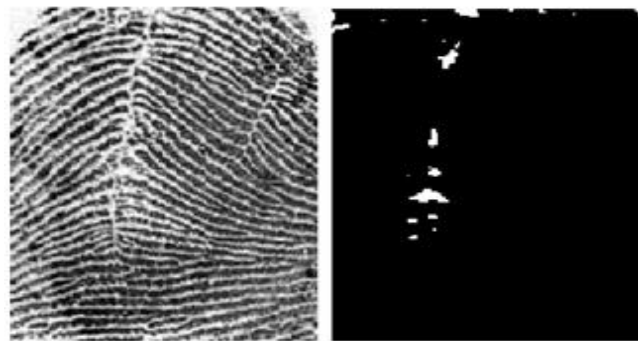


Fig. 4.7 (b) Scar detected from imitation type of altered FP

Fig. 4.7 shows the scars detected from distortion and imitation type of altered FPs. Scar is present in both types altered FP along the surgical cuts.

## **4.5. Feature Extraction and Classification**

Fingerprint image analysis can be considered as a pattern recognition problem and the important step for pattern classification is the creation of feature vectors. The feature vectors from the ridge discontinuity map, minutiae density map and scar is constructed by local histograms in  $3 \times 3$  cells. All these features are combined by concatenating local histograms in each cell to create feature vectors. These feature vectors are fed into SVM for classification [13].

## 4.6. Experiments and Results

Experiments are conducted on both real and synthetically altered FPs. The database consists of 70 real altered FP images of obliteration, distortion and imitation and synthetically altered FP of 60 images each of all type. Normal FPs of 60 numbers obtained from FVC 2004 database are also used.

Each type of altered FP is separately tested along with normal FP. In fact, features from both normal and altered FP are fed into SVM for training and testing. The classes ‘1’ and ‘0’ is assigned for altered and normal FP respectively. SVM gives a class of ‘1’ for altered FP and ‘0’ for normal FP leads to the conclusion of true classification and false classification respectively. Tables 4.1 to 4.3 shows the result. Experiment is performed on real altered FPs.

Table 4.1 Detection of distortion type of alteration

FP	No. of FP	No. of FP detected as	
		Distortion	Normal FP
Distortion	25	25	0
Normal FP	60	7	53

Table 4.2 Detection of Imitation type of alteration

FP	No. of FP	No. of FP detected as	
		Imitation	Normal FP
Imitation	20	11	9
Normal FP	60	8	52

Table 4.3 Detection of obliteration type of alteration

FP	No. of FP	No. of FP detected as	
		Obliteration	Normal FP
Obliteration	25	22	3
Normal FP	60	5	55

Table 4.4 Result of detection in terms of TPR and FPR

Type of alteration	TPR in %	FPR in %
Distortion	100	12
Imitation	56	13.33
Obliteration	88	8

Table 4.4 shows the detection performance in terms of TPR and FPR computed from tables 4.1 to 4.3. Altered FP is taken as positive class. Thus the detection of altered FP as altered one belongs to TPR and detection of normal FP as altered one belongs to FPR. Proposed method detected all distorted FP with 12% of FPR. It means that proposed method detected all the distorted FPs as distorted one and 12% of normal FP as distorted FP. Detection of imitated type of FP is less. It also detected 87% of obliterated FP with 8% FPR and 56.25% of imitated FP with 8% FPR.

Possible combinations of features are also tested on synthetically altered FP of obliteration and distortion type. Number of altered FP and normal FP considered for the experiment is 120 and 60 respectively. Table 4.5 and 4.6 shows the detection performance. Table 4.6 gives the detection performance in terms of TPR and FPR.

Table 4.5 Alteration detection by different combination of features

Features	No. of Normal FP Detected as		No. of Altered FP Detected as	
	Normal FP	Altered FP	Altered FP	Normal FP
RD & MD	49	11	104	16
RD & Scar	47	13	102	18
MD & Scar	48	12	96	24
RD, MD & Scar	53	7	115	5

Table 4.6 TPR and FPR for combination of features.

Features	TPR in %	FPR in %
RD & MD	87	18
RD & Scar	85	21.2
MD & Scar	80	20
RD, MD & Scar	94	10

Comparison of the proposed method with method developed by S Yoon and Jain[13] is performed using the synthetically altered FPs except on imitation type. Table 4.7 gives the result. Performance of the proposed method is better since it detected more altered FP with the aid of an extra feature namely scar present in the obliteration type of FP and surgical cuts of distortion type of FP.

Table 4.7. Comparison of proposed method with existing method

Method	TPR	FPR
Proposed method	94	10
Existing Method (Jain and S Yoon)	87.5	13

ROC curve that shows the alteration detection performance of the proposed method on both real and synthetic altered FP is plotted as shown in Fig. 4.8.

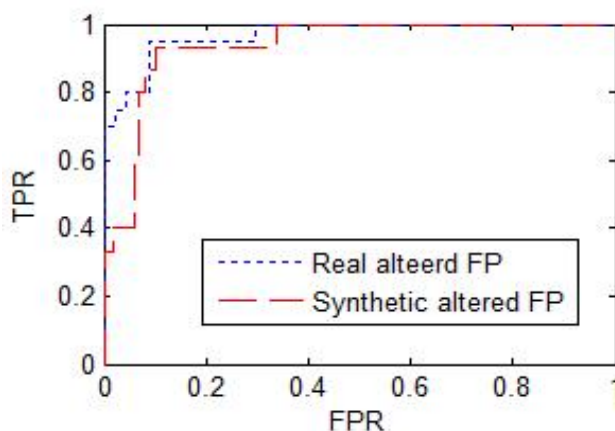


Fig. 4.8. ROC curve for altered FP detection

## **4.7. Conclusion**

In this chapter, a method for detecting altered FP s is discussed. Altered FP s consist of three features, Ridge Discontinuity (RD), Non uniform Minutiae Density (MD), and absence of ridges and valleys known as Scars(S). The standard method developed for alteration detection by Jain and S Yoon has used RD and MD for alteration detection. The proposed method uses scar along with RD and MD. The results shows that the addition of the scar increased the detection rate while reduced the FPR

Once the FP detection is completed, it goes to classification stage. Classification of alteration is needed to take appropriate counter measures or to help the matching stage. If the detected altered FP is classified as obliteration type, it can directly go to the matching stage. If it belongs to imitation or distortion, necessary steps have to be taken to restore the altered region for matching. Next chapter gives a method for FP alteration classification based on Hough transform.





# Chapter 5

## Altered Fingerprint Classification

---

### **Abstract**

This chapter gives an overview of different types of alterations namely obliteration, distortion and imitation. A Hough transform based method for classification of a given FP into normal FP and different types of altered FP have been developed. This method uses variation of ridge ending density possessed by normal and different types of altered FP. Hough transform is applied on the ridge end image extracted from the FP. Due to the variation in ridge ending density, Hough accumulator cells possess different peaks with respect to type of alteration. Classification is made possible by the selection of a threshold value for Hough accumulator. Hough accumulator is enhanced to isolate the peak from other values so that the result of classification is improved. The enhanced accumulator is also used for the separation of scar of altered FP from the normal FP



## **5.1. Introduction**

Different mechanical and chemical process used in alteration creates various patterns on the ridge structure. Subjective analysis of the ridge patterns and process leads to the classification of altered FP into three groups [12] [13]. They are

1. Obliteration
2. Distortion
3. Imitation

### **5.1.1. Obliteration**

Obliteration type of altered FP is obtained by processes like cutting and abrasion with blades or knives, burning and poring strong chemicals. Obliteration is again divided into scar and mutilation. Obliteration is the most popular form of alteration since the process of alteration is easier than the surgical procedure of alteration involved in imitation and distortion [12] [13].

However the processes used for making obliteration creates large amount of broken ridges or ridge endings since possibility of obliterating a small selected portion of the fingertip is less. The number of ridge endings also depends upon the area of alteration. For FP images having less area of alteration, the ridge ending are less.

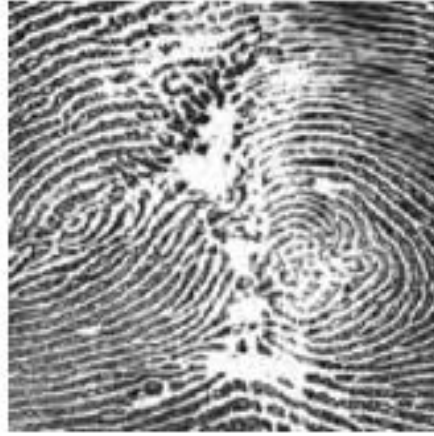
### **5.1.2. Distortion**

This type of altered FP is obtained by surgical ways. The interchanging of one portion of the fingertip with other portion of the same fingertip or with the palm or leg print leads to distortion type of altered FP. The broken ridges produced by this process present only along the surgical cuts and is less than that of obliteration type of altered FP. Researchers have found a special type of distortion known as ‘Z’ cut.

The path of the surgical cut forms the alphabet Z. This is formed by taking two triangles, stretching it, transformed each other and joining back on the fingertip.



(a) Mutilation



(b) Scar



Fig. 5.1 (c) Z type distortion



(d) Imitation

### **5.1.3. Imitation**

This type of alteration is created by the replacement of large area of fingertip with other fingertip, palm print or leg print by plastic surgery. Imitation type consists of broken ridges along surgical cuts and is less as compared to distortion type. This is

because the distortion is created by replacement of number of small portion while imitation is created by replacement of large area. Fig. 5.1 shows different types of altered FP.

The main characteristics of altered FP that leads to the development of automatic method for the classification is the variation in number of ridge endings due to the different processes used for the creation of alteration. In order to depict this variation, ridge endings are found using binarization method as explained in section 4.2 and ridge ending density map is obtained using Parzen window method.

Fig. 5.2 shows the ridge ending density map for different types of altered FP. Normal FP possess lowest ridge ending density and obliteration is having highest ridge ending density. Distortion and imitation falls in between normal FP and obliteration. Compared to imitation, distortion possess high ridge ending density.

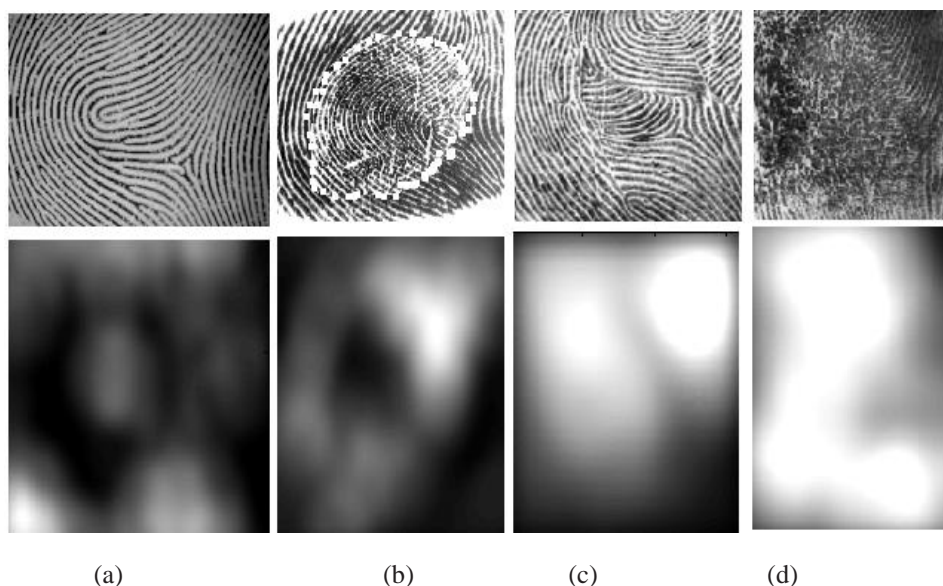


Fig. 5.2 Variation of ridge ending density in (a) normal FP, (b) Imitation, (c) distortion and (d) obliteration

The quality of the altered FP cannot affect the variation of ridge ending density since NIST quality assessment software have detected only 20% of altered FP [12]. In order to efficiently utilize this variation in ridge ending density to classify altered FP, Hough transform is used. The ridge end points in normal and altered FPs are collinear even though they are distributed randomly in the image space. Due to the variation of ridge ending density, the number of collinear ridge end points is also varying with respect to normal and different types of alteration. Hough accumulator cell value also vary with respect to number of collinear ridge end points. Making use of this, a threshold is selected in the Hough accumulator to perform detection and classification of fingerprint alteration.

The performance of the minutiae extraction algorithm relies heavily on quality of the fingerprint images. Noises and dryness on the unaltered fingerprint image causes broken ridges and can be wrongly detected as altered fingerprint images. Therefore fingerprint image is enhanced by FFT as explained in section 4.1 before the extraction of ridge end points by binarization method. This is to reduce the broken ridges produced by dryness and noises in the FP image. This enhanced image is used by binarization method to produce ridge ending image. Then Hough transform is applied to this ridge ending image for detection and classification of altered FP.

## **5.2. Detection and Classification of FP Alteration by Hough Accumulator**

Hough transform has been used for fingerprint matching of poor quality images [164] and latent fingerprints [165], even though traditionally it is widely used for the detection of lines and objects in the form of circles and ellipses [166], [143], [167]. Junhong and Chen presented a method to detect lines in noisy images by enhancing the Hough accumulator [168].

Hough transform is applied to ridge ending image of normal and altered fingerprint to detect line through the collinear ridge end points. Due to the increase in ridge ending density from normal FP to obliteration type of altered FP (see Fig. 5.2), number of ridge end points lying on the line detected by Hough transform is also increases. Thus the peak of the Hough accumulator increases from normal FP to obliteration type of altered FP.

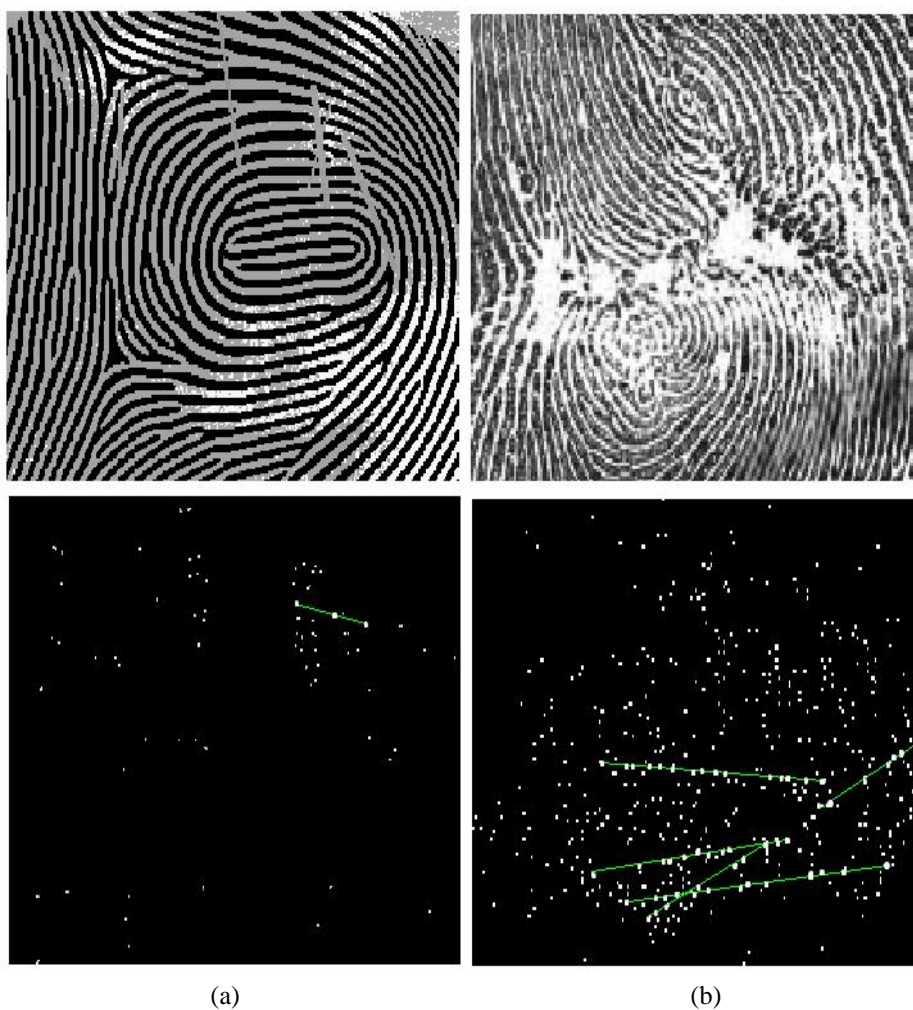


Fig. 5.3 Collinear ridge end points detected by Hough transform from (a) normal FP and (b) altered FP.

For every ridge end point in the fingerprint image, Hough transform space consists of a sinusoidal curve with corresponding  $(i, j)$  values. The ridge end points lying on single line have same value of  $i$  and  $j$ . These values are recorded on a 2D array known as Hough accumulator. The  $i$  and  $j$  axes of accumulator are divided into a number of equal divisions of resolution  $\Delta i$  and  $\Delta j$  respectively. As the number of ridge end points lying on a single line increases, values in the corresponding cell of Hough accumulator also increases. Number of ridge end points is higher in altered fingerprint and this in turn leads to higher number of collinear ridge end points as compared to normal fingerprints and is shown in Fig. 5.3.

In fact the peak of the Hough accumulator of altered fingerprints becomes high. Increase in ridge ending density from imitation, through distortion to obliteration causes the increase in peak of Hough accumulator. This makes the classification of altered fingerprints possible. In order to detect collinear ridge end points, it is necessary to select a threshold that is low enough to ensure all possible cells are included while high enough to exclude unwanted cells. To ensure this condition, we defined two thresholds  $H_{th1}$  and  $H_{th2}$  as given in equations (5.1) and (5.2) respectively.

$$H_{th1} = 0.5 * H_{max} , \quad (5.1)$$

$$H_{th2} = m + 3 * \sigma , \quad (5.2)$$

where  $H_{max}$  is the maximum value of Hough accumulator ,  $m$  &  $\sigma$  are mean and standard deviation of Hough accumulator respectively. Fig. 5.4 illustrates the variation of  $H_{th1}$  and  $H_{th2}$  for normal and real altered fingerprints. Same fingerprints are used to plot the values of  $H_{th1}$  and  $H_{th2}$ . The normal and altered fingerprints are taken along x axis in such a way that the ridge ending density increases along positive direction. Both the thresholds are increasing with the increase in ridge ending density and  $H_{th1}$  and  $H_{th2}$  of normal and altered fingerprint is overlapping



each other. This overlapping in both thresholds increases the FPR in classification. This is due to the fact that Hough accumulator consists of number of peaks and the exact peaks are not well defined. To alleviate this effect Hough accumulator is enhanced.

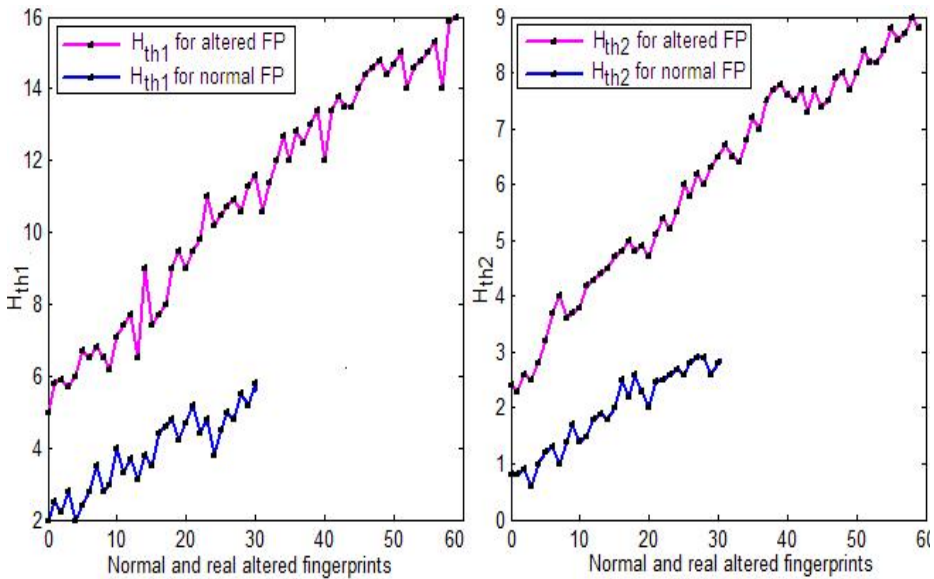


Fig. 5.4 (a) Variation of  $H_{th1}$

(b) Variation of  $H_{th2}$

### 5.2.1. Hough Accumulator Enhancement

The objective of enhancement is to isolate the most dominant or ideal peaks from other cells of the Hough accumulator to reduce the nonlinearity and FPR with increase in TPR. Many methods have been proposed in literature for highlighting the peaks by voting schemes and localization. All of these methods require prior knowledge about the peak and do not provide exact peak separation or isolation. A method for enhancement of Hough accumulator by isolating the peak based on the characteristics of butterfly structure is provided in [168]. This method is used in the proposed work to reduce the False Positive Rate in alteration classification.

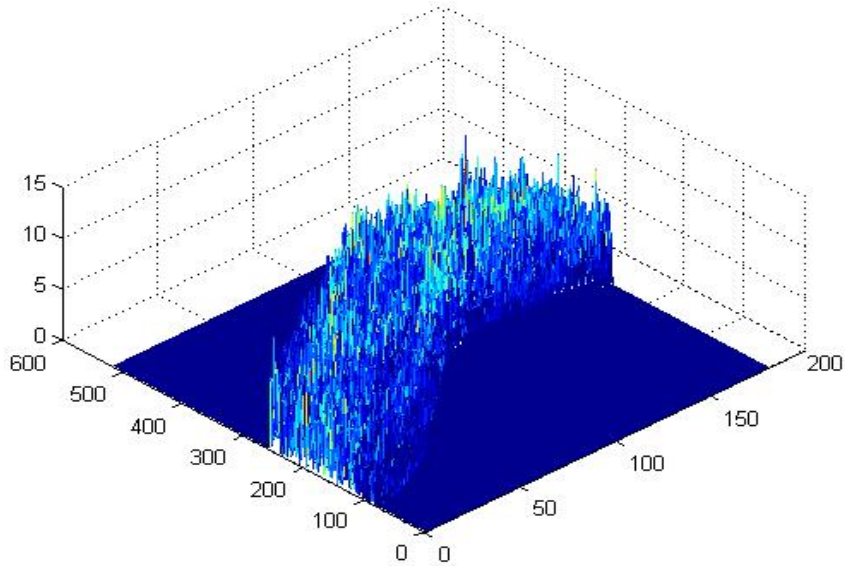


Fig. 5.5 Mesh plot of Hough accumulator

Hough accumulator always possesses a butterfly structure as shown in Fig. 5.5. The value of cells outside the butterfly is normally zero. Consider the cell to be enhanced in the butterfly structure of Hough accumulator  $H$  as  $H_i$  corresponding to  $(x_i, y_i)$ . Mapping of the cell  $H_i$  into an enhanced cell  $R_i$  is performed by implementing a local operator by projecting the sum of difference between value in  $H_i$  and its  $3 \times 3$  neighborhood on to an angle  $\theta_i$  that depends on average normal direction of  $H_i$ . Where  $R$  is the enhanced accumulator having the same dimension of  $H$ . A cell in  $H$  consists of number of sine curves passing through it. The average normal direction of a cell is defined as the average of the normal direction of number of sine curves in it and is obtained by using the equation (5.3), (5.4) and (5.5).

1. Cell in the accumulator have a sine curve passing through it. Curve's normal direction's slope rate is given by

$$\eta_l = \frac{1}{x_l \sin \theta - y_l \cos \theta} \quad (5.3)$$

where  $l = 1, \dots, q$ ; ( $q$  = value registered in the cell.),  $x_l$  = value of the axis corresponding to the cell

2. Angle the normal makes with axis in anticlockwise direction is

$$\psi_l = \arctan (n_l) , l = 1, \dots, q \quad (5.4)$$

3. Average normal direction of cell is

$$\psi_{avg} = \frac{1}{q} \sum_{l=1}^q \psi_l \quad (5.5)$$

After finding the average normal direction of cell, the local operator is defined as follows. Consider a 3×3 neighborhood around the cell of interest. Angles that the central element makes with neighboring cells in anticlockwise direction  $\theta_i$  ( $i = 1, \dots, 9$ ). are ( $\theta_1$  to  $\theta_9$  except  $\theta_5$ )  $3\pi/2, \pi/2, \pi/4, \pi, 0, 5\pi/4, 3\pi/2$  and  $7\pi/2$  respectively. Then  $\theta_i$  is defined as the deviation between  $\theta_i$  and the angle  $\psi_{avg}$ . The angle  $\theta_i$  is obtained by pseudo codes from 1 to 4.

```

1:    $\theta_i = | \theta_i - \psi_{avg} |$ ;
2:   if  $\theta_i > 2$  then
        $\theta_i = \theta_i - 2$ 
3:   if  $\theta_i > \pi$  then
        $\theta_i = 2\pi - \theta_i$ 
4:   if  $\theta_i > \pi/2$  then
        $\theta_i = \pi - \theta_i$ 

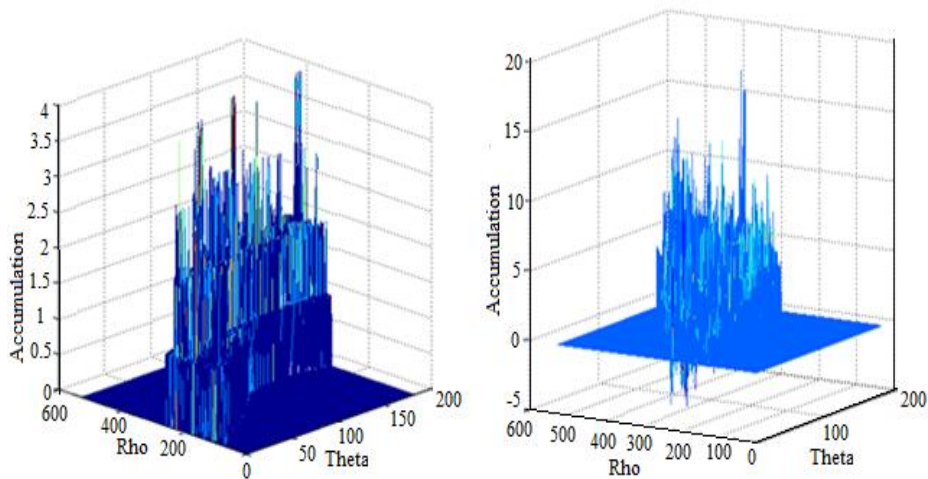
```

The varying angle  $\theta_i$  is projected to the sum of difference between cell to be enhanced and neighboring cell values. Thus the cell corresponding to H5 in enhanced accumulator R is obtained as

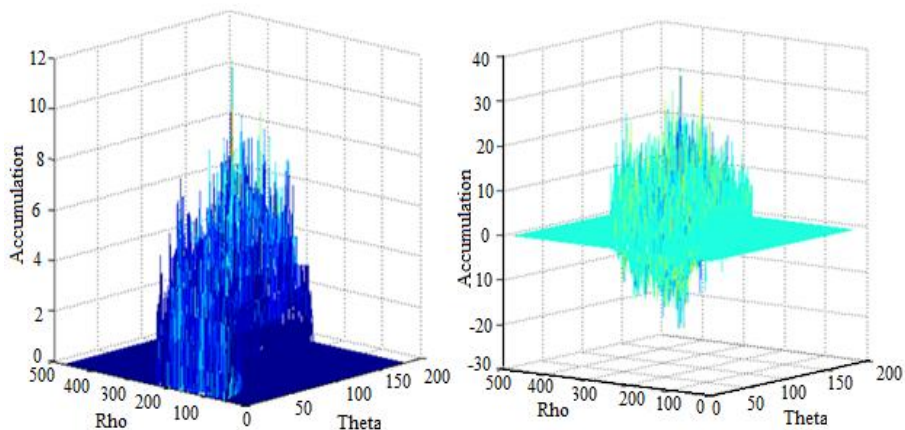
$$R_5 = \sum_{i=1}^9 (H_5 - H_i) \cos \theta_i \quad (5.6)$$

If any of the value in H is zero, corresponding value of R is also taken as zero. Figs 5.6 and 5.7 illustrate the effect of accumulator enhancement. Fig. 5.6(a) and (b)

shows the mesh diagram of Hough accumulators and enhanced accumulators of normal fingerprint image and Fig. 5.7(a) and (b) shows these of altered fingerprint image. After enhancement, the peaks become more prominent or isolated from other cell values and negative peaks are also introduced in the accumulator.



(a) Before enhancement (b)After enhancement  
 Fig. 5.6 Mesh plot of Hough accumulator of normal FP



(a) Before enhancement (b) After enhancement.  
 Fig. 5.7 Mesh plot of Hough accumulator of altered FP.

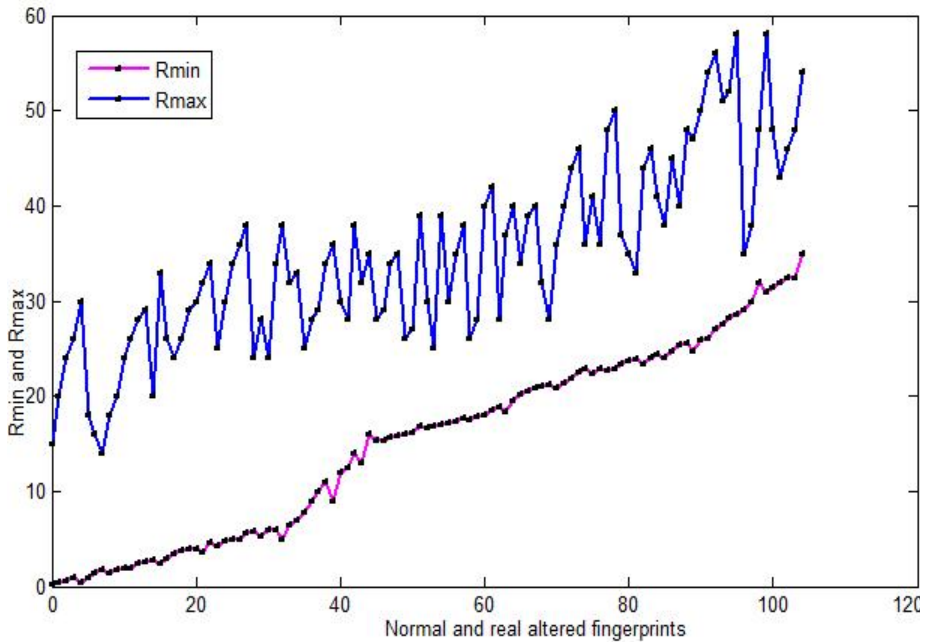


Fig. 5.8 Variation of Rmin and Rmax of enhanced accumulator

The threshold  $H_{th2}$  given in equation (5.2) is not applicable for enhanced accumulator since the mean is almost equal to zero due to negative peaks. Absolute value (modulus) of the negative and positive peaks of enhanced accumulator  $R$  is denoted as  $Rmin$  and  $Rmax$  respectively.  $Rmin$  and  $Rmax$  are plotted with the increase in ridge ending density in Fig. 5.8 for the same FPs used in Fig. 5.4. It is seen from the Fig. that for all types of fingerprints,  $Rmax$  is nonlinearly varying and is not suitable for alteration detection and classification. The value of  $Rmin$  is linearly increasing with the increase in ridge ending density. In fact the enhancement improved the classification accuracy by reducing the FPR. An alteration classification algorithm is developed based on experiments on real altered fingerprint. It is observed that for obliteration type of alteration, the value of  $Rmin$  is greater than or equal to 25. For distortion type of alteration  $Rmin$  lies in between 20 and 25. For imitation type,  $Rmin$  varies between 15 and 20. In case of normal

fingerprints, value of  $R_{min}$  is less than 10. The classification algorithm is shown in Fig. 5.9.

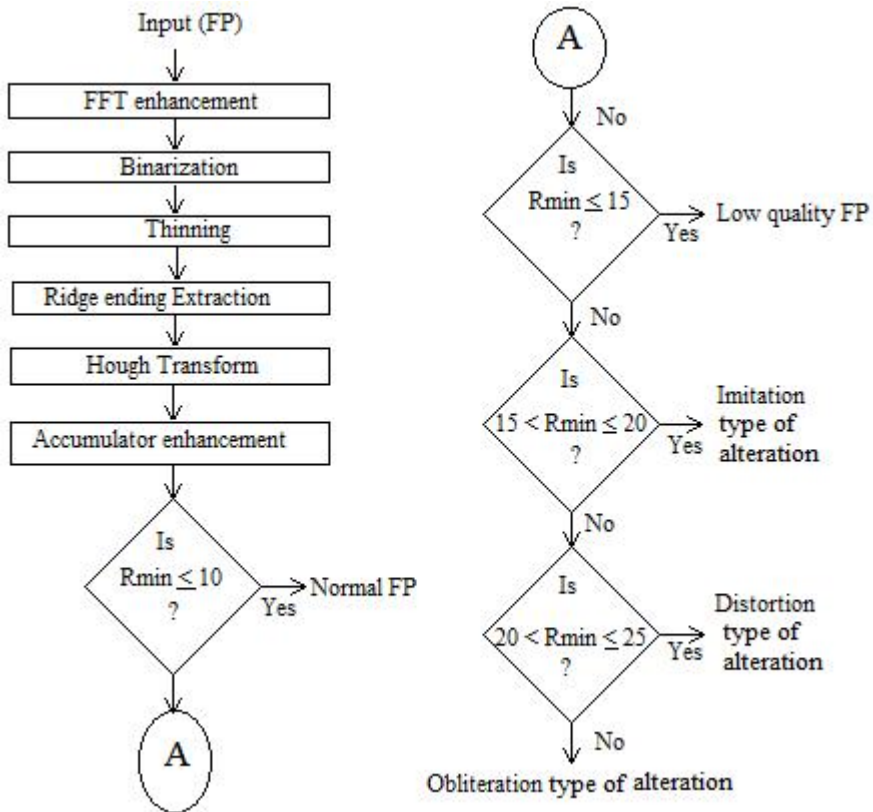


Fig. 5.9 Algorithm for classification of given FP into normal, low quality and different types of altered FP.

### 5.3. Separation of Natural Scar from Altered Scar

Popular methods used for scar detection are Gabor filtering and average filtering followed by thresholding [163]. Scar detected from normal and altered FP by average filtering and thresholding is shown in Fig. 5.10. Fig. 5.10(a) shows scar detected from normal FP and 5.10(b) and (c) shows scar detected from altered FPs.



Presence of scar in normal FP increases the chance of classifying normal FP as altered one.

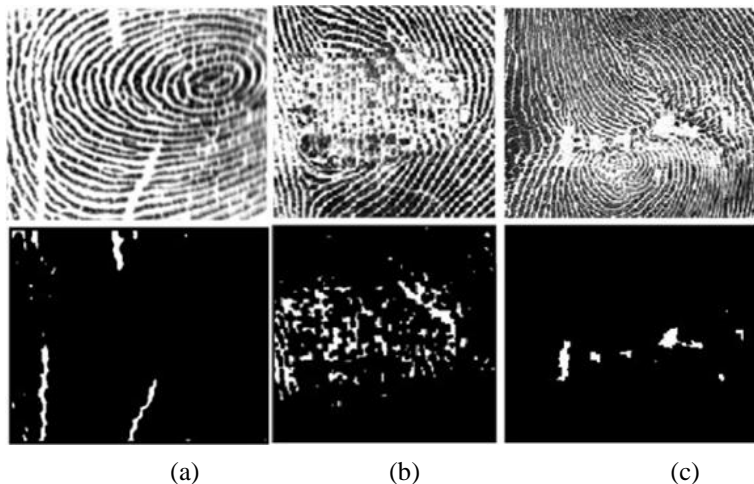


Fig. 5.10 (a) scar in normal Fingerprint, (b) and (c) scar in altered fingerprints

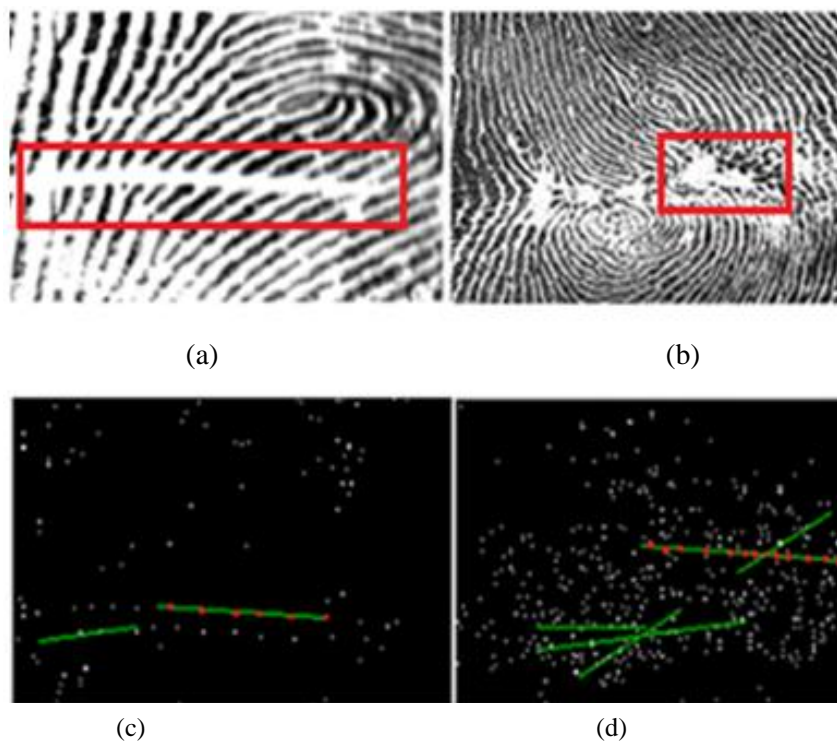


Fig. 5.11 (a) Normal FP with scar, (b) Altered FP with scar, (c) line detected from ridge ending image of normal FP, (d) line detected from ridge ending image of altered FP

Rectangle drawn in the FP images in Fig. 11(a) and (b) shows scar present in normal and altered FP respectively. Ridge end points are detected from these images. Fig. 5.11 (c) and (d) shows the lines detected by Hough transform from ridge ending images indicating that the number of collinear ridge endings at the boundary of the natural scar is less than that in the altered scar. Thus the peak in the Hough accumulator of altered fingerprint scar is higher than that of natural scar. Hence it is possible to separate the natural scar from altered scar by setting a threshold in the Hough accumulator.

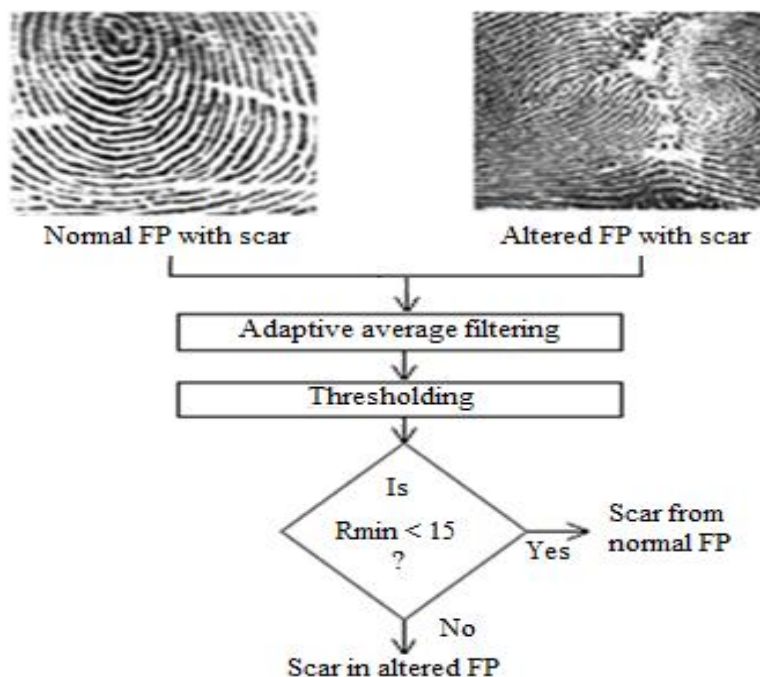


Fig. 5.12 Classification of Scar

Experiments are conducted on normal fingerprint having scar along with scar type of altered FP. It is seen that fingerprints with  $Rmin < 15$  is classified as normal fingerprints with scar and  $Rmin > 25$  is classified as altered one with scar. Fig. 5.12 shows the classification algorithm.



## 5.4. Database

An altered FP database consisting of real and synthetically altered fingerprints is used for the experiments. Fig 5.13 and 5.14 shows some of synthetically altered fingerprints from the database. Real altered FPs of 60 numbers consisting of all types of alteration along with normal FPs is used to set the threshold for classification. Using this threshold, the algorithms are tested with a database of 60 normal FPs, 60 numbers of each of synthetically made altered FPs of obliteration, imitation and distortion.



(a) Obliteration type synthetically altered FP



Fig. 5.13 (b) Distortion type synthetically altered FP



Fig. 5.14 Imitation type synthetically altered FP.

## 5.5. Results

The proposed method is tested on synthetically altered FP database of all types of alteration. Result of classification before and after the Hough accumulator enhancement is tabulated in terms of TPR and FPR. Consider the case of imitation as positive class. Then the classification of imitation as imitation gives TPR and classification other class as imitation gives FPR.

### 5.5.1. Classification Based on Normal Hough Accumulator

Table 5.1 and 5.2 gives the classification results using threshold  $H_{th1}$ . Out of 60 normal FPs, 7 images were classified as imitation and 4 as distortion (See row for normal FP in table 5.1). Out of 60 imitation types of images, 3 FPs classified as normal, 12 as distortions and 6 images classified as obliteration. Five images of distortion classified as obliteration and 30 images classified as imitation. For obliteration type, 5 images are classified as imitation and 32 images are classified as distortion. Table 5.2 gives the classification rate in terms of TPR and FPR. The

classification of normal FP as normal one belongs to TPR and classification of other FP as normal one belongs to FPR. Similarly this is calculated for other type of altered FP.

Table 5.1. Classification results on altered and normal FP using  $H_{th1}$

FP images	No. of FP	No. of FP classified as			
		Normal FP	Imitation	Distortion	Obliteration
Normal	60	49	7	4	0
Imitation	60	3	39	12	6
Distortion	60	0	30	25	5
Obliteration	60	0	5	32	23

Table 5.2 Classification results using  $H_{th1}$  in terms TPR and FPR

<i>Fingerprints</i>	<i>TPR in %</i>	<i>FPR in %</i>
Normal FP(60 images) $H_{th1} = 6$	81.667	1.667
Imitation(60 images) $6 < H_{th1} = 10$	65	23.33
Distortion(60 images) $10 < H_{th1} = 13$	41.667	26.667
Obliteration(60 images) $H_{th1} > 13$	38.33	6.11

Table 5.3 Classification results using threshold  $H_{th2}$ .

FP images	No. of FP	No. of FP classified as			
		Normal FP	Imitation	Distortion	Obliteration
Normal	60	56	2	0	2
Imitation	60	1	44	11	4
Distortion	60	0	14	41	5
Obliteration	60	0	0	17	43

Table 5.4 Classification result using  $H_{th2}$  in terms of TPR and FPR

<i>Fingerprints</i>	<i>TPR in %</i>	<i>FPR in %</i>
Normal FP(60 images) $H_{th2} = 3$	93.33	0.56
Imitation(60 images) $3 < H_{th2} = 5$	73.33	8.89
Distortion(60 images) $5 < H_{th2} = 7.5$	68	15.55
Obliteration(60 images) $H_{th2} > 7.5$	71.66	6

Table 5.3 and 5.4 gives the classification results of threshold  $H_{th2}$ . Comparison of table 5.2 and 5.4 shows that the performance of  $H_{th2}$  is better than  $H_{th1}$ .

### 5.5.2. Classification Based on Enhanced Hough Accumulator

Table 5.5 shows the result of enhanced accumulator on testing database. Out of 60 normal FP images, 49 images are classified as normal FP, 5 images are classified as imitation, 4 images are classified as distortion and 2 images as obliteration (see row wise). Out of 60 imitation type of altered FP, 51 images classified as imitation, 4 images are classified as normal FPs, 3 FPs as distortion and 2 images as obliteration. Similarly the distortion and obliteration are also classified. Based on the table 5.5, TPR and FPR are calculated and is tabulated in table 5.6. The comparison of table 5.4 and 5.6 shows that, after enhancement, TPR is increased and FPR is reduced except for normal FP.

Table 5.5 Classification results on altered and normal FP using  $R_{min}$

FP images	No. of FP	No. of FP classified as			
		Normal FP	Imitation	Distortion	Obliteration
Normal	60	49	5	4	2
Imitation	60	4	51	3	2
Distortion	60	0	4	46	10
Obliteration	60	0	4	4	52

Table 5.6 Classification results using Rmin in terms of TPR and FPR

FP images	TPR in %	FPR in %
Normal FP	81.667	2.22
Imitation	85	7.22
Distortion	76.67	6.11
Obliteration	86.67	7.78

### 5.5.3. Two Stage Classification

Based on above results, a two stage classification algorithm is developed. A given FP is first classified as normal or altered based on  $H_{th2}$ . If it is classified as normal, the process ends. Otherwise it is again classified using enhanced Hough Accumulator. The results of two-stage classification are given in tables 5.7, 5.8 & 5.9.

Table 5.7 Altered Detection by  $H_{th2}$

FP	No. of FP	No. of FP Classified as		TPR in %	FPR in %	FNR in %
		Altered FP	Normal FP			
Altered FP	180	179	1	99.44	-	0.55
Normal FP	60	4	56	93.33	6.677	

Table 5.7. shows the result of first stage. When Altered fingerprint is taken as positive class, the detection of altered FP as altered one is TP detection and detection of altered FP as normal one is FN (False Negative) detection. Similarly, when real FP is taken as positive class, a real FP detected as real is a TP detection and a real FP detected as altered is a FP detection. Out of 180 altered FP, 179 FP is detected and 4 of normal FP is false detected as altered FP. Thus the corresponding TPR, FPR and FNR are given in table 5.7. First stage produced FNR of 0.55%. Detected altered FP goes to second stage. Table 5.8 and 5.9 shows the classification result in second stage. The number of FP in imitation type is reduced from 60 to 59

since one FP is falsely classified as normal one. Distortion and obliteration remains at 60 numbers each. The advantage of two stage classification is that possibility of classification of all types of altered FP as normal one can be reduced since all these FPs are already declared as altered FP in first stage. If the value of Rmin of these altered FP goes less than the threshold of normal FP, it is taken as imitation type. This is due to the fact that the probability of classification of obliteration and distortion as normal FP is very less (see table 5.5) Out of 59 imitation type, three FPs are classified as distortion and two FP classified as obliteration (see table is 5.8). Left behind 54 FPs are correctly classified. Out of 60 distortion type, 4 and 10 FPs are falsely classified as imitation and obliteration respectively. Similarly, 4 each of obliteration is classified as imitation and distortion. Lingering 46 of distortion and 52 of obliteration is properly classified. Table 5.9 shows the resultant TPR and FPR. As compared to the classification result of Rmin alone, the two stage classification performs better since there is increase in TPR and decrease in FPR.

Table 5.8 Classification results using Rmin in second stage

FP images	No. of FP	No. of FP classified as		
		Imitation	Distortion	Obliteration
Imitation	59	54	3	2
Distortion	60	4	46	10
Obliteration	60	4	4	52

Table 5.9 Classification results in second stage in terms of TPR and FPR

FP images	TPR in %	FPR in %
Imitation	91.52	6.667
Distortion	76.67	5.83
Obliteration	86.67	10

#### 5.5.4. Classification of Scar

Classification of scar is performed by the parameter Rmin. The algorithm developed for classification of scar is tested on a database consisting of 30 images each of normal scar and altered scar FP. Table 5.10 shows the results in terms of percentage

of detection. It detected 85% of altered FP with scar and 83.33% of normal FP with scar.

Table 5.10 Classification results on altered and normal FP scar

FP images	Detection rate in %
Altered Scar	85
Normal scar	83.33

### **5.5.5. Comparison with State of the Art Algorithm**

Altered FP detection performance of the proposed method is compared with the method proposed by Soon and Jain [13] which uses minutiae density and orientation field discontinuity as feature for altered FP detection.

Table 5.11 Comparison results on altered detection

Method	TPR in %	FPR in %
Proposed( $H_{th2}$ )	99.44	2.22
Proposed(Rmin)	97.778	18.33
Existing algorithm	87.5	40

Performance comparison is done using synthetically altered FP database consist of all types of alteration and normal FPs. Table 5.11 shows the TPR and FPR for the two methods. Existing algorithm produced a FPR of 40% since it detected normal FP as imitation type of altered FP.

## **5.6. Conclusion**

Ridge ending density is increased as we go from normal FP to obliteration type of altered FP. The ridge ending present in the fingerprint images are collinear. As ridge ending density varies, the number of collinear ridge points also varies. This fact helped us to make use of Hough transform for alteration detection and

classification. Classification accuracy of normal Hough accumulator is less. To overcome this, accumulator has enhanced to make the peak more prominent than other cell values. Maximum value of the enhanced Hough accumulator ( $R_{max}$ ) varies randomly with respect to normal and altered fingerprints. The parameter  $H_{th2}$  is used for alteration detection and absolute value of the minimum of the enhanced accumulator ( $R_{min}$ ) is used for alteration classification due to its linear variation with respect to increase in ridge ending density. The classification fails when area of alteration is very less. A two stage classification method is also implemented.  $H_{th2}$  is used to detect the altered FP and  $R_{min}$  is used to classify these detected FP into three types.  $H_{th2}$  in alteration detection has produced  $FNR < 1\%$ . This method improved the classification accuracy as compared to classification by  $R_{min}$  alone.



# Chapter 6

## Orientation Field Reconstruction

---

### **Abstract**

This chapter illustrates the proposed method for ridge orientation field reconstruction of altered FP based on orthogonal wavelet transform. The ridge orientation is represented as a complex function and the real and imaginary part of the complex function is decomposed using orthogonal wavelet transform and reconstructed using the approximation coefficients. The ridge orientation is reconstructed from approximated real and imaginary parts of the complex function. The selection of correct level of decomposition for optimum reconstruction is discussed. Three orthogonal wavelets are compared based on reconstruction performance.



The different processes used for FP alteration are cutting and abrasion with blades, burning, application of strong chemicals and surgery. These processes create the discontinuous ridge orientation field in the altered region. Ridge orientation field reconstruction of obliteration type of alteration is possible and that of distortion and imitation type are not possible since these are produced by transplantation of ridge structure. This chapter presents a method proposed for orientation reconstruction using orthogonal wavelet transform.

Orientation estimation methods in literature can be categorized into two groups [56][61]. They are approximation methods and deterministic mathematical model. They can also be classified according to whether they need prior information about the position and type of singular points. Most of the approximation-based methods do not need the prior information about the singular points to estimate the orientation field. In approximation-based method, the orientation field is represented as series of basis function with corresponding coefficients. Once this representation is complete, orientation can be modeled by finding the approximation coefficients. The proposed method belongs to approximation-based method and it does not take any prior information about the singular points.

## **6.1. Transformation of Orientation Into Continuous Complex Function**

Denoting  $\theta(x, y)$  as orientation and  $U(x, y)$  as transformed function, the mapping can be described as [3]

$$U = \text{Re } U(x,y) + i \text{Im } U(x,y) = \cos 2\theta - i \sin 2\theta \quad (6.1)$$

where RE and IM denote respectively the real and imaginary part of complex function  $U(x, y)$ . The orientation angle  $\theta(x, y)$  can be easily reconstructed from the values of  $\text{RE}(x, y)$  and  $\text{IM}(x, y)$  using the equation (4.8).

In general, the approximation of a two dimensional function  $f(x, y)$  is performed by expanding it using a basis function and finding out the coefficients [4]. This is explained by the following equation.

$$f(x, y) = b_1 U_1(x,y) + b_2 U_2(x,y) + \dots + b_k U_k(x,y) + e(x,y) \quad (6.2)$$

where  $b$  is the coefficients to find out,  $U(x,y)$  is the basis function and  $e(x,y)$  is the error between original and approximated function. In wavelet multiresolution approximation, at a decomposition level of  $k$ ,  $f(x, y)$  can be decomposed as

$$f(x, y) = d_1 + d_2 + d_3 + \dots + d_k + A_k \quad (6.3)$$

where  $d_1, d_2, d_3$  and  $d_k$  are the detailed coefficients at the corresponding levels and  $A_k$  is the approximation coefficients at the level  $k$ [4]. Hence an orthogonal wavelet is chosen as the basis function in this work.

Comparison of the images of  $\sin^2(x, y)$  and  $\cos^2(x, y)$  of normal and altered FP shows that the alteration process introduced more irregularity or discontinuity. These images are decomposed using orthogonal wavelet and energy of the approximation and detailed coefficients are compared. This comparison is made on number of images and the result reveals that the energy of the detailed coefficients of  $\sin^2(x, y)$  and  $\cos^2(x, y)$  of altered FP is higher than that of normal FP while energy of approximation coefficients of  $\sin^2(x, y)$  and  $\cos^2(x, y)$  of altered FP is less than that of normal FP. This suggests that alteration increases high frequency components or irregularity in the real and imaginary part of complex function. Thus the sum of detailed coefficients in equation (6.3) can be taken as error function  $e(x, y)$ . Accordingly equation (6.3) becomes

$$f(x, y) = e(x, y) + A_k \quad (6.4)$$

where  $e(x, y)$  is the sum of detailed coefficients ( $e(x, y) = d_1 + d_2 + d_3 + \dots + d_k$ ). The equation (6.4) is similar to equation (6.3). To make  $f(x, y)$  equal to the approximated function,  $e(x, y)$  is taken as zero. Thus the real and imaginary part of

complex function can be reconstructed from the approximation coefficients by keeping the detailed coefficients to zero at every stage. The block diagram of proposed method of orientation reconstruction is shown in Fig. 6.1.

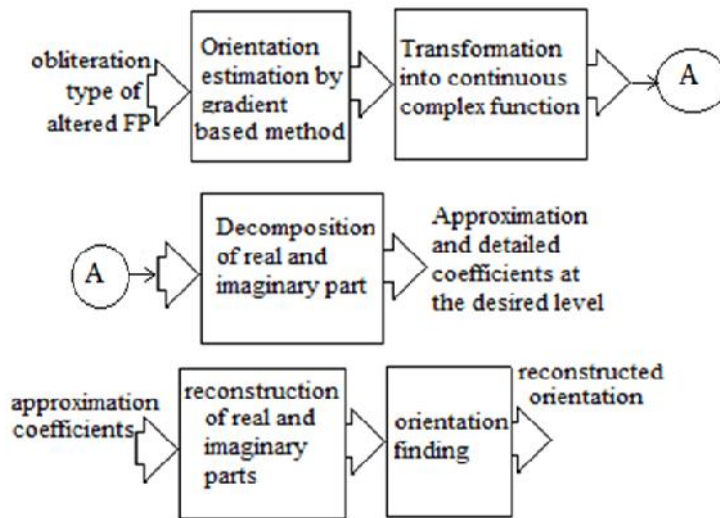


Fig. 6.1 Block diagram of the proposed method

Decomposition of real and imaginary parts are performed according to the equation

$$w_{\phi}(j_0, m, n) = \frac{1}{MN} \sum_{x=0}^{M-1} \sum_{y=0}^{N-1} f(x, y) \cdot j_{0,m,n}(x, y) \quad (6.5)$$

$$w_{\psi}^i(j, m, n) = \frac{1}{MN} \sum_{x=0}^{M-1} \sum_{y=0}^{N-1} f(x, y) \cdot i_{j,m,n}(x, y) \quad (6.6)$$

where  $i=\{H,V,D\}$ ,  $j_0$  is an arbitrary starting scale,  $w(j_0,m,n)$  define the approximation coefficients and  $w_{\psi}^i(j, m, n)$  defines the detailed coefficients in horizontal, vertical and diagonal directions. Reconstruction of  $\sin 2\theta(x, y)$  and  $\cos 2(x, y)$  is performed according to equation (6.7) by keeping  $w_{\psi}^i(j, m, n)$  to zero in every stage.

$$f_{rec}(x, y) = \frac{1}{MN} \sum_n \sum_n w_\phi(j_0, m, n) \phi_{j_0, m, n}(x, y) + \frac{1}{MN} \sum_{i=H, V, D} \sum_{j=j_0}^{\infty} \sum_m \sum_n w_\psi^i(j, m, n) \psi_{j, m, n}^i(x, y) \quad (6.7)$$

## 6.2. Selection of Level of Decomposition

The selection of level of decomposition depends upon whether the image is smoother or not. If the irregularity present in the image is higher, level of decomposition to decay the detailed coefficients is increased. More smoother the function  $f(x, y)$ , then faster the decay of detailed coefficients so that the level of decomposition is also reduced. Fig. 6.2 shows the normal FP and its altered version.



Fig. 6.2 (a) Normal FP

(b) Altered FP

Fig. 6.3(a) and 6.3(b) shows  $\sin^2(x, y)$  and  $\cos^2(x, y)$  of normal FP and altered FP respectively of fig. 6.2. Irregularity found in the images of  $\sin^2(x, y)$  and  $\cos^2(x, y)$

of altered FP corresponds to the cause of discontinuity in the ridge orientation field. Consequently, the level of decomposition increases.

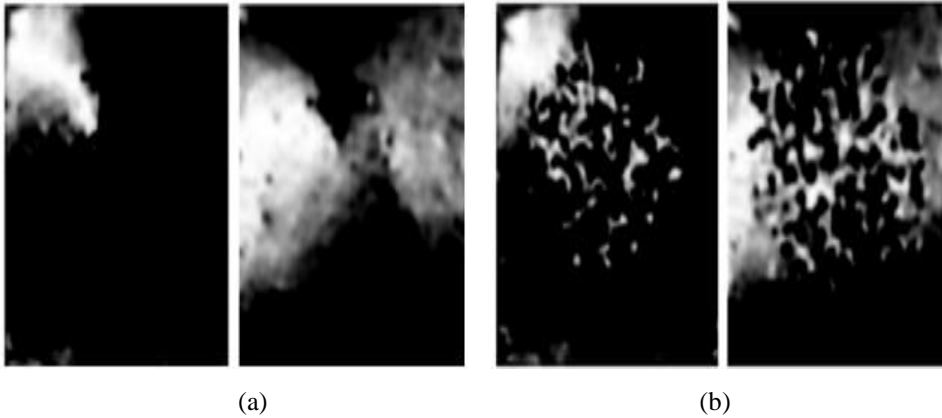


Fig. 6. 3 (a)  $\sin^2(x,y)$  and  $\cos^2(x,y)$  of normal FP, (b)  $\sin^2(x,y)$  and  $\cos^2(x,y)$  of altered FP

In order to select the correct level of decomposition, ridge orientation difference (ROD) is computed. The ridge orientation difference is defined as difference between reconstructed ridge orientation of altered FP and ridge orientation of its unaltered mates and is found using the equation 6.8 given below.

$$ROD = \min (| \theta_{un}(i, j) - \theta_{rec}(i, j) |, -| \theta_{un}(i, j) - \theta_{rec}(i, j) |) / \sqrt{2}, \quad (6.8)$$

where  $\theta_{un}(i, j)$  is the orientation of unaltered mate and  $\theta_{rec}(i, j)$  is the reconstructed orientation. Fig. 6.4 shows the ridge orientation difference map for different levels of decomposition. From the Fig., it is clear that as the levels of decomposition increases ROD decreases up to level 6 and then again it increases. At 7<sup>th</sup> and 8<sup>th</sup> levels of decomposition, ridge orientation difference is increasing because of the fact that necessary information for restoration is lost. Since 6 levels of decomposition produce minimum ROD, it is selected as optimum level of decomposition for this study.

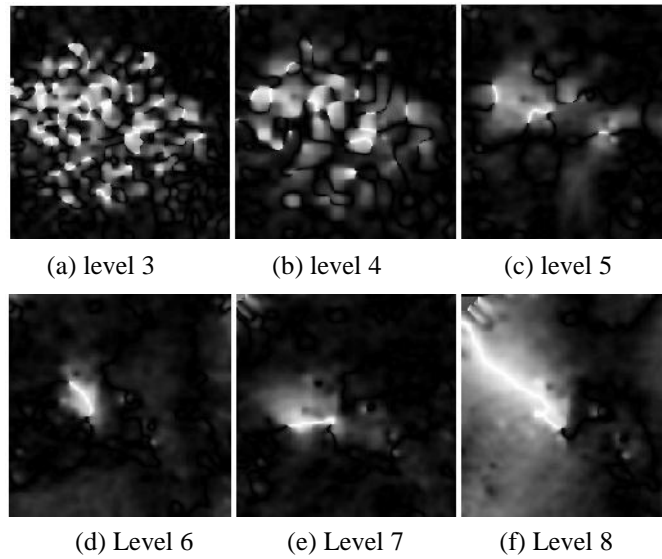


Fig. 6.4 R.O.D. map of FPs reconstructed from different levels of decomposition

Fig. 6.5 show the reconstructed orientation of altered FP given in Fig. 6. 2 (b) at different levels of decomposition. Fig. 6.5(a) shows the orientation of unaltered mate. The approximated orientation at level 6 is similar to the orientation of unaltered mate. Daubchies wavelet db5 is used for reconstruction.

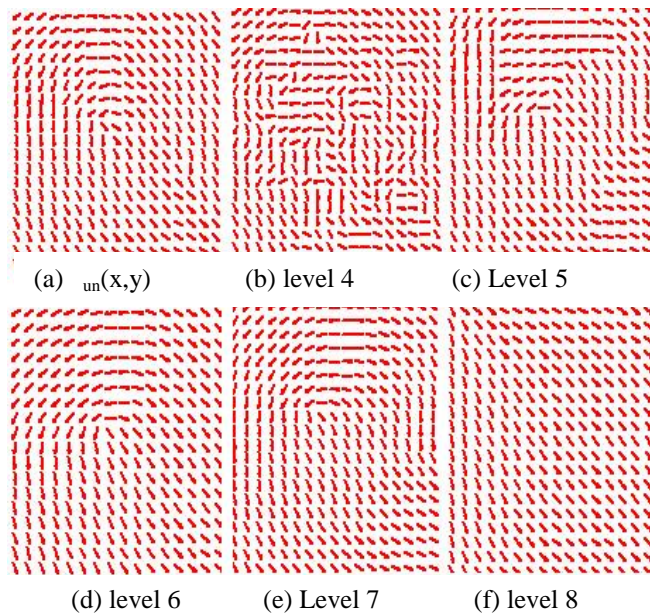


Fig. 6.5(a) Orientation of unaltered mate, (b), (c), (d), (e) & (f) reconstructed orientation of altered FP at different levels.

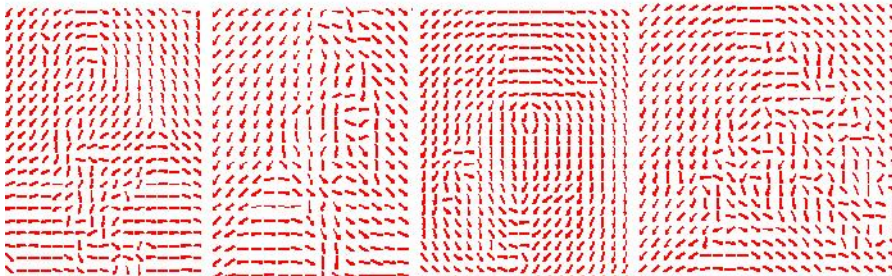


### 6.3. Comparison of Orthogonal Wavelets

Even though the wavelets are similar in orthogonal property, other characteristics are different. In fact a comparison of different wavelets on ridge orientation reconstruction is needed to find out an orthogonal wavelet which gives maximum output in terms of approximation. Performance of Daubichies (db5), Symlet (sym5) and Coiflet (coif5) wavelets on ridge orientation approximation is compared based on ROD map.



(a) Altered FP



(b) Orientation of altered FP

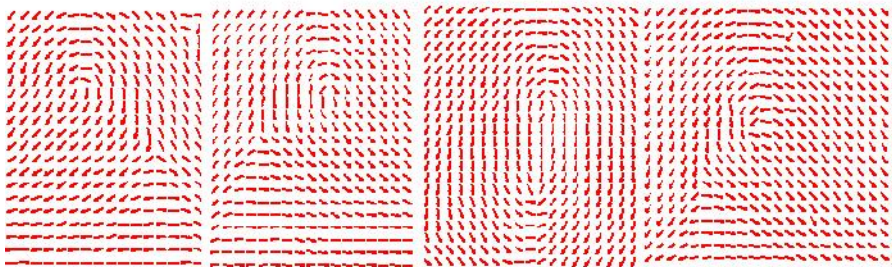


Fig. 6.6 (c) Orientation of unaltered FP mates

The ROD map between approximated ridge orientation and orientation of its unaltered mates is found as explained in equation (6.8). Fig. 6.6 shows the altered FP and its orientation. It also shows the orientation of unaltered mates. The orientation field difference for the altered FPs given in Fig. 6.6 (a) with different wavelet is shown in Fig. 6.7. Performance of the proposed method is good at all regions except at singular point. All orthogonal wavelets produced error at the core points during ridge orientation field reconstruction.

Out of three wavelets, the performance of *coif5* is better at the singular points. Fig. 6.7(c) shows that the error produced by *coif5* wavelet at the singular point is less especially at delta point. Hence *Coiflet* wavelet is more accurate at singular points than *Symlet* and *Daubichies*. Based on this comparison, *coif5* is selected for orientation approximation of altered FP.

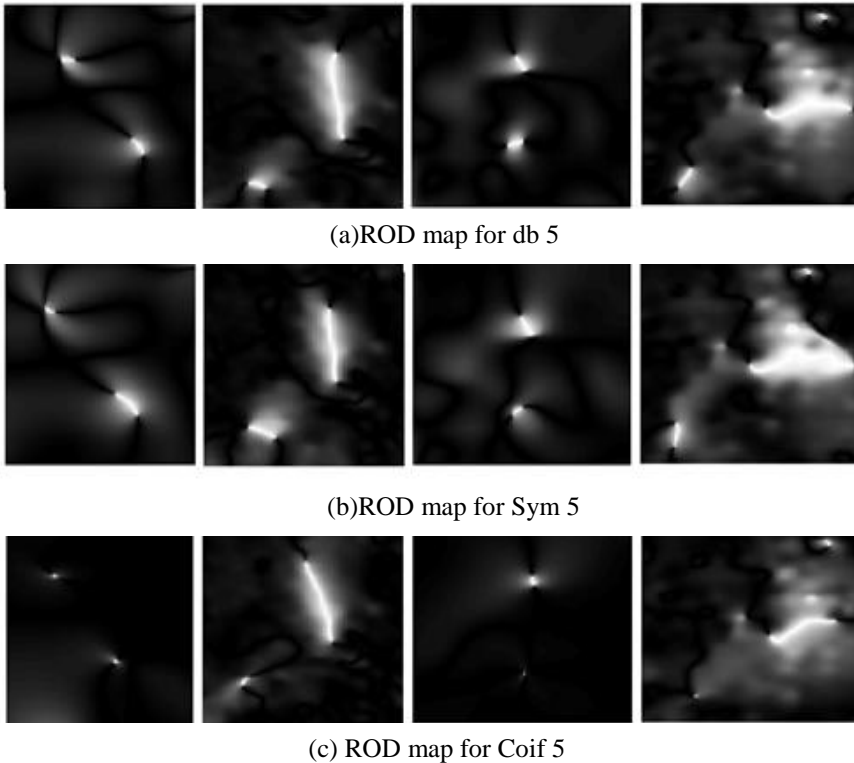
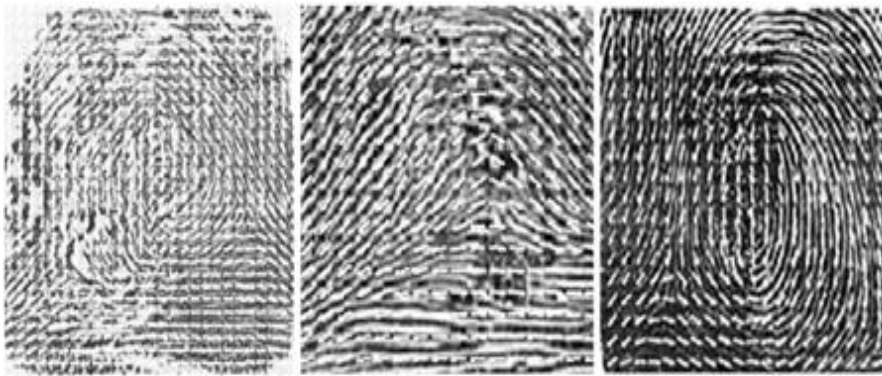


Fig. 6.7 ROD map of altered FP given in Fig. 6.6 (a) for different orthogonal wavelets

## 6.4. Results

The proposed method is tested on real altered FPs, synthetically altered FP and low quality FP images.

### 6.4.1. Reconstructed Orientation of Altered FPs



(a) Reconstructed orientation of Mutilation type of altered FP

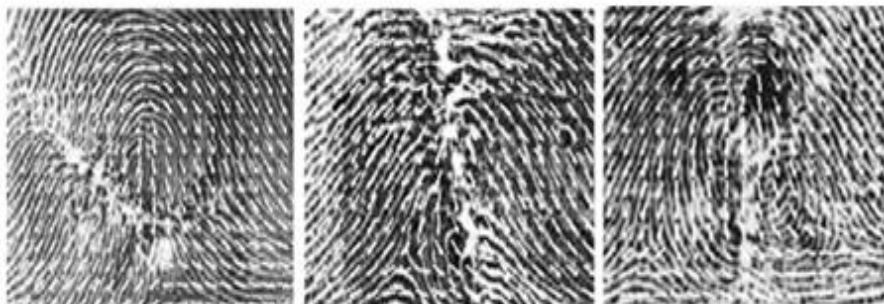


Fig. 6.8 (b) Reconstructed orientation of Scar type of altered FP

The proposed method is tested on real altered FP obtained from NIST SD14 database. Fig. 6.8 shows the approximated ridge orientation field by the proposed method on both scar and mutilated type of altered FPs. Coiflet wavelet with  $N=5$  is used for reconstruction. Orientation at the singular point is also approximated without giving the prior information about its type and location.



### 6.4.2. Reconstructed Orientation of Synthetically Altered FPs



Fig. 6.9 (a), (b) & (c) Synthetically altered FPs

Proposed method is tested on synthetically FPs. Fig. 6.9 shows the synthetically altered FP. Fig. 6.10, 6.11 and 6.12 shows the Ridge Orientation Field (ROF) of its unaltered mates and reconstructed orientation.

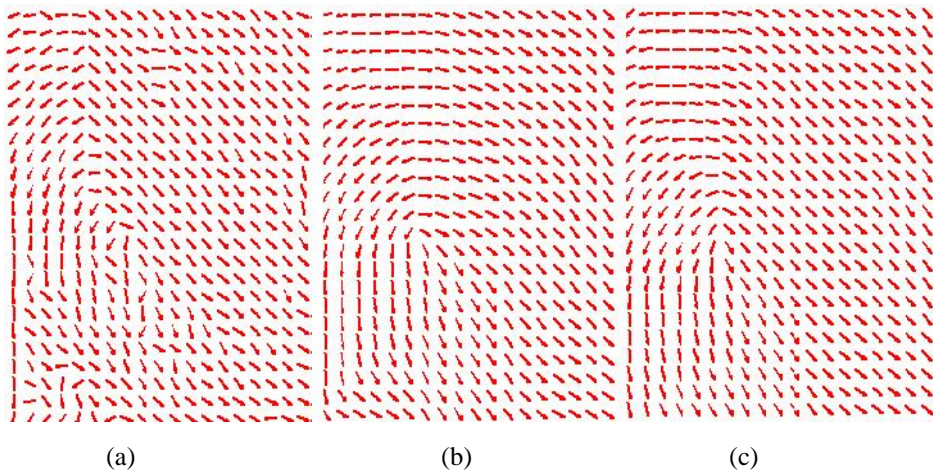


Fig. 6.10 (a) ROF of altered FP in 6.9(a) (b) ROF of unaltered mate (c) Reconstructed ROF

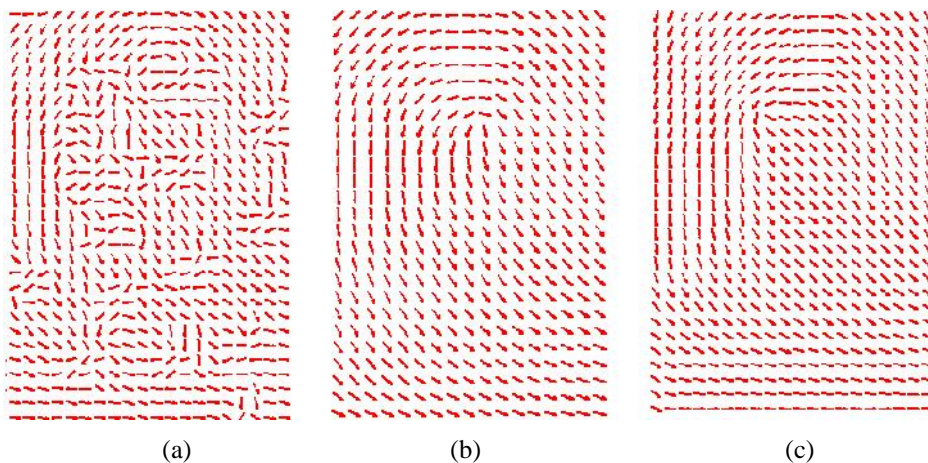


Fig. 6.11 (a) ROF of altered FP in Fig. 6.9 (b), (b) ROF of unaltered mate, (c) Reconstructed ROF

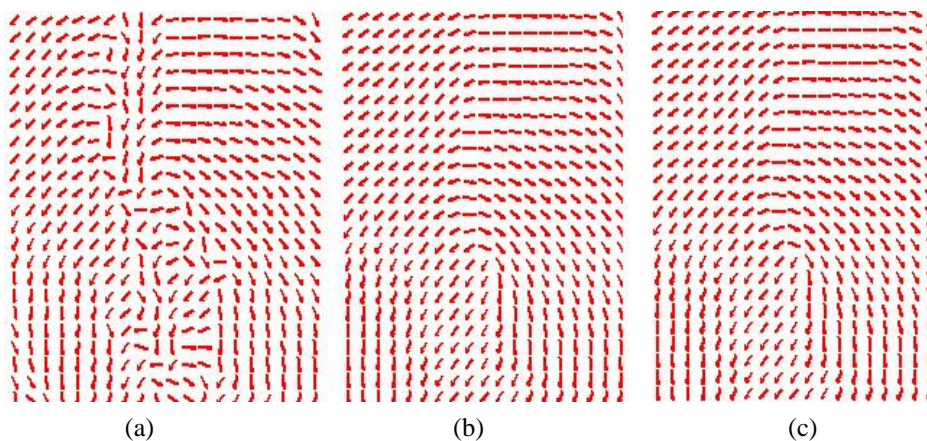


Fig. 6.12 (a) ROF of altered FP in Fig. 6.9 (c), (b) ROF of unaltered mate, (c) Reconstructed ROF

### **6.4.3. Reconstructed Orientation of Low Quality FPs**

FP images become low quality due to various reasons such as pressure applied by the individual on the scanner, non linear distortions, noise, and aging of the people and skin diseases. Orientation estimations with gradient based method fails in low quality images.



Fig. 6.13 Reconstructed orientation of low quality FP.

Dry images have absence of ridges and valleys and wet images do not have well separated ridges and valleys. Fig. 6.13 shows the reconstructed ridge orientation by the proposed method on low quality images obtained from FVC database.

## 6.5. Conclusion

Orthogonal wavelet based ridge orientation reconstruction is proposed in this chapter. The comparison of three orthogonal wavelets on ridge orientation reconstruction is performed and concluded that the Coiflet5 gives better performance than Daubichies5 and Symlet5. Reconstructed ridge orientation is used to match the altered FP against its unaltered mate.

# Chapter 7

## Altered Fingerprint Matching

---

### **Abstract**

This chapter presents a method proposed for matching of obliteration type of altered FP implemented in two stages. After classifying the given FP into obliteration, successful matching is essential since it helps to find the criminals and also prevents the breaking of FP based security system. Altered FP matching can be done in two ways. First method needs the reconstruction or restoration of altered region and matching is performed in the same way as normal FP matching. In second method, matching is performed using the features in the unaltered region. These two methods fail when whole region of the FP is altered. Minutiae based altered FP matching is difficult since the alteration process creates large amount of spurious minutiae. However minutiae based matching is possible if altered area is small. Proposed method uses the reconstructed ridge orientation and features in the unaltered region. A verification of detected altered FP is also performed before going to the matching stage.





Once the detection and classification of altered FP is completed, matching is the next step to conquer the altered FP threats against Automatic Fingerprint Identification System. Matching of altered FP helps to identify the criminals by searching the unaltered mates available in the database.

We have developed a wavelet transform based method for ridge orientation reconstruction in previous chapter. Since this approximated ridge orientation can be used to find out the RD in the altered region, a verification of the alteration detection is performed by using this RD before the matching stage begins. In fact, RD obtained by FFT based enhancement is replaced with that obtained by wavelet based approximation method. This RD is used along with MD and scar to perform the alteration detection.

## **7.1. Verification of Altered Fingerprint Detection**

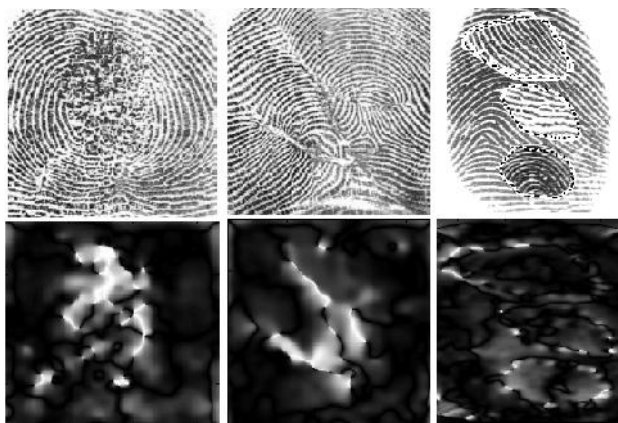


Fig. 7.1 RD obtained by wavelet based approximation

RD is obtained by comparing the wavelet based approximated ridge orientation with original orientation. Minutiae density is determined by Parzen window method and scar is determined by adaptive average filtering and thresholding as explained in chapter 4. Fig. 7.1 shows the RD obtained by wavelet based approximation of

ridge orientation. After the extraction of RD, MD and scar, feature vectors are created and fed into SVM for detection. Once this alteration detection is confirmed, FP goes to Hough transform based classification stage.

## **7.2. Proposed Method**

The FP classified as obliteration type by Hough transform method comes to the matching stage. The proposed matching method uses three features namely Ridge Orientation Field (ROF), Ridge Texture (RT) and Ridge Frequency (RF). RT and RF are extracted from the unaltered region of the altered FP. The computation of a single matching score from these three features is not possible since automatic selection of unaltered region from the altered FP is not possible in one to many matching. Thus the proposed method is implemented in two stages. First stage reduces the number of normal FP to be matched in the second stage so that manual selection of unaltered region becomes easier.

First stage utilizes the approximated ridge orientation for matching. This stage starts with orientation estimation of altered and unaltered mate by orthogonal wavelet based method proposed in previous chapter. Alignment between normal and altered FP is performed by using the estimated orientation. Matching score is computed in terms of Euclidian distance. The altered FP is matched with normal FPs in the database until it becomes successful. The FP goes to next stage once it is successful.

Second stage starts with Region of Interest (ROI) selection from both altered and unaltered FP. Fused matching between RT and RF is computed to confirm the successful matching of the first stage. A matching is declared as successful, if genuine match occurs in both the stage. Fig. 7.2 shows the block diagram of the proposed method.

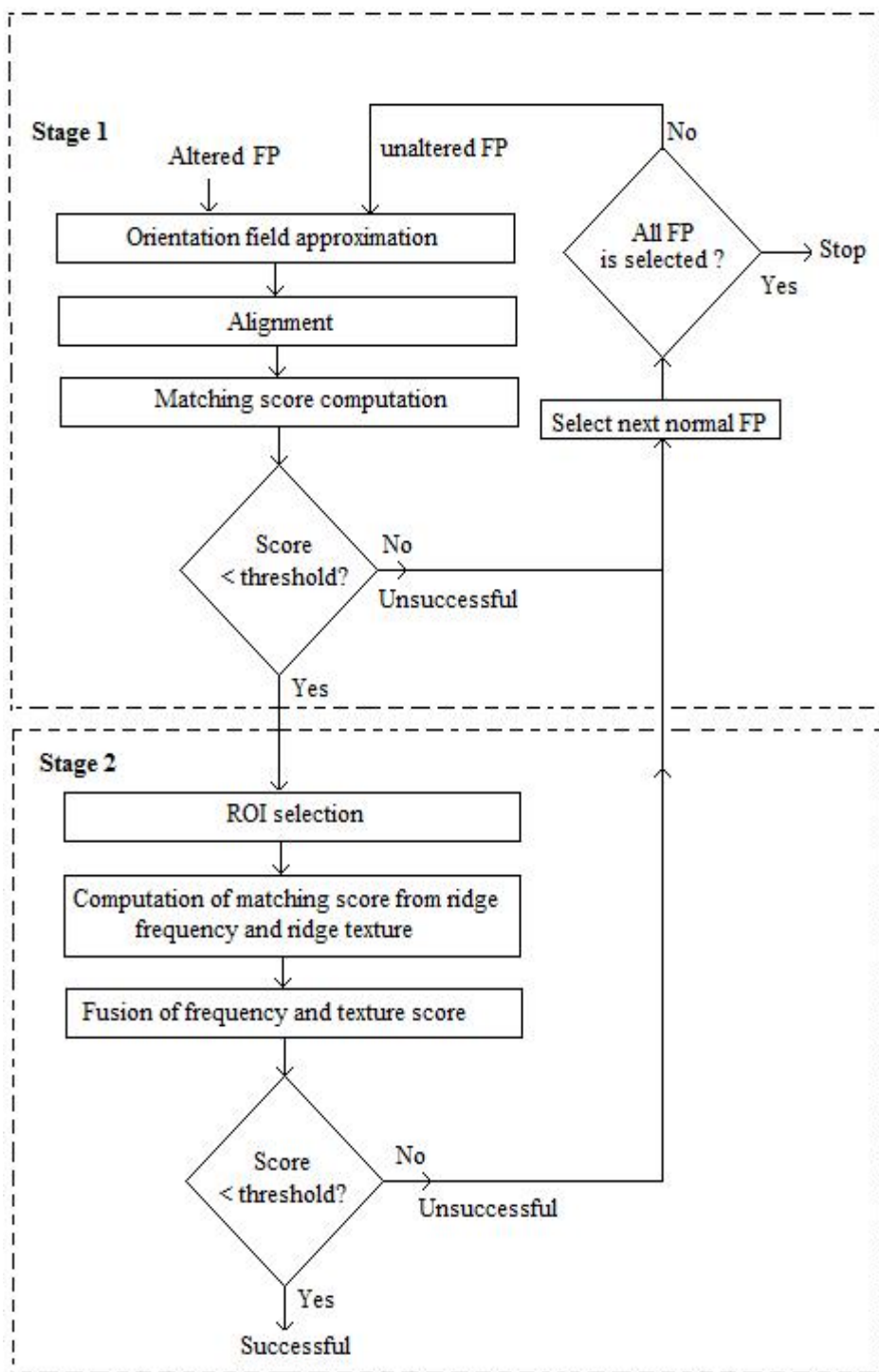


Fig. 7.2 Block diagram of the proposed method

### 7.3. Ridge Orientation Based Matching (Stage 1)

Alignment of the FP and its mate is an important step in FP matching to compensate the rotation of the image, which is taken place during scanning process. Alignment is usually performed by taking the core and delta points as reference points. Identification of these points in altered FP is difficult since these points sometimes belong to the altered region. Thus, the orientation field has used to perform the alignment.

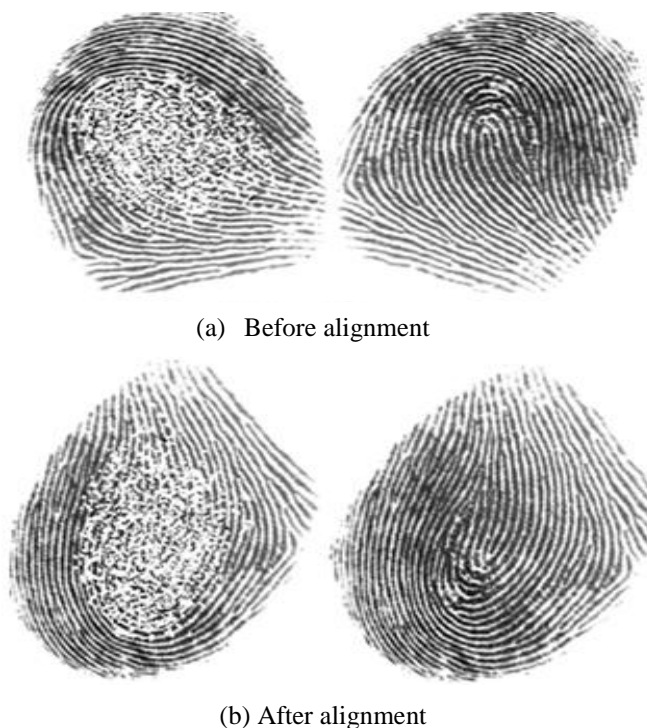


Fig. 7.3 Altered and its unaltered mate

Ridge orientation of altered FP is reconstructed using orthogonal wavelet based approximation as explained in chapter 6. This reconstructed orientation is used to match the altered FP against the orientation of its unaltered mate. The orientation field of the unaltered mate is also found using the orthogonal wavelet transform based approximation. These two orientations are used to perform alignment of the

two FPs to prevent the unsuccessful matching of the FP due to rotation. The alignment of the fingerprints is performed in such a way that both fingerprints are rotated to make the ridges points to the vertical direction. Fig. 7.3(a) shows the altered FP rotated in anticlockwise direction and its unaltered mate rotated in clockwise direction. Fig. 7.3(b) shows the two fingerprints after performing the alignment. Ridge direction of both altered and unaltered mates point to the vertical direction. These aligned fingerprints are used in all the successive stages of matching.

### 7.3.1. Orientation Based Matching Score

Matching score based on ridge orientation field is computed using the method proposed by [17]. Let the reconstructed orientation of altered FP and orientation of its unaltered mates are denoted as A and B respectively. Take ‘ $\cap$ ’ as the common area of intersection from two orientation fields and N as the total number of points in  $\cap$ . Then matching score between two orientation fields A and B is computed as follows.

$$s(A, B) = \frac{1}{N} \sum_{(i,j) \in \Omega} \theta(i, j) \quad (7.1)$$

In (6.1),  $\theta(i, j)$  is the difference between the orientation values at the point,  $(i, j)$  in A and B which is given as

$$\theta(i, j) = \theta_0(i, j), \quad \text{if } \theta_0(i, j) \leq \pi/2 \quad (7.2)$$

$$\theta(i, j) = \pi - \theta_0(i, j), \text{ otherwise} \quad (7.3)$$

$\theta_0(i, j)$  is defined as

$$\theta_0(i, j) = | \theta_A(i, j) - \theta_B(i, j) | \quad (7.4)$$

where  $\theta_A(i, j)$  and  $\theta_B(i, j)$  are the direction of point,  $(i, j)$  in image A and B. If the matching score  $s(A, B)$  is higher than a certain threshold, two orientation fields are said to be matched.

## 7.4. Selection of Region of Interest



Fig. 7.4 (a) Altered FP (b) Segmented FP

Automatic segmentation of unaltered region from the altered FP is performed based on ridge discontinuity analysis. If the ridge discontinuity is present, corresponding pixels in both altered and unaltered FP is kept at zero value. This is not effective since some of pixels in the unaltered region also becomes zero. This is shown in Fig. 7.4. Thus the unaltered region or Region Of Interest (ROI) is manually selected.

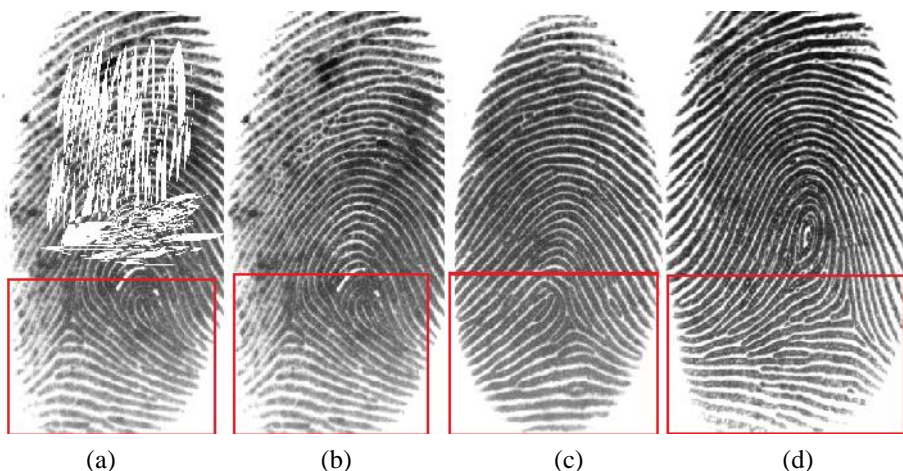


Fig. 7.5 ROI marked as rectangle in (a) Synthetically altered FP, (b) Unaltered mate, (c) & (d) Unaltered FP in the database.



ROI is the unaltered region selected from the altered FP. Before the ROI extraction, alignment is made as explained in section 3. Similar region is also selected from the entire normal fingerprint in the database consisting of unaltered mates. Fig. 7.5 shows the synthetically altered FP and its unaltered mate along with other normal fingerprints. ROI is marked as rectangle in Fig. 7.5. Unaltered region belongs to bottom of the altered FP and hence similar region with same size is selected from normal fingerprints as shown in Fig. 7.5(b), (c) and (d). Selection of unaltered area is performed with respect to position of the altered region. If the alteration is at the bottom region, then the top end region of fingerprint is selected. See Fig. 7.6.



Fig. 7.6 ROI selected from altered FPs

## **7.5. Ridge Frequency Extraction**

After the selection of ROI, RF extraction is done as explained below. The local ridge frequency (or density)  $f_{xy}$  at point  $[x, y]$  is the number of ridges per unit length along a hypothetical segment centred at  $[x, y]$  and orthogonal to the local ridge orientation. A frequency image  $\mathbf{F}$ , analogous to the orientation image  $\mathbf{D}$ , can be defined if the frequency is estimated at discrete positions and arranged into a matrix. The local ridge frequency varies across different fingers, and may also vary

across different regions of the same fingerprint [1]. The method proposed by Hong, Wan, and Jain [126] is used in this paper to estimate ridge frequency. To find the frequency  $f_{ij}$  at a point  $(x_i, y_j)$ , a rectangular window of size  $32 \times 32$  centered at  $(x_i, y_j)$  is considered. Then the window is rotated in such a way that the ridges point in the vertical direction. This is shown in Fig. 7.7.

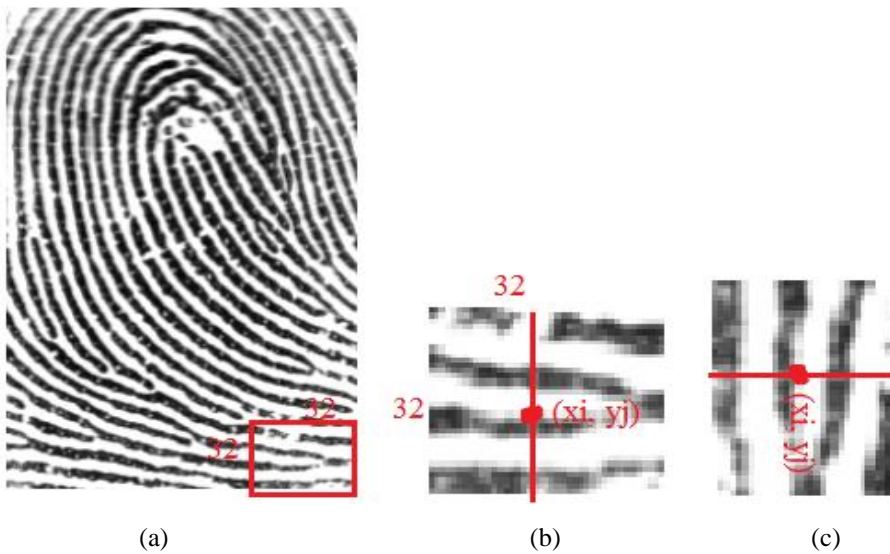


Fig. 7.7 (a)  $32 \times 32$  window is marked with rectangle, (b)  $32 \times 32$  window with center  $(x_i, y_j)$ , (c) Rotated window with ridges points in the vertical direction.

After the rotation, the gray levels in the each column are accumulated to obtain x-signature. This is shown in Fig. 7.8. Then  $f_{ij}$  is determined as the inverse of the average distance between two consecutive peaks of the x-signature.

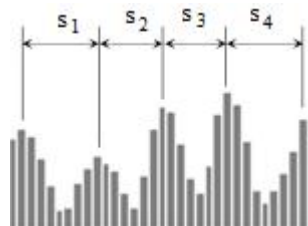


Fig. 7.8 x-signature



Frequency  $f_{ij}$  at  $(x_i, y_j)$  is given by

$$f_{ij} = 4/(s_1+s_2+s_3+s_4) \quad (7.5)$$

Fig. 7.9 shows the ridge frequency obtained.



Fig. 7.9 (a) Fingerprint, (b) Ridge frequency image

## 7.6. Matching Score Computation from Ridge Frequency

Ridge frequency images for both altered FP and normal FP are obtained as explained in section II. These frequency images are decomposed up to four levels using Haar wavelet with respect to equations given below.

$$w_{j_0, m, n} = \frac{1}{MN} \sum_{x=0}^{M-1} \sum_{y=0}^{N-1} f(x, y). \quad w_{j_0, m, n}(x, y) \quad (7.6)$$

$$w_{\psi^i}^i(j, m, n) = \frac{1}{MN} \sum_{x=0}^{M-1} \sum_{y=0}^{N-1} f(x, y). \quad w_{j, m, n}^i(x, y) \quad (7.7)$$

Then the mean of approximation coefficients at the 4<sup>th</sup> level and detailed coefficients at all the levels are found. The Matching score is obtained by finding the Euclidian distance between these two feature vectors as follows.

$$ERF = \sqrt{\sum_{N=1}^{13} ((mRF\_AFP(N) - mFP\_NFP(N))^2)} \quad (7.8)$$

where ERF is Euclidian distance for ridge frequency, mRF\_AFP(N) and mFP\_NFP(N) is the mean of the coefficients of ridge frequency image of altered FP and normal FP respectively. N varies from 1 to 13.

### 7.7. Matching Score Computation from Ridge Texture

The ROI from altered and normal FP is decomposed to fourth level by Haar wavelet to find out ridge texture feature vectors. Procedure followed is same as explained for ridge frequency.

$$ERT = \sqrt{\sum_{N=1}^{13} ((mRT\_AFP(N) - mFN\_NFP(N))^2)} \quad (7.9)$$

where ERT is Euclidian distance for ridge texture, mRF\_AFP(N) and mFP\_NFP(N) is the mean of the coefficients of ridge texture image of altered FP and normal FP respectively.

### 7.8. Matching Score Fusion

Matching scores obtained by ridge frequency features and ridge textures are combined to get a single matching score. This is done by using weighted sum rule [121].

Final matching score EFS is generated as explained in the equation (7.10) below.

$$EFS = \alpha \cdot ERF + (1 - \alpha) \cdot ERT \quad (7.10)$$

where  $\alpha$  varies between 0 and 1. The value of ERT is very high as compared to ERF. Thus  $\alpha$  is taken as 0.98 to normalize ERT to a value in between 0 and 1.

## 7.9. Results and Discussion

An altered FP database consisting of 70 synthetically altered fingerprints is used for the experiments. Normal fingerprints obtained from FVC 2000 and FVC 2004 database is used for creating synthetically altered fingerprints. Each group in this database consists of 8 impressions of 10 fingers and is captured by optical and capacitive sensors. The resolution of each fingerprint is 500dpi. Synthetically altered obliteration of different area is created by making scar and scratches in the image.

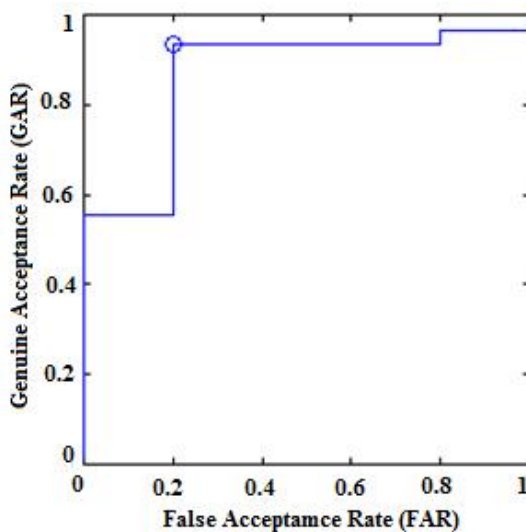


Fig. 7.10: ROC curve for the matching scores in first stage

In one to many matching, one altered FP is matched against all the unaltered FP. The actual mates with matching scores less than a threshold belongs to Genuine match and greater than threshold belongs to false non match. Different FP mates having scores less than threshold is considered as false match. The ROC curve between Genuine Acceptance Rate (GAR) and False Acceptance Rate (FAR) for each stage is plotted. ROC curve gives the performance of the matching system for different threshold. Given the matching score, it computes the GAR and FAR for different thresholds and plotted the graph. ROC curve for first stage is shown in Fig. 7.10 and second stage is shown in Fig. 7.11. The threshold that gives maximum matching results is marked as circle. These cut-off point for best GAR and FAR is 0.2213 and 0.0520 for first and second stage respectively.

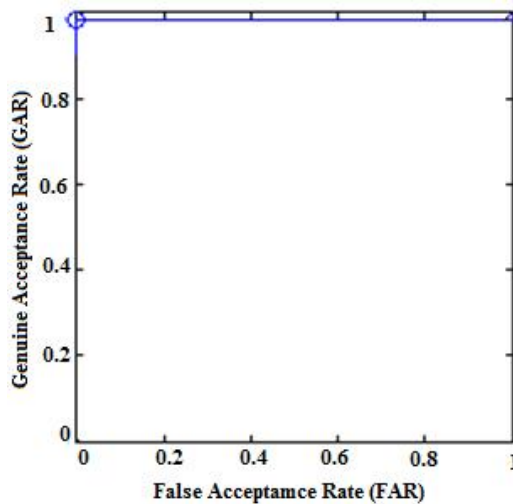


Fig. 7.11 ROC curve for matching scores in second stage.

Table 7.1 shows the GAR and FAR of the proposed method for the optimum threshold found by ROC curves. Two fingerprints image are considered as from same fingertip only when the value of  $s(A, B)$  and EFS are less than 0.2213 and 0.0520 respectively. Different FP mates with matching score less than above mentioned threshold in both stages are considered for FAR. True FP mates with

both matching score less than above mentioned threshold is taken for GAR. The second stage reduced the FAR produced at the first stage.

Table 7.1 GAR and FAR for the thresholds 0.2213 and 0.0520

No. of altered of FP	GAR in %	FAR in %
Altered FP(70)	87.14	0

This method is tested on another database of synthetically altered fingerprints. These fingerprints are created by normal fingerprints obtained from casia fingerprint database. It consists of 70 images of obliteration type. The Table 7.2 shows the results of matching.

Table 7.2 GAR and FAR for synthetically altered FP created from casia

No. of altered of FP	GAR in %	FAR in %
Altered FP(70)	90	3.33

## **7.10. Conclusion**

This chapter presents a two stage method to match obliteration type of altered fingerprint with its unaltered mates. Reconstructed orientation based matching is performed in the first stage and it filter out the non mated fingerprints. In second stage, ridge frequency and ridge texture in the unaltered region of the altered FP is used for matching. Region of Interest selection is performed manually since the automatic selection is difficult. As the number of FP images to be matched increases, the manual ROI selection becomes difficult. The two stage matching reduces this difficulty.



# Chapter 8

## Conclusion and Future Scope

---

### 8.1. Conclusion

This thesis presents a solution to prevent altered FP threats against AFIS by detection, classification and matching using ridge and minutiae features. First step to defeat the altered FP threat is the detection. Chapter 4 proposed a method for altered FP detection based on Minutiae Density (MD), Ridge Discontinuity (RD) and Scar(S). Scar is an important feature present in altered FP since all process of alteration creates the absences of ridges and valleys. Scar detection is performed by average filtering and thresholding. Extraction of scar from low quality FP images is difficult. This difficulty is overcome by changing the window size with respect to dryness of the FP. Thus the average filtering process becomes adaptive. It is concluded that addition of scar increases the TPR and decreases FPR as compared to the methods proposed in literature.

Once the detection of altered FP is performed, it needs to be automatically classified into different types to take appropriate countermeasures and also to help the matching stage. A Hough transform based method that utilizes the variation in ridge ending density for the classification of altered FP is proposed in chapter 5. This method classifies the altered FP in to imitation, distortion or obliteration. If FP is classified as distortion or imitation, the reconstruction of transplanted region have to be performed or can go for the identification of doctor who had done the surgery.

If the altered FP is classified as obliteration, it goes to the matching stage. Minutiae based matching is not possible to perform for obliterated FP since the alteration process causes the large amount of spurious minutiae. Thus the matching is performed using the reconstructed ridge orientation and ridge texture features in the unaltered region. A method based on orthogonal wavelet is proposed to reconstruct the ridge orientation of altered FP. This reconstructed orientation is used to confirm the alteration detection and also used as a feature in matching stage. Matching is performed in two stages. First stage utilizes the reconstructed ridge orientation and second stage uses the ridge texture and frequency in the unaltered region.

## **8.2. Future Scope**

Classification accuracy is affected if the area of alteration is very less. Obliteration type of altered FP with very less area of alteration produces the ridge ending density similar to that of imitation or distortion type and can be misclassified as imitation type or distortion type. The increase in FPR due to less area of alteration can be compensated by making the threshold values adaptive with respect to area of alteration.

Proposed two stage matching method discussed in chapter 7 can be improved in following ways. Make the ROI selection automatic so that the speed of matching process can be increased. Matching of distortion or imitation type of altered FP is also needed to completely defeat the altered FP threats against AFIS. The distortion or imitation type is produced by the transplantation of ridge structure. Reconstruction of the transplanted region or restoration of minutiae points is needed to perform the matching of these FPs. Methods are to be developed for marking the the transplanted region automatically and use the features in the unaltered region for matching since the reconstruction of transplanted region is difficult.



## References

- [1] Maltoni D., Maio D., A.K. Jain and S. Prabhakar, “Hand Book of Fingerprint Recognition”, Springer Verlag, New York, 2009.
- [2] H.T.F. Rhodes, “Alphonse Bertillon: Father of Scientific Detection, Abelard-Schuman”, New York, 1956.
- [3] G.S. Sodhi and Jasjeet Kaur “A tale of two fingerprint experts”, Indian Journal of History of Science, pp. 151-159, 2001.
- [4] Francis Galton “Fingerprints”, Macmillan and Company, London and New York, 1892.
- [5] National Science and Technology Council (NSTC) subcommittee, “Iris recognition”, August 2006.
- [6] J. L. Wayman, “Fundamentals of biometric authentication technologies”, International Journal of Image and Graphics, Vol. 1, No. 1, pp. 93–113, 2001.
- [7] Anil K. Jain, Arun Ross, and Salil Prabhakar, “An introduction to biometric recognition”, IEEE Transaction on Circuits and Systems for Video Technology, Vol. 14, No. 1, January 2004.
- [8] Arun Ross and Anil K Jain “Biometric sensor interoperability: A case study in fingerprints”, Proceeding of International Workshop on Biometric Authentication (IWBA), Prague, Czech Republic, pp. 134-145, Springer publishers, May 2004.
- [9] A. K. Jain, L. Hong, and B. R. “On-line fingerprint verification”, IEEE Transactions on Pattern Analysis and Machine Intelligence, Vol. 19, No. 4, pp. 302–314, 1997.
- [10] W. Bicz, “The idea of description (reconstruction) of fingerprints with mathematical algorithms and history of the development of this idea at Optel”, <http://www.optel.pl/article/english/idea.htm>, Optel, 2003.

- [11] R. Cappelli, A. Lumini, D. Maio, and D. Maltoni, "Fingerprint image reconstruction from standard templates", *IEEE Transactions on Pattern Analysis and Machine Intelligence*, Vol. 29, No. 9, pp. 1489-1503, September 2007.
- [12] Feng, A.K. Jain, and A. Ross, "Detecting altered fingerprints", *Proceeding of 20<sup>th</sup> International Conference on Pattern Recognition (ICPR)*, pp. 1622-1625, August 2010.
- [13] Soweon Yoon, Jianjiang Feng, and Anil K. Jain, "Altered fingerprints: analysis and detection", *IEEE Transactions on Pattern Analysis and Machine Intelligence*, Vol. 34, No. 3, March 2012.
- [14] Mail online "Doctor jailed for plotting to surgically alter fingerprints of illegal immigrants", *Press Report*, 11 February 2011.
- [15] N. K. Ratha, J. H. Connell, & R.M.Bolle, "Enhancing security and privacy in biometrics-based authentication systems", *IBM Systems Journal*, pp. 614-634, 2001.
- [16] S. A. C. Schuckers, "Spoofing and anti-spoofing measures", *Information security technical report*, pp. 56-62, 2002.
- [17] Osten, H. M. Carim, M. R. Arneson, and B. L. Blan, "Biometric personal authentication system," *U.S. Patent No. 5719950*, 1998.
- [18] P. D. Lapsley, J. A. Less, D. F. Pare, and N. Hoffman, "Anti-fraud biometric sensor that accurately detects blood flow", *U.S. Patent No. 5737439*, 1998.
- [19] D. R. Setlak, "Fingerprint sensor having spoof reduction features and related methods", *U.S. Patent No. 595344*, 1999.
- [20] K. A. Nixon, R. K. Rowe, J. Allen, S. Corcoran, L. Fang et al., "Novel spectroscopy-based technology for biometric and liveness verification", *Proceedings of SPIE*, pp. 287-295, 2004.
- [21] D. Baldisserra, A. Franco, D. Maio, and D. Maltoni, "Fake fingerprint detection by odor analysis", *Proceedings of International Conference on Biometric Authentication (ICBA)*, 2006.

- [22] Arun Ross, Anil K. Jain, and Jian Z. Qian, “Information fusion in biometrics”, Lecture notes on Computer Science, Vol. 24, No. 13, pp. 2115-2125, September, 2003.
- [23] Lin Hong and Anil K. Jain. “Integrating faces and fingerprints for personal identification”, IEEE Transactions on Pattern Analysis and Machine Intelligence, Vol. 20, No 1, pp. 295–1307, 1998.
- [24] Anil K. Jain, Lin Hong, and Yatin Kulkarni “A multimodal biometric system using fingerprint, face, and speech”, Technical report, MSU-CPS-98-32, Department of Computer Science, Michigan State University, East Lansing, Michigan, November 1998.
- [25] Benoit Duc, Elizabeth Saers Bigiin, C Josef Bigiin D, Gilbert Maitre, and Stefan Fischer “Fusion of audio and video information for multi modal personal authentication”, Pattern Recognition Letters, Elsevier, No. 18, pp. 835–843, 1997.
- [26] Heeseung Choi, Raechoong Kang, Kyoungtaek Choi, Andrew Teoh Beng Jin and Jaihie Ki “ Fake-fingerprint detection using multiple static features”, Optical Engineering, April 2009.
- [27] Harold Cummins, “Attempts to alter and obliterate fingerprints”, American Institute of Criminal Law & Criminology, Vol. 982, pp. 1934-1935.
- [28] A press report “John Dillinger shot dead by federal agents in front of a movie theater in Chicago”, New York Times, July 22, 1934.
- [29] K. Wertheim “altering prints”, [http://omin.com/cgi-bin/fp/board-admin.cgi?action=quick&do=print&http\\_referer=4/1494&postindex=415](http://omin.com/cgi-bin/fp/board-admin.cgi?action=quick&do=print&http_referer=4/1494&postindex=415), July 1993.
- [30] K. Wertheim “An extreme case of fingerprint mutilation”, International Journal of Forensic Identification, Vol. 48, 1998.
- [31] A press report by BBC news, “Fake fingerprint Chinese woman fools Japan controls”, [http://news.bbc.co.uk/2/hi/asia\\_pacific/8400222.stm](http://news.bbc.co.uk/2/hi/asia_pacific/8400222.stm), December 2009.
- [32] M. Hall, “Criminals go to extremes to hide identities”, USA Today, [http://www.usatoday.com/news/nation/2007-11-06criminal\\_extreme\\_N.htm](http://www.usatoday.com/news/nation/2007-11-06criminal_extreme_N.htm), November, 2007.

- [33] Press report “Woman alters fingerprints to deceive Taiwan immigration fingerprint identification system”, [http://www.zaobao.com/special/news/papers/2008/10/hongkong\\_081002r.shtml](http://www.zaobao.com/special/news/papers/2008/10/hongkong_081002r.shtml), October 2008.
- [34] Press report “Surgically altered fingerprints help woman evade immigration”, <http://abcnews.go.com/Technology/Gadget/Guide/surgically-altered-fingerprints-woman-evade-immigration/story?id=9302505>, 2011.
- [35] Adina Petrovici and C. Lazar “Altered fingerprint analysis based on SIFT key points”, Automatic Control and Applied Informatics Department, Technical University “Gheorghe Asachi”, Iasi, Romania, September, 2012.
- [36] Adina Petrovici and C. Lazar “Identifying fingerprint alteration using the reliability map of the orientation field”, Automatic Control and Applied Informatics Department, Technical University “Gheorghe Asachi”, Iasi, Romania, 2012.
- [37] John H Ellingsgaard “Fingerprint alteration detection”, M.Sc thesis, Department of Applied Mathematics and Computer Science, Technical University of Denmark, 2013.
- [38] A. K. Jain, L. Hong, S. Pankanti, R. Bolle, “An identity authentication system using fingerprints”, IEEE Explore, Vol. 85, No. 9, pp. 1365-1388, September 1997.
- [39] D. Maio, D. Maltoni. “Direct gray-scale minutiae detection in fingerprints”, IEEE Transactions on Pattern Analysis and Machine Intelligence, Vol. 19, No. 1, 27-39, January, 1997.
- [40] A. Almansa, T. Linderberg “Fingerprint enhancement by shape adaptation of scale-space operators with automatic scale operation”, IEEE Transactions on Image Processing, Vol. 9, No. 9, pp. 2027-2042, December 2000.
- [41] X. D. Jiang, “On orientation and anisotropy estimation for online fingerprint authentication”, IEEE Transactions on Signal processing; Vol. 53, No. 10, pp. 4038—4049, October 2005.
- [42] K. Karu K, A. K. Jain, “Fingerprint classification”, Pattern Recognition, Elsevier, Vol. 29, No. 3, pp. 389-404, March 1996.

- [43] A. K. Jain, S. Prabhakar, L. Hong, "A multichannel approach to fingerprint classification", *IEEE Transactions on Pattern Analysis and Machine Intelligence*, Vol. 21, No. 4, pp. 348-359, April 1999.
- [44] R. Cappelli, A. Lumini, D. Maio, D. Maltoni, "Fingerprint classification by directional image partitioning", *IEEE Transactions on Pattern Analysis and Machine Intelligence*, Vol. 21, No. 5, pp. 402-421, May 1999.
- [45] X. D. Jiang, W. Ser. "Online fingerprint template improvement", *IEEE Transactions on Pattern Analysis and Machine Intelligence*, Vol. 24, No. 8, pp. 1121-1126, August 2002.
- [46] C. H. Park, H. Park , "Fingerprint classification using fast Fourier Transform and nonlinear discriminant analysis", *Pattern Recognition*, Elsevier, Vol. 38, No. 4, pp. 495-503, April 2005.
- [47] J. L. Araque, M. Baena, B. E. Chalela, D. Navarro, and P. R. Vizcaya, "Synthesis of fingerprint images," *Proceedings of 16<sup>th</sup> International Conference on Pattern Recognition (ICPR)*, pp. 422-425, Aug. 2002.
- [48] R. Cappelli, A. Lumini, D. Maio, and D. Maltoni, "Fingerprint image reconstruction from Standard templates", *IEEE Transactions on Pattern Analysis and Machine Intelligence*, Vol. 29, No. 9, pp. 1489-1503, September 2007.
- [49] Jianjiang Feng and Anil K. Jain, "Fingerprint reconstruction: from minutiae to phase", *IEEE Transactions on Pattern Analysis and Machine Intelligence* Vol. 33, No. 2, February 2011.
- [50] B. Sherlock, D. Monro, and K. Millard. "Fingerprint enhancement by directional Fourier filtering", *IEEE proceedings of Vision, Image and Signal Processing*, Vol. 141, pp. 87-94, April 1994.
- [51] Soweon Yoon and Anil K. Jain, "Is there a fingerprint pattern in the image?", *Proceedings of International Conference on Biometrics (ICB)*, Madrid, Spain, June, 2013.
- [52] P. Vizcaya and L. Gerhardt. "A nonlinear orientation model for global description of fingerprints", *Pattern Recognition*, Elsevier, Vol. 29, No. 7, pp. 1221-1231, 1996.

- [53] J. Zhou and J. Gu. “A model-based method for the computation of fingerprints orientation field”, *IEEE Transaction on Image Processing*, Vol. 13, No. 6, pp. 821-835, 2004.
- [54] J. Li, W. Y. Yau, and H. Wang, “Constrained nonlinear models of fingerprint orientations with prediction”, *Pattern Recognition*, Elsevier, Vol. 39, No. 1, pp. 102–114, 2006.
- [55] S. Ram, H. Bischof, and J. Birchbauer, “Modelling of fingerprint ridge orientation using Legendre polynomials”, *Pattern Recognition*, Elsevier, Vol. 43, No, 1, pp. 342–357, 2010.
- [56] Y. Wang, J. Hu, and D. Phillips, “A Fingerprint orientation model based on 2D Fourier expansion (FOMFE) and its application to singular-point detection and fingerprint indexing”, *Special issue on biometrics: progress and directions, IEEE Transactions on Pattern Analysis and Machine Intelligence*, Vol. 29, No. 4, pp. 573-585, April 2007.
- [57] S. Huckemann, T. Hotz, and A. Munk, “Global models for the orientation field of fingerprints: an approach based on quadratic differentials”, *IEEE Transactions on Pattern Analysis and Machine Intelligence*, Vol. 30, No. 9, pp. 1507- 1519, 2008.
- [58] S. Dass, “Markov random field models for directional field and singularity extraction in fingerprint images”, *IEEE Transaction on Image Processing*, Vol. 13, No. 10, pp. 1358- 1367, 2004.
- [59] M. Ask, Bazen, Sabih H. Gerez, “Systematic methods for the computation of the directional fields and singular points of fingerprints”, *IEEE Transactions on Pattern Analysis and Machine Intelligence*, Vol. 24, No. 7, July 2002.
- [60] M. Asker, Bazen, Niek J. Bouman, and Raymond N. J. Veldhuis, J, “A multi-scale approach to directional field estimation”, *Proceedings of RISC 2004*.
- [61] Yi Wang, Jiankun Hu, Fengling Han, “Enhanced gradient-based algorithm for the estimation of fingerprint orientation fields”, *Applied Mathematics and Computation*, Vol. 185, pp. 823–833, 2007.
- [62] En Zhu, Jian-Ping Yin, Guo-Min Zhang, Chun-Feng Hu, “Fingerprint ridge orientation estimation based on neural network”, *Proceedings of*

- International Conference on Signal Processing, Robotics and Automation, Madrid, Spain, pp. 158-164, February, 2006.
- [63] Qinzhi Zhang, Hong Yan, “Fingerprint orientation field interpolation based on the constrained Delaunay triangulation”, *International Journal of Information and Systems Sciences*, Vol. 3, No. 3, Pages 438–452, 2007.
- [64] Ji Luping, Yi Zhang , “Fingerprint orientation field estimation using ridge projection”, *Pattern Recognition*, Elsevier Vol. 41, pp. 1491 – 1503, 2008.
- [65] N. Kiryati, Y. Elar, and A. Bruckstein, “A probabilistic Hough transform”. *Pattern Recognition*, Elsevier Vol. 24, pp. 303–316, 1991.
- [66] D. Shaked, O. Yaron. O, N. Kiryati. N, “Deriving stopping rules for the probabilistic Hough Transform”. *Computer Vision and Image Understanding*, Elsevier, Vol. 63, pp. 512–526, 1996.
- [67] L. Xu, E. Oja., P. Kultanen , “A new curve detection method: randomized Hough transform (rht)”, *Pattern Recognition Letters*, Elsevier, Vol. 11, No. 5, pp. 331–338, May 1990.
- [68] L. Xu, E. Oja, “Randomized Hough Transform: basic mechanisms, algorithms and computational complexities”. *CVGIP: Image understanding*, Vol. 57, pp. 2134–154, March 1993.
- [69] P. Ser, and W. Siu, “Sampling Hough algorithm for the detection of lines and curves” *IEEE International Symposium on Circuits and System*, pp. 2497-2500, 1992.
- [70] N. Kiryati, A. Bruckstein, “Heteroscedastic Hough Transform (htht): an efficient method for robust line fitting in the errors in variables problem”, *Computer Vision and Image Understanding*, Vol. 78, pp. 69–83, 2000.
- [71] J. Mata, C. Galambos, and J. Kittler, “Robust detection of lines using the progressive probabilistic Hough Transform”, *Computer Vision and Image Understanding*, Vol. 78, pp. 119–137, 2000.
- [72] Zezhong Xu, Bok-Suk Shin, “A statistical method for peak localization in Hough space by analyzing butterflies”, *Proceedings of PSIVT*, Springer, Lecture notes in computer science, pp. 111-123, 2014.

- [73] Palmer, P., Kittler, J. and Petrou, M. "An optimizing line finder using a Hough transform algorithm", *Computer Vision and Image Understanding*, Elsevier, Vol. 67, No. 1, pp. 1–23, 1997.
- [74] A. M. Bazen, G. T. B. Verwaaijen, S. H. Gerez, L. P. J. Veelenturf, and B. J. Vander Zwaag. "A correlation based fingerprint verification system", *Proceedings of Workshop on Circuits Systems and Signal Processing*, pp. 205–213, 2000.
- [75] Kumar, M. Savvides, C. Xie, K. Venkataramani, J. Thorntonb and A. Mahalanobis, "Biometric verification with correlation filters," *Applied optics*, Vol. 43, No. 2, pp. 391–402, 2004.
- [76] K. Nandakumar, A. K. Jain, "Local correlation-based fingerprint matching", *Proceedings of International Conference on Computer Vision, Graphics and Image Processing*, pp. 503–508, 2004.
- [77] T. Hatano, T. Adachi, S. Shigematsu, H. Morimura, S. Onishi, Y. Okazaki, H. Kyuragi, "A fingerprint verification algorithm using the differential matching rate", *Proceedings of the 16<sup>th</sup> International Conference on Pattern Recognition*, pp. 799–802, 2002.
- [78] A. Cavusoglu, S. Gorgunoglu, "A robust correlation based fingerprint matching algorithm for verification", *Journal of Applied Science*, pp. 3286–3291, 2007.
- [79] N. K. Ratha, K. Karu, S. Chen, and A. Jain, "A real-time matching system for large fingerprint databases," *IEEE Transactions on Pattern Analysis and Machine Intelligence*, Vol. 18, No. 8, pp. 799–813, 1996.
- [80] R. Germain, A. Califano, and S. Colville, "Fingerprint matching using transformation parameter clustering," *Journal of the Computational Science and Engineering, IEEE*, Vol. 4, No. 4, pp. 42–49, 1997.
- [81] S.H. Chang, F.H. Cheng, W.H. Hsu, and G.Z. Wu, "Fast algorithm for point pattern matching: invariant to translations, rotations and scale changes", *Journal of Pattern Recognition*, Vol. 30, No. 2, p. 311320, 1997.
- [82] S. Pan, Y. Gil, D. Moon, Y. Chung, and C. Park, "A memory efficient fingerprint verification algorithm using a multi resolution accumulator array," *Journal of the Electronics and Telecommunications Research Institute (ETRI)*, Vol. 25, No. 3, pp. 179–186, 2003.



- [83] S. Pan, D. Moon, and K. Kim, "A fingerprint matching hardware for smart cards," *Journal of the Institute of Electronics, Information and Communication Engineers (IEICE) Electronics express*, Vol. 5, No. 4, pp. 136–144, 2009.
- [84] A. Lomte and S. Nikam, "Biometric fingerprint authentication by minutiae extraction using USB token system," *International Journal of Computer Technology and Applications*, Vol. 4, No. 2, pp. 187–191, 2013.
- [85] T. Chouta, J. Danger, L. Sauvage, and T. Graba, "A small and high-performance coprocessor for fingerprint match-on-card," *15<sup>th</sup> Euromicro Conference on Digital System Design, IEEE*, pp. 915–922, 2012.
- [86] F. Chen, X. Huang, and J. Zhou, "Hierarchical minutiae matching for fingerprint and palm print identification," *IEEE Transactions on Image Processing*, Vol. 22, No. 11-12, pp. 4964–4971, 2013.
- [87] R. Zhou, D. Zhong, and J. Han, "Fingerprint identification using SIFT-based minutia descriptors and improved all descriptor-pair matching," *Academic Journal of Sensors*, Vol. 13, No. 3, pp. 3142–3156, 2013.
- [88] F. R. Johannesen, S. Raaschou, O.V. Larsen and P. Jurgensen, "Using weighted minutiae for fingerprint identification," *Proceedings of International Conference on Advances in Structural and Syntactical Pattern Recognition*, pp. 289–299, August, 1996.
- [89] Y. Jie, Y. Y. Fang, Z. Renjie, and S. Qifa, "Fingerprint minutiae matching algorithm for real time system," *Pattern Recognition, Elsevier*, Vol. 39, No. 1, pp. 143–146, 2006.
- [90] X. Luo, J. Tian, Y. Wu, "A minutia matching algorithm in fingerprint verification" *Proceedings of the 15<sup>th</sup> International Conference on Pattern Recognition*, Vol. 4, pp. 833–836, 2000.
- [91] T. Y. Jea, V. Govindaraju, "A minutia-based partial fingerprint recognition system" *Pattern Recognition, Elsevier*, Vol. 38, No. 10, pp. 1672–1684, 2005.
- [92] Haiyong Chen, Hongwei Sun, Kwok-Yan Lam, "A fast and elastic fingerprint matching algorithm using minutiae-centered circular regions",

- proceedings of International Conference on Emerging Security Information, Systems and Technologies, IEEE, October 14-20, 2007.
- [93] Neeta Nain, B. M. Deepak, Dinesh Kumar, Manisha Baswal, and Biju Gautham “Optimized minutiae-based fingerprint matching”, Proceedings of the World Congress on Engineering, Vol. 1, WCE July 2008, London, U.K.
- [94] A. K. Jain, S. Prabhakar, L. Hong, and S. Pankanti, “Filter bank-based fingerprint matching,” IEEE Transactions on Image Processing, Vol. 9, pp. 846–859, 2000.
- [95] Zin Mar Win and Myint Myint Sein, “Robust fingerprint recognition system using orientation and texture features”, 2<sup>nd</sup> International Conference on Computer Science and Information Technology (ICCSIT'2012) , Singapore April 28-29, 2012.
- [96] Jayant V. Kulkarni, Bhushan D. Patil, Raghunath S. Holambe “Orientation feature for fingerprint matching”, Pattern Recognition, Elsevier, Vol. 39, pp. 1551 – 1554, March 2006.
- [97] Xinjian Chen, Jie Tian, and Xin Yang “A new algorithm for distorted fingerprints matching based on normalized fuzzy similarity measure” IEEE Transactions on Image Processing, Vol. 15, No. 3, March 2006.
- [98] Wenzhen Zhou and Wenzhao Zhang “Fingerprint matching based on global orientation field and local features”, International Journal of Digital Content Technology and its Applications, Vol. 6. No. 19, pp. 279-287, October 2012.
- [99] Soweon Yoon, Qijun Zhao, and Anil K. Jain, “On matching altered fingerprints”, International conference on Biometrics, New Delhi, India, March 2012.
- [100] Marius Tico and Pauli Kuosmanen “Fingerprint matching using an orientation-based minutia descriptor”, IEEE Transaction on Pattern Analysis and Machine Intelligence, Vol. 25. No. 8, August 2003.
- [101] Fanglin Chen, Jie Zhou, and Chunyu Yang “Reconstructing orientation field from fingerprint minutiae to improve minutiae-matching accuracy”, IEEE Transaction on Image Processing, Vol. 18, No. 7, July 2009.

- [102] Jin Qi, Suzhen Yang, Yangsheng Wang “Fingerprint matching combining the global orientation field with minutia” *Pattern Recognition Letters*, Elsevier, Vol 26, pp. 2424–2430, June 2005.
- [103] J. Yang, L. Liu, T. Jiang. and Y. Fan, “A modified Gabor filter design method for fingerprint image enhancement,” *Pattern Recognition Letters*, Elsevier, Vol. 24, No. 12, pp. 1805–1817, 2003.
- [104] Zhu, Yin and Zhang (2004). Zhu E., Yin J. and Zhang G., “Fingerprint enhancement using circular Gabor filter,” *Proceedings of International Conference on Image Analysis and Recognition*, pp. 750–758, 2004.
- [105] W. Wang, J. Li J, F. Huang F. and H. Feng, “Design and implementation of Log-Gabor filter in fingerprint image enhancement”, *Pattern Recognition Letters*, Elsevier, Vol. 29, No. 3, pp. 301–308, 2008.
- [106] V. Areekul, U. Watchareeruetai, K. Suppasriwasuseth. and S. Tantaratana, “Separable Gabor filter realization for fast fingerprint enhancement”, *Proceedings of International Conference on Image Processing*, Vol. 3, pp. 253–256, 2005.
- [107] W. Jang, D. Park, D. Lee and S. J. Kim, “Fingerprint Image Enhancement based on a half Gabor filter”, *Proceedings of International Conference on Biometrics*, LNCS 3832, pp. 258–264, 2006.
- [108] S. Chikkerur, A. N. Cartwright and V. Govindaraju, “Fingerprint enhancement using STFT analysis” *Pattern Recognition*, Elsevier, Vol. 40, No. 1, pp. 198–211, 2007.
- [109] S. Jirachaweng and V. Areekul, “Fingerprint enhancement based on Discrete Cosine Transform”, *Proceedings of International Conference on Biometrics*, LNCS 4642, pp. 96–105, 2007.
- [110] Vipin Kakkar, Abhishek Sharma, T.K.Mangalam, Pallavi Kar “ Fingerprint image enhancement based on Wavelet Transform and Gabor filtering”, *Acta technica napocensis Electronics and Telecommunication*, Vol. 52, No. 4, 2011.
- [111] Ching-Tang Hsieh, Eugene Lai, You-Chuang Wang “An effective algorithm for fingerprint image enhancement based on Wavelet

- Transform”, *Pattern Recognition*, Elsevier, Vol. 36, No. 2, pp. 303-312, February 2003.
- [112] Naeim Karimimehr, Ali Asghar Beheshti Shirazi and Mehdi Keshavars “Fingerprint image enhancement using Gabor Wavelet Transform”, *Proceedings of ICEE, IEEE Explore*, May 11-13, 2010.
- [113] Xiukun Yang, Yong Chai and Zhigang Yang “ A fingerprint image enhancement method based on Contourlet Transform”, *Electrical and Power System Computers, LNEE*, pp. 331-338, Springer Verlag, 2011.
- [114] A. Almansa and T. Lindeberg, “Fingerprint enhancement by shape adaptation of scale-space operators with automatic scale selection,” *IEEE Transactions on Image Processing*, Vol. 9, No. 12, pp. 2027–2042, 2000.
- [115] H. Cheng, J. Tian and T. Zhang, “Fingerprint enhancement with dyadic scale-space,” *Proceedings of 16<sup>th</sup> International Conference on Pattern Recognition*, Vol. 1, pp. 200–203, 2002.
- [116] H. Fronthaler, K. Kollreider and J. Bigun “Pyramid-based image enhancement of fingerprints”, *Proceedings of Workshop on Automatic Identification of Advanced Technologies*, pp. 45–50, 2007.
- [117] H. Fronthaler, K. Kollreider and J. Bigun, “Local features for enhancement and minutiae extraction in fingerprints”, *IEEE Transactions on Image Processing*, Vol. 17, No. 3, pp. 354–363, 2008.
- [118] B. M. Mehtre, N. N. Murthy, S. Kapoor and B. Chatterjee , “Segmentation of fingerprint images using the directional image”, *Pattern Recognition*, Elsevier, Vol. 20, No. 4, pp. 429–435, 1987.
- [119] B. M. Mehtre, B. Chatterjee “Automatic fingerprint identification”, *Journal of the Institution of Electronics and Telecommunication Engineers (special issue on pattern recognition)*, Vol. 37, No. 5–6, pp. 493–499, 1991.
- [120] N. K. Ratha, S. Y. Chen and A. K. Jain, “Adaptive flow orientation-based feature extraction in fingerprint images”, *Pattern Recognition*, Elsevier, Vol. 28, No. 11, pp. 1657–1672, 1995.
- [121] D. Maio and D. Maltoni, “Direct gray-scale minutiae detection in fingerprints”, *IEEE Transaction on Pattern Analysis and Machine Intelligence*, Vol. 19, No. 1, pp. 27-40, 1997.

- [122] Shen L., Kot A. and Koo W.M., “Quality measures of fingerprint images”, Proceedings of 3<sup>rd</sup> International Conference on Audio and Video Based Biometric Personal Authentication, pp. 266–271, 2001.
- [123] E. Zhu, J. Yin, C. Hu and G. Zhang, “A systematic method for fingerprint ridge orientation estimation and image segmentation”, Pattern Recognition, Elsevier, Vol. 39, No. 8, pp. 1452– 1472, 2006.
- [124] X. Chen X., Tian J., Cheng J. and Yang X., “Segmentation of fingerprint images using linear classifier,” EURASIP Journal on Applied Signal Processing, Vol. 2004, No. 4, pp. 480–494, 2004.
- [125] L. Hong, A. K. Jain , S. Pankanti and R. Bolle, “Fingerprint enhancement”, Proceedings of Workshop on Applications of Computer Vision, pp. 202–207, 1996.
- [126] B. G. Kim and D. J. Park, “Adaptive image normalization based on block processing for enhancement of fingerprint image”, Electronics Letters, Vol. 38, No. 14, pp. 696–698, 2002.
- [127] S. Greenberg, M. Aladjem, D. Kogan and I. Dimitrov, “Fingerprint Image Enhancement Using Filtering Techniques”, Proceedings of 15<sup>th</sup> International Conference on Pattern Recognition, Vol. 3, pp. 326–329, 2000.
- [128] L. Hong, Y. Wan and A. K. Jain, “Fingerprint image enhancement: algorithms and performance evaluation”, IEEE Transactions on Pattern Analysis Machine Intelligence, Vol. 20, No. 8, pp. 777–789, 1998.
- [129] S. Greenberg, D. Kogan, “Structure-adaptive anisotropic filter applied to fingerprints”, Optical Engineering, Vol. 44, No. 12, 2005.
- [130] A. Erol, U. Halici and G. Ongun, “Feature selective filtering for ridge extraction”, in intelligent biometric techniques in fingerprint & face recognition, CRC Press, Baco Raton, 1999.
- [131] C. Wu, Z. Shi and V. Govindaraju, “Fingerprint image enhancement method using directional Median filter,” Proceedings of International SPIE Conference on Biometric Technology for Human Identification, 2004.

- [132] J. P. Egan, “Signal detection theory and roc analysis. series in cognition and perception”, Academic Press, New York, 1975.
- [133] J. A. Swets, R. M. Dawes, J. Monahan, “Better decisions through science” Scientific American, Available in [http://www. psychologicalscience.org/newsresearch/publications/ journals/%siam.pdf.](http://www.psychologicalscience.org/newsresearch/publications/journals/%siam.pdf), Vol. 283, pp. 82–87. 2000.
- [134] J. Swets, J.” Measuring the accuracy of diagnostic systems”, Science, Vol. 240, pp. 1285–1293, 1988.
- [135] K. H. Zou, “Receiver Operating Characteristics literature research”, On-line bibliography available from <http://splweb.bwh.harvard.edu:8000/pages/ppl/zou/roc.html>, 2002.
- [136] K. A. Spackman, “Signal detection theory: valuable tools for evaluating inductive learning”, Proceedings of the 6<sup>th</sup> International Workshop on Machine Learning, Morgan Kaufman, pp. 160–163, December 1989.
- [137] Tom Fawcett, “ROC graphs: notes and practical considerations for data mining researchers hp laboratories”, January, 2003.
- [138] Vojislav Kecman, “Support Vector Machines Basics, An Introduction Only”, School of Engineering, University of Auckland, April, 2004.
- [139] Max Welling “Support Vector Machines”, Department of Computer Science, University of Toronto, M5S 3G5, Canada.
- [140] Christopher J.C. Burges, “A Tutorial on Support Vector Machines for Pattern Recognition, Data Mining and Knowledge Discovery”, Kluwer Academic publishers, pp. 121–167. Boston, 1998.
- [141] Steve R Gunn “Technical report on Support Vector Machines for Classification and Regression”, Faculty of Engineering, Science and Mathematics, School of Electronics and Computer Science, University of Southampton, May 1998.
- [142] Arthur Coste “Image Processing Project 4 using Hough Transform”, November, 2012.
- [143] D. H. Ballard, “Generalizing the Hough Transform to detect arbitrary shapes”, Pattern Recognition, Elsevier, Vol. 13, No. 2, pp. 111-122.

- [144] C. Liu, T. Xia and H. Li “A hierarchical Hough Transform for fingerprint matching”, Proceedings of 1<sup>st</sup> International Conference on Biometric Authentication, LNCS 3072, pp. 373–379, 2004.
- [145] David Vernon “Automatic detection of secondary creases in fingerprints”, Optical Engineering, Vol. 32. No. 10, pp. 2616-2623. October, 1993.
- [146] D. Gabor, "Theory of communication", Journal of IEE, Vol. 93, No. 26, pp. 429-457, November, 1946.
- [147] M. R. K. Khansari and A. Leon-Garcia, “Sub band decomposition of signals with generalized sampling”, IEEE Transaction on Signal Processing, Vol. 41, No. 12, pp. 3365- 3376,1993.
- [148] M.Vetterly and Kovacevic, “Wavelets and sub band coding”, Prentice-Hall, 1995.
- [149] O.Rioul, “Regular Wavelets: a discrete time approach”, IEEE Transaction on Signal Processing, Vol. 41, pp. 3572-3579, December 1993.
- [150] O.Rioul,”A discrete time multiresolution theory”, IEEE Transaction Signal Processing, Vol. 41, pp 2591-2606, August 1993.
- [151] O. Rioul and P. Duhamel, “Fast algorithm for continuous and discrete Wavelet Transforms”, IEEE Transaction on Information Theory, Vol. 38, pp. 569-586, March 1992.
- [152] S. Mallat, “A Wavelet tour of signal processing”, 2/E. San Diego, Academic Press, pp. 2-121, 1999.
- [153] J. J. Ding and N. C. Shen, “Sectioned Convolution for discrete Wavelet Transform,” June, 2008.
- [154] Justice information services division, Federal Bureau of Investigation, “WSQ gray-scale fingerprint image compression” Washington D.C., December, 1997.
- [155] Mela G. Abdul-Haleem, Loay E. George, Huda M. Al-Bayti “Fingerprint recognition using Haar Wavelet Transform and local ridge attributes only” International Journal of Advanced Research in Computer Science and Software Engineering Vol. 4, No. 1, January 2014.

- [156] Xu Cheng , Wuhan, Cheng, Xin-Ming “An algorithm for fingerprint identification based on Wavelet Transform and Gabor feature”, 3rd International Conference on Genetic and Evolutionary Computing, IEEE Explore, pp. 827-830, Oct. 2009.
- [157] A. Javier, Montoya Zegarra, Neucimar J. Leite, Ricardo da Silva Torres “Wavelet-based fingerprint image retrieval”, Journal of Computational and Applied Mathematics, Science Direct, Elsevier, Vol. 227, No. 2, pp. 294–307, May 2009.
- [158] H.Selavrej, S. Arivazhagan, L. Ganesan, “Fingerprint verification using Wavelet Transform”, Proceedings of 5<sup>th</sup> International Conference on Computational Intelligence and Multimedia Applications (ICCIM), September, 2003.
- [159] T. Arulkumar<sup>1</sup>, P.E.Sankaranarayanan , G.Sundari, “Fingerprint based age estimation using 2D discrete Wavelet Transforms and principal component analysis”, International Journal of Advanced Research in Electrical, Electronics and Instrumentation Engineering Vol. 2, pp. 3, March 2013.
- [160] P. Gnanasivam, S. Muttan “Estimation of age through fingerprints using Wavelet Transform and Singular Value Decomposition”, International Journal of Biometrics and Bioinformatics (IJBB), Vol. 6, No. 2, 2012.
- [161] K. Mangesh, Shinde<sup>1</sup> , S. A. Annadate “Study of different methods for gender identification using fingerprints”, International Journal of Application or Innovation in Engineering & Management, Vol. 3, No. 10, October 2014.
- [162] Pontus Hymer, “Extraction and application of secondary crease information in fingerprint recognition system”, Department of Science and Technology, Linköping University, Electronic press, March 2005.
- [163] A. N Marana. and A. K. Jain.“Ridge-Based fingerprint matching using Hough Transform”, 18<sup>th</sup> Brazilian Symposium on Computer Graphics and Image Processing, October 2005.
- [164] A.A. paulino, jianjiang feng and a. k. jain, “Latent fingerprint matching using descriptor-based Hough Transform”, IEEE Transactions on Information Forensics and Security, Vol. 8 No. 1, January 2013.



- [165] Richard O. Duda, and Peter E. hart “Use of Hough Transform to detect lines and curves in pictures”, Graphics and image processing, Vol. 15, No. 1, January 1972.
- [166] M. Atiquzzman and M.W. Akhtar “A robust Hough Transform Technique for complete line segment description”, Real-time imaging 1, pp. 419-426, Academic Press Limited, 1995.
- [167] Junhong Ji, Guodong Chen, Lining Sun “A novel Hough Transforms method for line detection by enhancing accumulator array”, Pattern Recognition Letters, Elsevier. Vol. 32, pp. 1503–1510, 2011.



## **Publications**

### **Journals**

1. **T.R. Anoop**, M.G.Mini “Hough Transform based technique for fingerprint alteration detection and classification” *International Journal of Biometrics (IJBM)*, Inderscience, Vol. 7, No. 4, PP. 309-325, 2015
2. Mini M G, **Anoop T R**, “ Ridge orientation reconstruction of altered FP using orthogonal wavelet” *ICTACT Journal on Video and Image Processing*, Vol. 6, No. 2, pp. 1127-1132, November 2015.
3. **Anoop.T.R**, Mini.M.G, “Comparison of ridge discontinuity analysis methods of altered FP”, *International Journal of Innovative Trends in Engineering*. Vol. 5, No. 1, pp. 43-46, 2015.
4. **Anoop T R**, Mini M G “Altered FP matching using ridge texture and ridge frequency in the unaltered region” *Bonfring International Journal of Advances in Image Processing*. Vol. 5, No. 2, pp. 6-9, May 2015.
5. **Anoop T R**, Mini M G “Two stage framework for altered fingerprint matching” *ICTACT Journal on Video and Image Processing*, Vol. 5, No. 4, pp. 1024-1029, May 2015.
6. **Anoop T R**, Mini M G, “ Fingerprint alteration detection using scars, minutiae density, and ridge discontinuity” *International Journal of Scientific and Engineering Research*, Vol. 4, No. 8, August 2013.

### **Conferences**

1. **Anoop T R**, Mini M G, “ Fingerprint obliteration detection using minutiae density, ridge discontinuity and scar” proceedings of *International Conference on Global Innovation in Technology and Science* , April 2013.

2. **Anoop T R**, Mini M G, “ Hough accumulator threshold based method for fingerprint alteration detection and classification” proceedings of ICETTAS-15, April 2015.

## **Resume**

### **Personal Profile**

Name: Anoop T.R.

Sex: Male

Date of Birth: 20-3-1982

Area of Interest: Digital Image Processing, VLSI design

Languages Known: English, Hindi, Malayalam, Tamil

Computational skills: C, MATLAB, VHDL, Verilog

Professional Experiences: 8 years of Teaching Experience

Research Experience: 3.5 years Research Scholar in the field of image processing in Department of Electronics, Model Engineering College, Thrikkakara

### **Professional Membership**

Associate Member of Institution Engineers (India), Life Time Member- ISTE

### **Publications**

International /National Conferences : 10

Journal Publications : 6

<b>Qualification</b>	<b>Branch /Specialization</b>	<b>Year</b>	<b>University</b>	<b>Percentage/ CGPA</b>
AMIE	Electronics and Communication Engineering	2006	IEI	CGPA 6.45
M.E	VLSI Design	2008	Anna University, Chennai	70%
Ph.D.	Image Processing	Doing	CUSAT (Model Engineering College)	CGPA 7.5 (Course Work)

Email Address :

[anooptr234@gmail.com](mailto:anooptr234@gmail.com)

Permanent Address :

Thazhathumanakal (H)  
Asamannoor P.O.  
Punnayam  
Perumbavoor  
Ernakulam(Dist.)  
PIN: 683549

Phone No (Mob) :

9961927628, 8589901806

## Subject Index

### A

Abrasion.....25, 65, 83, 107  
AFIS.....9, 14, 15, 46, 67, 135, 136  
Altered fingerprint.....15, 16, 17, 18,  
19, 24, 29, 65, 67, 74, 76, 78, 81, 86,  
87, 88, 92, 93, 96, 124, 133  
Alteration.....13, 14, 15, 17, 24, 25,  
26, 27, 65, 67, 76, 77, 79, 81, 83, 85,  
86, 90, 94, 98, 100, 104, 105, 107,  
108, 119, 121, 122, 127, 135, 136,  
140, 155, 156  
Average filter..... 73

### B

Biometrics..... 3, 5, 7, 21, 22, 137,  
138, 144, 145, 149, 150  
Bifurcation.....11, 34, 37, 68, 69  
Binarization.....69, 85, 86

### C

Classification.....10, 13, 14, 15,  
16, 17, 27, 28, 43, 49, 50, 52, 63, 75,

76, 79, 81, 83, 85, 86, 88, 89, 93, 94,  
96, 97, 98, 100, 101, 102, 103, 121,  
122, 135, 140, 141, 155

Comparison.....7, 17, 18, 61,  
78, 100, 102, 105, 108, 113, 155

Coiflet.....113, 114, 116

Criminal.....4, 24, 25

### D

Daubichies.....113, 114

Detection.....13, 14, 15, 17,  
19, 21, 22, 23, 26, 27, 28, 32, 41, 49,  
54, 62, 65, 67, 68, 73, 76, 77, 78, 79,  
86, 93, 94, 101, 102, 103, 121, 122,  
135, 138, 139, 140, 142, 143, 148,  
150, 153, 155

Decomposition.....41, 58, 60,  
61, 105, 108, 110, 111, 112, 151

Distortion.....9, 11, 12, 15,  
16, 17, 36, 37, 38, 75, 76, 77, 78, 79,  
81, 83, 84, 85, 88, 93, 97, 98, 100,  
107, 135, 136

### E

Euclidian distance.....122, 130

Enhancement.....10, 13, 19, 28,  
32, 37, 40, 41, 43, 45, 46, 62, 67, 72,  
89, 91, 92, 93, 94, 100, 102, 121, 140,  
141, 147, 148, 149

## F

FAR.....48, 49, 132, 133  
FFT..... 47, 68, 72, 86, 121  
Fingerprint, 1, 4, 5, 8, 9, 10, 12, 13, 15,  
16, 17, 18, 19, 21, 22, 24, 25, 26, 27,  
28, 29, 30, 31, 34, 35, 36, 37, 38, 39,  
40, 41, 43, 45, 47, 48, 54, 65, 67, 69,  
70, 73, 74, 76, 77, 78, 79, 81, 83, 86,  
87, 88, 92, 93, 96, 102, 103, 105, 107,  
115, 119, 124, 127, 128, 131, 133,  
135, 137, 139, 140, 141, 142, 144,  
145, 146, 147, 148, 149, 152, 155  
FMR.....49  
FNR.....49, 50  
FPR.....27, 49, 50, 77, 78, 79,  
89, 93, 98, 99, 100, 101, 102, 103,  
135, 136  
FRR.....48, 49

## G

GAR.....49, 132, 133

## H

Haar wavelet.....129  
Hough transform.....17, 32,

33, 43, 53, 54, 73, 79, 81, 86, 88, 97,  
105, 122, 135, 143, 144, 153, 155

Hough Accumulator..... 32, 86, 89,  
98, 100, 101, 156

## I

Imitation..... 15, 16, 75, 76, 78,  
79, 81, 83, 85, 88, 93, 97, 98, 100,  
103, 107, 135, 136

## M

Matching score.....35, 122, 126,  
131, 132, 133

Matching.....5, 8, 10, 11, 13,  
14, 16, 17, 18, 19, 23, 24, 28, 33, 34,  
35, 36, 37, 38, 39, 43, 45, 47, 67, 79,  
86, 118, 119, 121, 122, 125, 126, 132,  
133, 134, 135, 136, 144, 145, 146,  
155

MD..... 65, 67, 70, 71, 77, 78,  
121, 122, 135

MRA.....56, 58

## O

Obliteration.....15, 16, 74, 76,  
77, 78, 79, 81, 83, 84, 85, 86, 87, 88,  
94, 98, 100, 102, 105, 107, 119, 122,  
131, 133, 135, 155



## P

Parzen window..... 27, 85, 121

## R

Reconstruction.....11, 15, 16,  
17, 28, 60, 105, 107, 109, 113, 114, 115,  
118, 119, 121, 135, 136, 141, 155

Ridge ending.....11, 17,  
68, 69, 70, 81, 83, 85, 86, 87, 88, 94, 97,  
105, 135, 136

Ridge frequency.....11, 18,  
47, 129, 130, 131, 134

Ridge orientation.....10, 28,  
31, 67, 124, 155

RD..... 65, 67, 72, 77, 78, 121, 135

ROC.....17, 49, 50, 131,  
132, 133, 149, 150

ROI.....122, 126, 127, 130, 134, 136

ROD.....111, 113, 114, 115

## S

Scar.....15, 17, 67, 73, 74,75, 78, 81, 83,  
94, 95, 96, 102, 115, 121, 131, 135

SNR.....13

SVM..... 27, 50, 52, 76, 122

Synthetically altered fingerprints.....27,  
78, 131, 133

Symlet.....113, 114

## T

Thinning.....69

Threshold,.....34, 35, 49,  
53, 73, 81, 86, 88, 93, 96, 97, 98, 99,  
100, 125, 132, 136

TPR..... 27, 49, 50, 77, 78,  
89, 98, 99, 100, 101, 102, 103, 135

## W

Wavelet transform.....17, 40,  
43, 55, 59, 61, 62, 63, 105, 107, 121,  
124, 147, 152

## X

X-signature.....128

## Z

Z cut.....15, 39, 84